Technologies for the Isolation of Circulating Tumor Cells

by

Ajay Mukesh Shah

B.S., Engineering, Harvey Mudd College (2006)
S.M, Mechanical Engineering, Massachusetts Institute of Technology (2008)

Submitted to the Division of Health Sciences and Technology
in partial fulfillment of the requirements for the degree of

Doctor of Philosophy in Medical Engineering

at the

MASSACHUSETTS INSTITUTE OF TECHNOLOGY

June 2012

Signature of the Author: _____
Harvard-MIT Division of Health Sciences and Technology
May 21, 2012

Certified by: _____
Mehmet Toner, PhD
Helen Andrus Benedict Professor of Biomedical Engineering and Health Sciences and Technology
Thesis Supervisor

Certified by: _____
Daniel A. Haber, MD, PhD
Isselbacher/Schwartz Professor of Oncology and Director of the Mass. General Hosp. Cancer Center
Thesis Reader

Certified by: _____
Ram Sassisekharan, PhD
Director, Harvard-MIT Division of Health Sciences and Technology
Edward Hood Taplin Professor of Health Sciences and Technology and Biological Engineering

Technologies for the Isolation of Circulating Tumor Cells

by

Ajay Mukesh Shah

Submitted to the Division of Health Sciences and Technology
in partial fulfillment of the requirements for the degree of
Doctor of Philosophy in Medical Engineering

Abstract

Metastasis, the spread and growth of tumor cells from the primary site to distant organs, is arguably the most devastating and deadly attribute of cancer, and is ultimately responsible for 90% of cancer-related deaths. Circulating tumor cells (CTCs) are exceedingly rare cells found in the whole blood of cancer patients which have the potential to serve as a 'blood biopsy'. The intricate characterization of these cells could result in an entire new class of therapies directly targeting metastasis.

Present technologies enable only a susbset of potential analyses to be conducted, principally due to sub-optimal cell isolation sensitivity, purity, throughput, or handling method. Here, we present two novel technologies to address the challenge of CTC isolation.

First, we build on affinity-based microfluidic cell capture platforms by developing sacrificial hydrogel coatings to enable the innocuous release of captured cells; we demonstrate that model CTCs captured from whole blood remain viable and proliferative following release and are compatible with downstream immunostaining and FISH analysis.

Second, we present a novel cell sorting system that interrogates over 10 million individual events each second, resulting in a high throughput, ultra-efficient rare cell sorter that delivers enriched cells in a vial, readily compatible with virtually any downstream assay. This is the first system combining the high sensitivity and single cell resolution that is characteristic of FACS with the practicality of MACS at a throughput and specificity afforded by inertial focusing, enabling operation in both 'positive selection' and 'negative depletion' modes. We find greater than 90% cell isolation efficiencies with over 2.5 log depletion of contaminating WBCs. Furthermore, the system is applied to clinical patient samples, and proof-of-concept is demonstrated in a cohort of breast, lung and prostate patients.

Working in a negative depletion mode to isolate target cells in an unbiased fashion, we used the system to assess single putative CTCs isolated from an endogenous pancreatic mouse model for gene expression of tumor markers. Initial data confirms CTC heterogeneity at the single cell level, and positions us to move forward with single cell transcriptome sequencing, which may reveal a broad array of CTC phenotypes including metastatic precursors.

Thesis supervisor: Mehmet Toner
Title: Helen Andrus Benedict Professor of Biomedical Engineering

Acknowledgments

I would like to first thank Mehmet Toner, my thesis advisor, for his tremendous support and guidance over the past six years. He has been incredibly supportive, enabling me to pursue whatever paths I found interesting while always being present to steer me when I needed his help. I will always treasure his continued mentorship. I also owe a large debt of gratitude to Daniel Haber, who co-leads the CTC efforts with Mehmet. Rising to the occasion, Daniel became a mentor to me, and taught me the ways of clinical research. He incorporated me into his group, giving me free reign, access to a world of resources, and introductions to folks across the clinical sphere. Thanks to these two incredible mentors, I feel I have truly been able to gain a deep understanding of the intersection between medicine and engineering; for this and for their profound impact on my life and career, I will be forever grateful.

Shyamala Maheswaran has been incredibly supportive of me during my time at the MGH Cancer Center, and in her no-nonsense way she made sure I remained on track! For this, I am much appreciative. I am grateful to Sangeeta Bhatia for graciously agreeing to chair my thesis committee and for helping me navigate the doctoral process. Her insights have been critical to guiding my path.

Over the course of my PhD work, I received tremendous guidance, support and encouragement from the numerous post-docs and fellows who passed through the Center for Engineering in Medicine and the MGH Cancer Center. To all of them, I am indebted tremendously for their actual day to day help in the lab, and for teaching me so many of the practical skills I know, as well as for listening sympathetically as I struggled through grad school! Of particular note, I would like to thank Shannon Stott, Min Yu, Kenneth Kotz, Emre Ozkumur, and David Ting for their incredible generosity and help. I also must thank Brian Nahed & Rick Lee for shaping my understanding of clinical oncology.

I was incredibly lucky to meet and work with Ravi Kapur, Tom Barber, and John Walsh, who joined the project early on and brought with them an industrial focus. When I'd get frustrated with aspects of academia, they were always there to support me, and fostered my entrepreneurial spirit. I'm especially grateful to Tom for discussing surface chemistry in detail with me, and for openly sharing his wisdom without hesitation.

I am thankful to the other graduate students in the group, Grace Chen, Sukant Mittal, Joseph Martel and Eugene Lim, for our shared camaraderie as we together navigated through the PhD process, and the unique attributes of working at MGH!

Two people deserve a special acknowledgement, as without them, the work shown in this thesis would not have been accomplished – Zev Nakamura and Jordan Ciciliano. They were both technicians at the Cancer Center who I had the pleasure to work with, and for whose help I am deeply grateful. I know that they are both headed on to successful careers of their own, and hope that I was able to help them as much as they helped me.

Finally, I am eternally thankful to my family and my fiancée, Ann Cai, for their unwavering support. I cannot express how deeply I am grateful for their love and their continual encouragement to pursue my dreams.

Table of Contents

Table of Figures

Chapter 1

Chapter 2

Chapter 3

Chapter 4

Chapter 6

Chapter 1: Introduction

Since the association of an imbalance in "black bile" with cancer by the Greek physician Galen in ancient Rome, to the post-mortem observation of tumor-like cells in the blood in 1869 by Ashworth, to the validation of circulating tumor cells (CTCs) as a prognostic tool in the early 2000's, the scientific community has had an ever-deepening interest in understanding these rare cells and their role in the deadly metastatic process. (Figure 1) (1-3) CTCs are exceedingly rare cells found in the whole blood of cancer patients. They have the potential to serve as a 'blood biopsy', enabling population-wide screening for early diagnosis, highly sensitive prognostic monitoring for cancer patients, and serial non-invasive molecular profiling to bring the science of personalized medicine to practical fruition in the clinic. Furthermore, while much has been hypothesized about their potential role in the hematogenous dissemination of cancer, the biological characterization of these cells could lead to an entirely new class of therapies targeting metastasis.

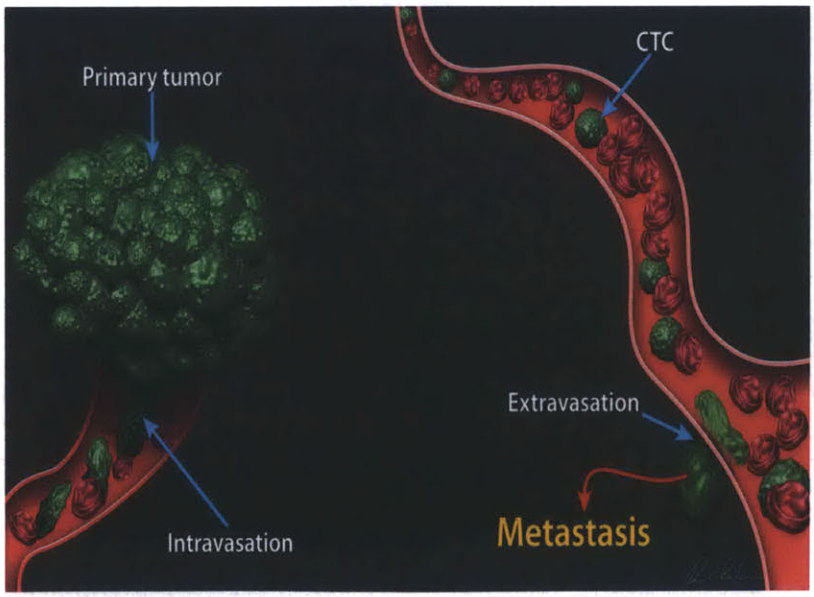

Figure 1. The potential role of circulating tumor cells in metastasis

Metastasis is the spread and growth of tumor cells from the primary site to distant organs, is arguably the most devastating and deadly attribute of cancer, and is ultimately responsible for 90% of cancer-related deaths, resulting in over 500,000 deaths each year in the United States alone. As discussed, circulating tumor cells have the potential to be highly informative with regards to our understanding of metastasis. Present technologies, however, enable only a susbset of potential analyses to be conducted, principally due to sub-optimal cell isolation sensitivity, purity, throughput, or handling method. Thus, the goal of this thesis is to address the challenge of CTC isolation by improving on existing techniques or developing new enrichment methods to enable a wide variety of endpoint analyses of CTCs. (Figure 2)

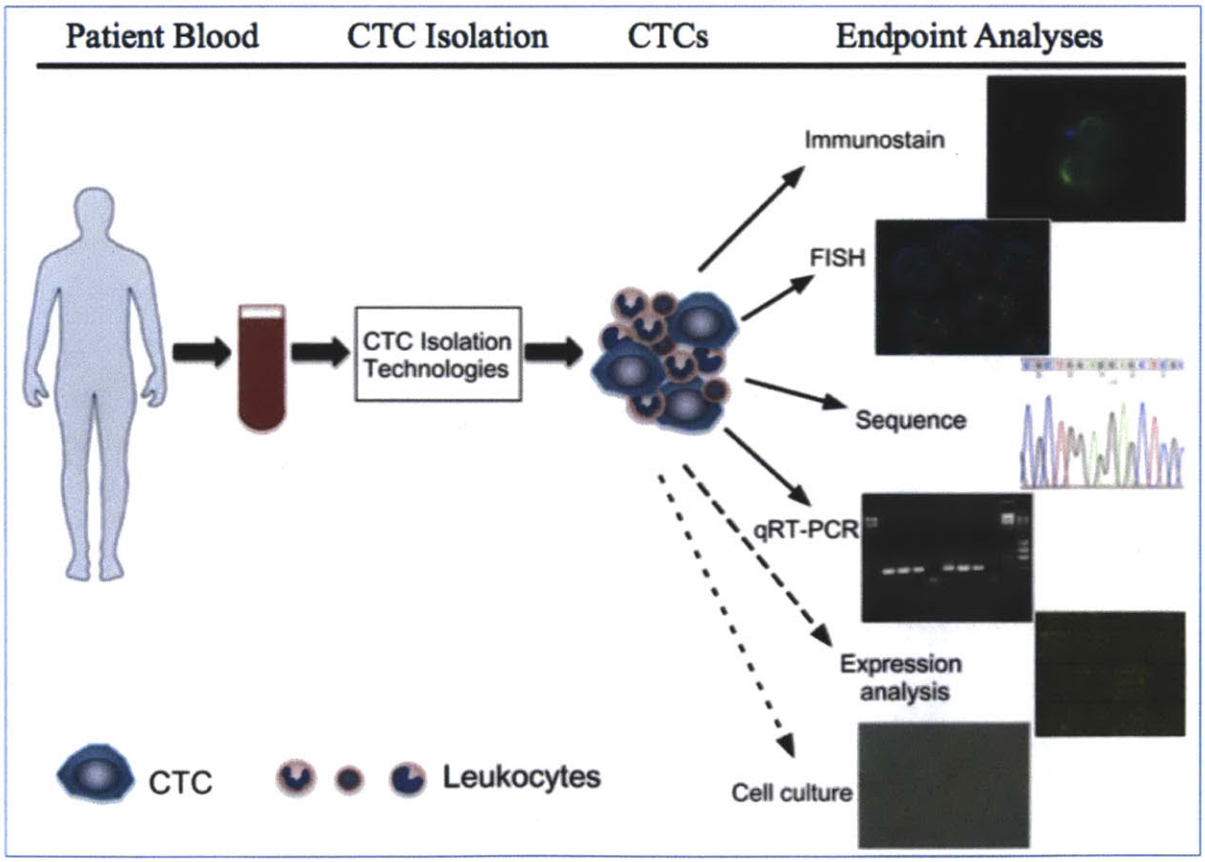

Figure 2. Current and potential downstream endpoint analyses of CTCs. Adapted from (*4*)

1.1 Thesis overview

This thesis presents two novel technologies that addresses current challenges in CTC isolation.

Chapter 2 first reviews existing rare cell enrichment technologies, including bulk immunomagnetic approaches, density-gradient isolation, and size-based separation methods as well as newer microfluidic affinity-based systems.

Chapter 3 presents a biofunctional sacrificial hydrogel coating for microfluidic chips that enables the highly efficient release of captured cells following gel dissolution. Such a coating is important because microfluidic systems for affinity-based cell capture have emerged as a promising approach for the isolation of specific cells from complex matrices (i.e., circulating tumor cells in whole blood). However, these technologies remain limited by the lack of reliable methods for the innocuous recovery of surface captured cells. The covalently crosslinked alginate biopolymer system discussed in chapter 3 is stable in a wide variety of physiologic solutions (including EDTA treated whole blood) and may be rapidly degraded via backbone cleavage with alginate lyase. The capture and release of EpCAM expressing cancer cells from whole blood using this approach was found to have no significant effect on cell viability or proliferative potential and recovered cells were demonstrated to be compatible with downstream immunostaining and FISH analysis.

Chapter 4 presents a novel cell isolation technology: Magnetophoretic Inertial Microfluidcs for Integrated Cell Sorting (MIMICS) - a cell sorting system that interrogates over 10 million individual events each second, resulting in a high throughput, ultra-efficient rare cell sorter that delivers enriched cells in a vial, readily compatible with virtually any downstream assay. This is the first system combining the high sensitivity and single cell resolution that is characteristic of

FACS with the practicality of MACS at a throughput and specificity afforded by inertial focusing, enabling operation in both 'positive selection' and 'negative depletion' modes. Whole blood is loaded into the three-component integrated system which enables (1) lossless sample debulking, (2) specific cell positioning and (3) highly sensitive magnetophoretic separation of target cells. In chapter 4, we demonstrate the operating parameters of each system component and then evaluate the performance of the integrated system for rare cell enrichment, finding greater than 90% target cell isolation efficiencies with over 2.5 log depletion of contaminating WBCs. Furthermore, the system is applied to clinical patient samples, and proof-of-concept is demonstrated in a cohort of breast, lung and prostate patients.

Chapter 5 presents an initial application of the MIMICS system aimed at deepening our fundamental understanding of CTC heterogeneity. The system was modified to work with an endogenous mouse model of pancreatic cancer and used in the negative depletion mode to isolate CTCs in an unbiased fashion. This application was validated using a cell line derived from the model, and recovery efficiencies were determined to be greater than 95% with approximately 3 log removal of contaiminating WBCs. This high recovery efficiency and low contamination, along with the relatively high number of CTCs found in the endogenous mouse model, results in an extremely high sample purity. We were thus able to individually micromanipulate putative CTCs and, following RNA extraction and cDNA amplification, assess individual cells for expression of potential CTC markers using qPCR. Interestingly, we observed a spectrum of expression, from cells expressing only a single keratin marker, to ones robustly expressing three keratins, to cells expressing no keratins but instead the pancreatic specific gene product PDX1. This initial data confirms CTC heterogeneity at the single cell level, and positions us to move

forward with single cell transcriptome sequencing, which is expected to reveal a broad array of CTC phenotypes.

Chapter 6 summarizes the contributions presented in this work and highlights the critical next steps to advance the biomaterials technology discussed in Chapter 3, development of the MIMICS technology discussed in Chapter 4, and the fundamental biological characterization of CTCs enabled by the work in Chapter 5.

Chapter 2: Techniques for CTC Identification

2.1 Introduction

A wide variety of technologies for CTC identification have been developed over the past 30 years to address the challenge of rare cell detection. (Figure 3) These range from non-enrichment based strategies, to enrichment strategies based on cells' physical properties, to those based on antigen expression.

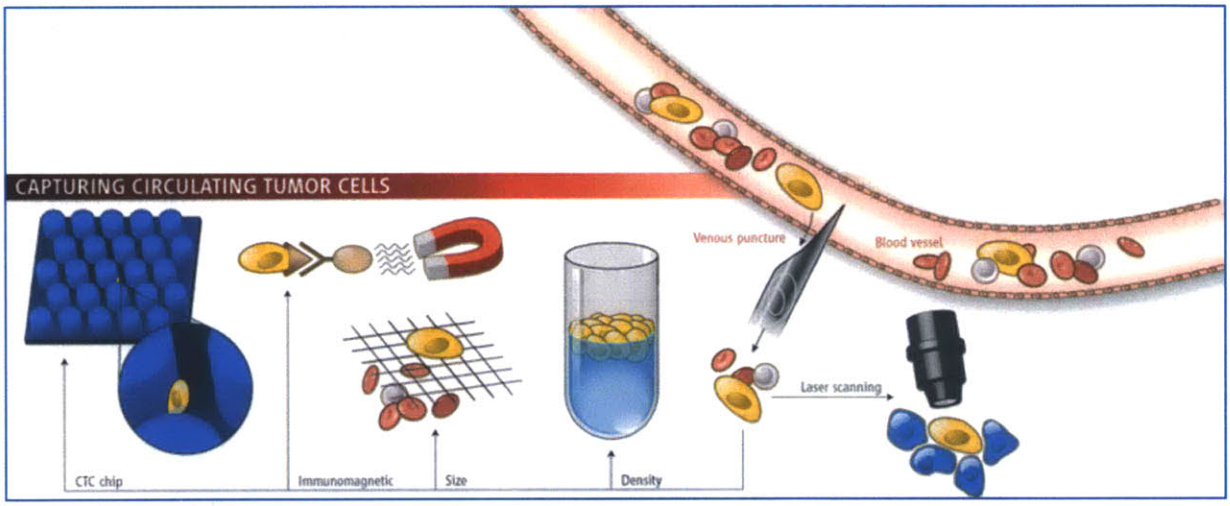

Figure 3. Approaches for circulating tumor cell capture. Adapted from (*5*).

2.2 Non-enrichment detection

One approach to identifying CTCs centers on detection without the need for selective enrichment. (*6*) In a recent embodiment of this approach, an 'HD-CTC' assay was developed. Here, RBCs are lysed in whole blood and nucleated cells are plated on specially coated glass slides at a density of ~ 3M cells / slide. The slides are then stained with anti-cytokeratin and anti-CD45 antibodies, scanned using a custom laser scanning microscope, and automated image processing software identifies positive targets for further human review. (*7*) The notable

advantage of this approach is that it is not reliant on any particular CTC feature for cell isolation, however the lack of enrichment limits its applicability to imaging-based analyses as the high numbers of hematogenous cells prevent molecular analyses.

2.3 Size based sorting

A number of technologies have been developed to isolate CTCs from whole blood based on their presumed larger size as compared to RBCs and WBCs. (*8*) Two examples of this approach include a microfabricated porous filter-based device and a shear-modulated inertial microfludics approach. In the filter-based device, a parleyne membrane with 8 micron pores is sandwiched between two PDMS slabs, and whole blood is pushed through the membrane. Cote et. al. demonstrate that larger cultured tumor cells are retained in the pores, while the bulk of WBCs and RBCs pass through and are collected on the other side of the filter. (Figure 4) (*9*)

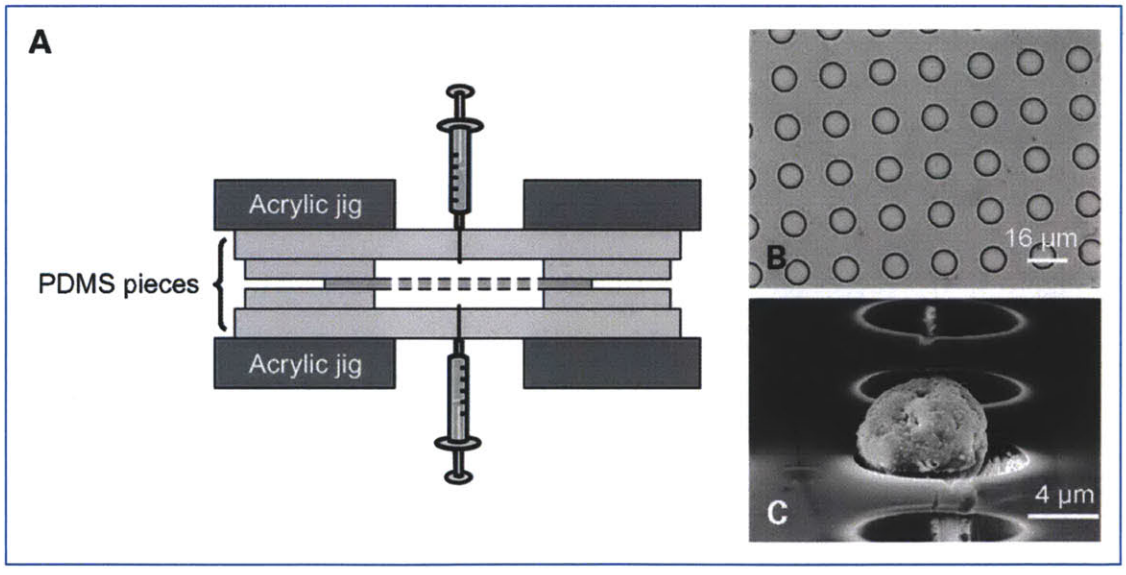

Figure 4. (A) A schematic of the microfilter device with (B) uniform 8 um pores that (C) retain larger cultured tumor cells. Adapted from (*9*).

Microfluidic approaches for sized-based separation are also being developed. Briefly, inertial lift forces may be used to create a cell-free zone in the center of the channel, by pushing all cells to two streamlines along the channel walls; larger cells are then pushed into the center stream as a result of flowing through a series of contraction-expansion regions that 'pinch', causing the center of inertia of these cells to align with the central flowstream. (*10*)

2.4 Density based approaches

Density gradient centrifugation across a Ficoll medium is commonly used to fractionate whole blood. This technique has been used to enrich disseminated tumor cells (DTCs) from bone marrow, and has further been adapted to enrich CTCs from blood. (*11*) The commercial product OncoQuick relies on similar principles (Figure 5); literature reports indicate over 600 fold depletion of mononuclear white blood cells from whole blood using this approach. (*12*)

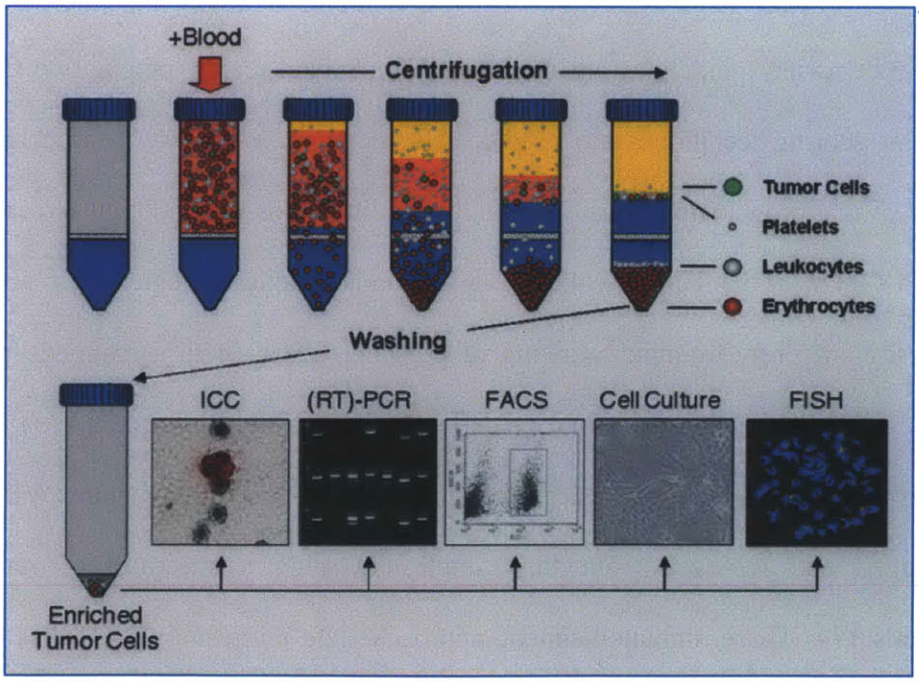

Figure 5. Overview of OncoQuick technology.

2.5 Immunological sorting techniques

Antigen based strategies are amongst the most compelling and commonly used for CTC isolation because they enable highly sensitive and specific targeting of particular cell populations. In particular, EpCAM (Epithelial Cell Adhesion Molecule) is a classically targeted cell surface marker in the CTC field as it is broadly expressed across epithelial tumors. Recently, however, additional disease-specific target antigens have gained prominence including EGFR, HER2 and PSMA.

2.5.1 Immunomagnetic strategies

The only FDA approved CTC isolation technique, CellSearch, is based on the application of a bioferrofluid to whole blood. The anti-EpCAM ferrofluid is used to label EpCAM expressing CTCs, and these cells are then magnetically separated. Importantly, the entire process is automated, from blood processing to the downstream staining, imaging, and potential target identification. Strict review guidelines are established for human review of putative CTCs to ensure that similar scoring techniques are used by all operators. While CellSearch has been clinically validated as a prognostic indicator, its utility is limited as the endpoint is essentially binary (> or < 5 CTCs / 7.5 mL). (*1*) Alternative immunomagnetic strategies have also been proposed; these similarly rely immuno-targeting of potential CTCs with a magnetic payload followed by binding to a magnetic substrate or deflection by a magnetic circuit. (*13*) Finally, similar strategies have been used for 'negative depletion' applications, where WBCs are magnetically tagged and removed from the sample, revealing a spectrum of rare non-hematogenous cells. (*14*) These immunomagnetic approaches are promising approaches for rare cell isolation, but are limited by their sensitivity as they often rely on bulk RBC-lysis methods which are inherently lossy. (*15*)

2.5.2 Microfluidic surface capture approaches

Over the last 5 years, our group has created and developed microfluidic affinity based chips to capture circulating tumor cells from whole blood; during this time we developed first a micropost chip (the 'CTC-Chip') and then a second generation chip (the 'HB-Chip'). (Figure 6) (*16-18*) Both manipulate the flow kinetics of complex solutions such as whole blood to allow sensitive detection of CTCs. In the first-generation CTC-Chip, whole blood was processed through a field of approximately 86,000 microposts, increasing the frequency of cell-surface interactions. (*16*) This technology was demonstrated to isolate CTCs in large numbers and with high frequencies, and additionally enabled the detection of EGFR mutations in lung cancer patients. (*16, 19*) However, the HB-Chip is more readily scalable and operates across a broader range of flow rates; also, in initial studies, the HB-Chip revealed the presence of CTC microclusters in patient blood. The herringbone chip is centered on the concept of passive mixing of blood through the generation of microvortices to increase cell-surface interactions. For cells traveling in a traditional flat microchannel, the laminar uniaxial flow restricts the degree of interaction between the cells and the antibody-coated capture surface; whereas, for cells traveling in the herringbone CTC-Chip, the grooves in the upper surface of the device generate helical flows that stretch and fold volumes of fluid over the cross section of the channel, effectively mixing the solution. As a result, the cells 'jump' the flow streamlines and consequently interact significantly more with the antibody-coated surface.

In our initial study evaluating the HB-Chip, samples from 15 prostate patients and 10 healthy donors were processed. Automated analysis of all samples for PSA+/CD45- cells found a median of 1 CTC / mL in healthy donors, and 63 CTCs/mL in patients. CTCs were found in 14 of 15 cases (93%), with counts ranging from 12 to 3,167 CTCs/mL. (*18*) As the first generation CTC-

chip detected CTCs in 64% of patients when evaluated using the same criteria, the herringbone clearly performs as well or superior to the initial technology while also revealing CTC microclusters and potentially enabling further biological insights. (*17*) Yet, these technologies remain limited by the inability to elute captured cells for further downstream analysis.

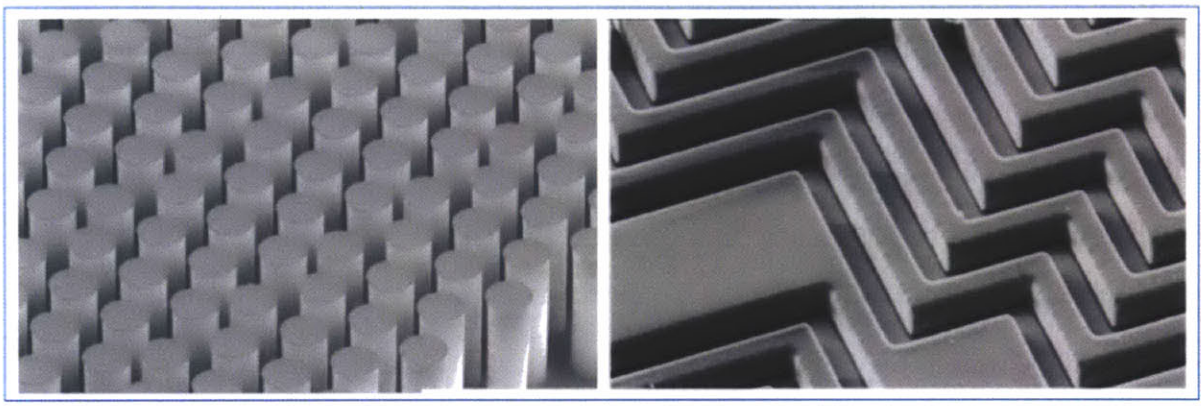

Figure 6. SEM images of the first generation micropost CTC-Chip (left) and the second generation herringbone HB-Chip (right). (*16, 17*)

2.6 Summary

A myriad of techniques have been developed for circulating tumor cell (CTC) detection, each with its own advantages and weaknesses. Non-enrichment strategies are amongst the most passive as they do not require prospective sorting, however they are limited to imaging based readouts, given the lack of purification. Size and density based approaches rely on assumed properties of CTCs; while sorting based on physical properties is reliable, little characterization of patient CTCs has been conducted to validate these assumptions. Immunological sorting techniques are arguably the most prominent of current approaches, and both bulk immunomagnetic sorting and microfluidic surface-based cell capture technologies have demonstrated reliable CTC isolation from a wide range of clinical samples.

Chapter 3: A Biopolymer System for Cell Recovery from Microfluidic Cell Capture Devices

3.1 Introduction

Continuous flow affinity-based microfluidic devices are emerging to fill an important niche in cell sorting. (*16, 20*) These technologies focus on coating a surface with a capture moeity and then utilize microfluidic architectures to precisely control and maximize cell–ligand interactions. (*17, 21, 22*) The label-free nature of these techniques enables the isolation of cell populations from complex solutions (i.e., whole blood) with minimal or no pre-processing. This allows for the rapid isolation of a wide variety of clinically relevant cell types, ranging from exceedingly rare circulating tumor cells,(*17*) to CD4+ T cells,(*23*) to more prevalent neutrophils.(*24, 25*) At present, only limited downstream analysis (most commonly, imaging-based approaches) may be conducted due to the inability to reliably elute viable cells from the microfluidic chips. For genetic analyses, mixed cell populations must be lysed on chip(*19*) and only limited amounts of material can be recovered, restricting the ability to do full genome wide studies of rare cell populations. Furthermore, the cells are unavailable for downstream purification, differentiation of complex sub-populations, single cell genomic analyses, or subsequent culture in vitro or in animal models.

3.2 Background

Cells initially captured on immuno-affinity substrates via specific antibody-antigen binding are likely to form other non-specific linkages with the surface over time. These non-specific linkages may confound any molecular release mechanisms which cleave only specific antibody linkages. (

Figure 7) Potential approaches for the release of surface captured cells range from chemical methods such as gradient elution to mechanical approaches such as the application of high shear stress and the use of bubbles within capillary systems.(*26, 27*) Both chemical and mechanical approaches have the potential to cause significant harm to the target cell populations. Even if cell integrity is preserved, the ability to extract phenotypic and functional information from target populations may be compromised as variations in chemical microenvironments and shear stress are known to cause significant changes in gene expression patterns. (*28*)

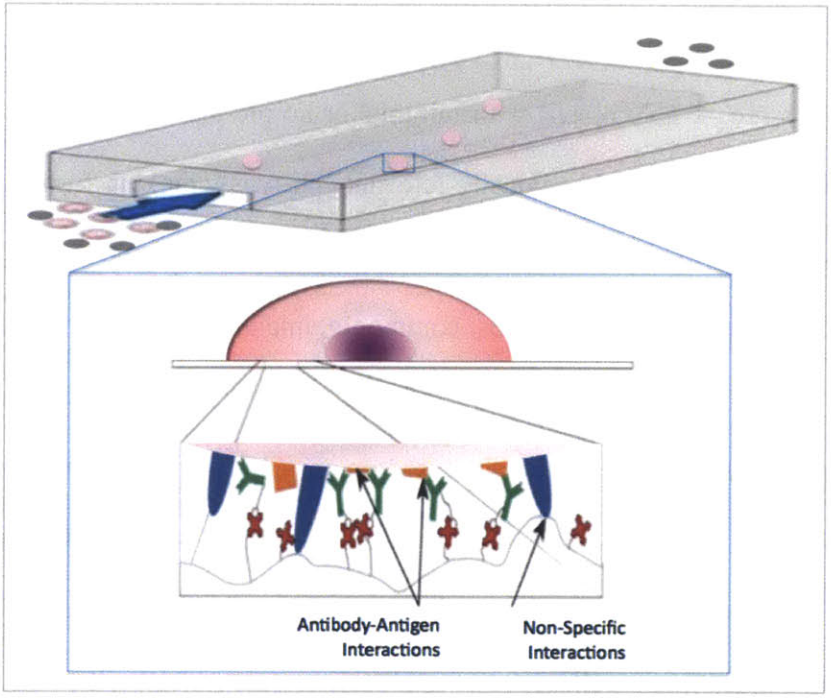

Figure 7. Nonspecific cell surface interactions confound targeted cell release mechanisms

In limited studies, the combination of a proteolytic enzyme and surfactant enabled the release of captured cells for immediate enumeration(*29-31*); the degradation of surface markers and potential membrane disruption due to the surfactant, however, may limit the feasibility of this approach for downstream biological analyses of target cells.

Phase-changing hydrogels, such as temperature(*32*) and UV sensitive gels,(*33*) have emerged as a potential method to regulate cell-surface interactions. Recently, Hatch et. al.,(*34*) demonstrated that ionically crosslinked hydrogels formed in situ enabled the capture, release, and FACS analysis of endothelial progenitor cells from heparinized whole blood. Notably, this study demonstrated the feasibility of a cation-crosslinked sacrificial hydrogel approach for microfluidic cell capture and release without enzymatic digestion of cell surface proteins. This system, while promising, has a limited scope of use as it cannot be used in conjunction with common anti-coagulation strategies that work on the principle of calcium chelation (EDTA, citrates, etc).(*35, 36*) Furthermore, during cell release, target cells are exposed to nonphysiologic levels of calcium chelating agents which may initiate unwanted signaling cascades within the target cells, and have the potential to alter the observed cell phenotype and proliferation state.(*37-39*)

3.3 Approach

Here we present a photocrosslinked, degradable biopolymer coating that enables the gentle, efficient release of antibody-captured cells from microfluidic devices (Figure 8). Our coatings are of controlled thickness, stable for extended periods of time, and may be used with a wide variety of buffers and physiological fluids (including EDTA-treated whole blood). The release mechanism we employ is the backbone degradation of our alginate biopolymer by a specific bacterial enzyme (alginate lyase) which is commonly used in combination with cell cultures. (*40-42*) We further demonstrate that released cells are viable and proliferative.

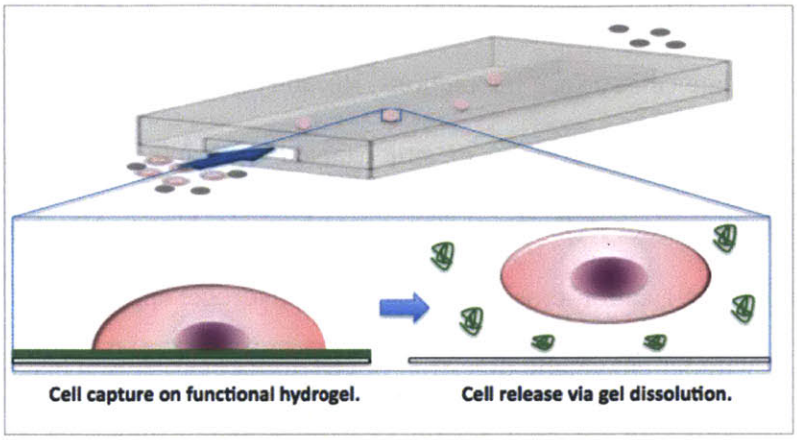

Figure 8. Sacrificial hydrogel coatings may be a compelling strategy for cell release from microfluidic devices, as they will release both specific and non-specific cell-surface linkages.

3.3.1 Biomaterial selection

Alginate is a naturally derived biomaterial isolated from brown algae that is used across a broad spectrum of applications, from food processing to cell culture. Within the biomedical community, alginate occupies a unique niche due to a number of favorable properties.(*40*) Alginate is a cytocompatible, non-fouling biomaterial that is generally regarded as safe (GRAS) by the U.S. FDA. A linear polysaccharide, alginate is composed of repeating mannuronic and guluronic acid monomers which form its backbone; this structure contains a readily functionalizable carboxylic acid on each monomer. (Figure 9) Alginate is often selected for various applications, most notably cell encapsulation, because of its ability to gently form temperature independent gels via divalent cation (generally calcium) crosslinking under physiologic conditions.(*40*) This crosslinking is thought to occur due to an 'eggbox' coordination between the divalent ions and the carboxylic acids, but the exact mechanism is not well understood.(*40*) The gelation is reversible by chelation of the crosslinking cation. Alternatively, alginate gels may be rapidly degraded by *alginate lyase*, a bacterial enzyme which specifically degrades the biopolymer's backbone and should have no affect on mammalian cells (Figure

9).(*41*) Alginate lyase has been well characterized and used for many *in vitro* and *in vivo* alginate systems.(*42*) This degradation strategy enables the dissolution of covalently crosslinked alginate films, overcoming the limitations of ionically crosslinked systems.

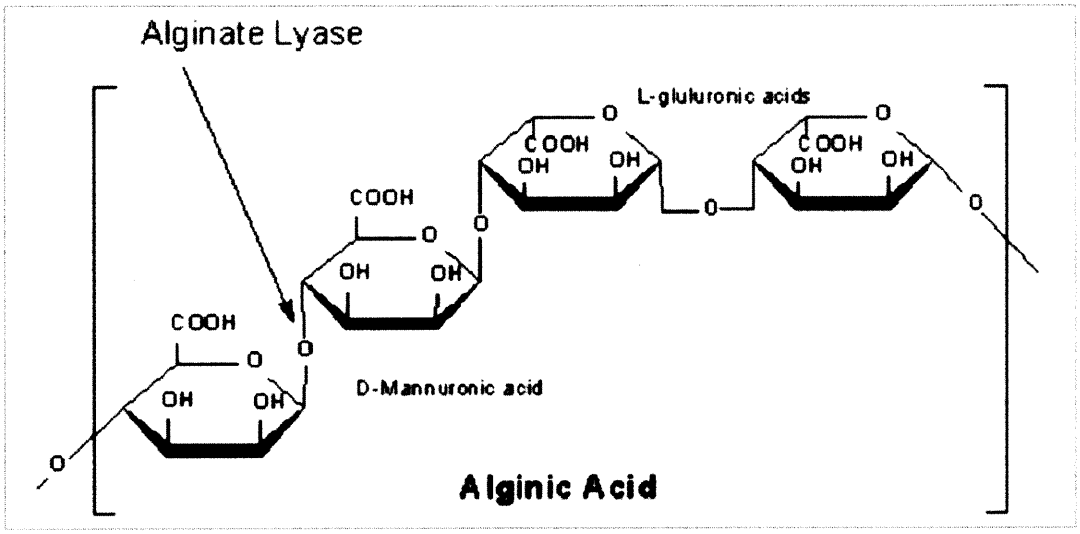

Figure 9. Structure of alginic acid polymer indicating backbone cleavage site of the enzyme Alginate Lyase.

3.4 Methods

3.4.1 Alginate modification

Pharmaceutical grade alginate (Pronova UP MVG, Novamatrix, Norway, 60% guluronate, 40% mannuronate) was modified with both N-(3-Aminopropyl)methacrylamide HCl (Polysciences 21200-5) and biotin hydrazide (Sigma B7639) using standard carbodiimide chemistry in a single reaction. Briefly, alginate was prepared at 1% by weight in MES buffer, pH = 6.0. Per 100 mL of alginate solution, 0-159 mg of biotin hydrazide, 225.63 mg of methacrylamide, 721 mg of 1-Ethyl-3-[3-dimethylaminopropyl]carbodiimide hydrochloride (EDC, Pierce 22980), and 408 mg

of hydroxysulfosuccinimide (Sulfo-NHS, Pierce 24510) were added and reacted for 3 hours, after which time the solution was dialyzed against dH2O for 48 hours and lyophilized. Alginate was reconstituted at 2% in dH2O prior to use.

3.4.2 Hydrogel formation

Substrates were pre-treated with a molecular-scale layer of alginate by first aminating the surface with a solution of 3-aminopropyltriethoxysilane (Pierce 80370, in 95% Ethanol, pH=5.0 for five minutes) followed by reacting the amine-surface overnight with a dilute alginate solution (0.1% in MES, pH = 6.0) containing 3.73 g of EDC and 2.11 g of Sulfo-NHS per 100 mL. Substrates were then rinsed and dried prior to spincoating. Alginate solutions were spun (spincoater WS-650SZ-6NPP/LITE, Laurel Technologies) at 3000 RPM for 30 seconds to control gel thickness, unless otherwise noted. Gels were then crosslinked using a 250 mM calcium chloride spray, followed by incubation in a 2.5 mM calcium solution, addition of the photoinitiator irgacure 2959 (Ciba Specialty Chemicals) (0.25%) to the solution, and then photocrosslinking in a nitrogen environment for 10 minutes using a 365 nm UV lamp (UVP XX-15-BLB). Following crosslinking, the gels were washed to remove calcium and dried prior to use.

3.4.3 Patterning and functionalizing gels inside simple microfluidic geometries

Gels were spatially templated onto ultraclean glass slides (Thermo C22-5128-M20) by first applying a laser-cut elastomeric stencil in the shape of the microchannel on top of the glass prior to hydrogel formation. Following gel formation as described above, the stencil was removed, and a PDMS microchannel was plasma treated for 30 seconds (ElectroTechnic Products BD-20) and bonded around the hydrogel.(*23*) The PDMS microchannels used in this study were rectangular chambers 50um tall, 4mm wide, and 50 mm long, fabricated using standard soft-lithography techniques.(*43*) The channels were flushed with PBS (rehydrating the gels), blocked

in a 1% BSA solution for a minimum of 30 minutes (blocking the gel and PDMS walls), and functionalized with neutravidin (Pierce 31000, 50 ug/mL in 1% BSA) for 45 minutes. The channels were rinsed with PBS and incubated with a biotinylated anti-EpCAM antibody (R&D Systems BAF960, 20 ug/mL in 1% BSA for 45 minutes) when used for cell capture. In this model system, only the bottom surface of the channel was coated with the hydrogel, limiting the available area for cell binding.

3.4.4 Hydrogel characterization

Hydrogel thickness was measured using a non-contact profilometer (Olympus LEXT OLS3100) after films were formed and dried. To characterize gel dissolution, 50 nm green fluorescent beads (Duke Scientific G50) were mixed into the alginate solution prior to gelation and thus impregnated in the resulting hydrogel; as the gel dissolved, beads were released and cleared away and the decrease in fluorescent signal intensity was monitored using time-lapse imaging. Initial steady-state intensity measurements were taken before treating the gel with alginate lyase at a particular concentration, and a final steady-state measurement was taken once the gel had fully degraded; these values were treated as 100% (initial) and 0% (final) relative intensities. For the control condition (0 ug/mL alginate lyase) all intensites were compared to the initial steady-state, as the gel did not degrade; the slight drop in intensity was observed to be caused by photobleaching of the sample by comparing the intensity of the gel immediately adjacent to exposed field of view. The experimental samples were observed to rapidly degrade, and so no notable photobleaching was observed.

Relative biofunctionality was measured using a sandwich assay in which the biotin incorporated into the hydrogel was coupled with neutravidin, rinsed with PBS, and then followed by a fluorescent biotinylated protein (biotin R-PE, 20 ug/mL for 45 min in 1% BSA, Life

Tecnologies). The 'standard chemistry' is a silane-based coupling chemistry used in our laboratory to functionalize microfluidic devices with neutravidin; it was followed by the same biotin R-PE solution to assay the biotinylated protein binding capacity of the surface.(*16*)

3.4.5 Cell capture, release and recovery

Cell capture and release was characterized using both a prostate cancer (PC3) and breast cancer (SKBR3) cell line. All cell lines were obtained from ATCC and cultured in accordance with their recommendations.

The relative cell capture efficiency was evaluated by patterning gels in 10 x 10 mm squares and functionalizing with the anti-EpCAM antibody as described. PC3s in PBS buffer were then spotted onto the areas in a static capture assay to compare the relative cell capture potential of the functional alginate coatings as compared to the standard chemistry (positive control, set to 100%) and nonfunctional alginate (negative control). Following a brief incubation period, unbound cells were removed by gently washing the area with PBS. Cells were counted before and after washing to determine capture efficiency. This static assay evaluates the effect of surface ligand presentation on cell capture efficiency, separate from the effects of the microfluidic geometry. Together, these two parameters determine cell capture efficiency in affinity-based microfluidic cell isolation devices.

To evaluate performance of the hydrogel system for cell release and recovery efficiency, a model system was employed; briefly, PC3s were spiked into whole blood (106 cells/mL, notably higher than the CTC load found in patient samples) and captured in a microfluidic in which the bottom of the channel was coated with an anti-EpCAM functionalized hydrogel. After PC3s were captured (2 uL / min) and blood was rinsed out with PBS (20 uL / min), the channel was imaged

and the total number of cells bound on the gel was counted. Alginate lyase (Sigma A1603, EC# 4.2.2.3, which targets the β-(1-4)-D-mannuronic bonds on the alginante backbone, 1 mg / mL in PBS) was then flowed through the channel (0.5 uL / min), releasing the cells which were recovered in an 8-well chamber slide and counted again. The ratio of cells recovered to cells captured was used to determine the recovery efficiency. The capture areas were re-imaged to confirm recovery efficiency by verifying the mass balance.

Cell release was observed under a fluorescent microscope (Nikon TiE, Japan) by first pre-labeling the cells with a dye (CellTracker Red, Life Technologies). Time-lapse images were taken every 200ms and then analyzed using the tracking module within the manufacturer's software (Nikon Elements) to chart cell movement as a function of time during the release process.

3.4.6 Analysis of released cells

Recovered cell viability was measured using a standard live/dead fluorescent assay (Life Technologies L3224) and compared to control cells which were never introduced into the microfluidic system. Colony formation was measured by recovering PC3 cells from a spiked sample and then diluting the cells with culture medium to form a single cell culture environment. After 96 hours, the number of colonies formed in the well were evaluated alongside the number of colonies formed from a similar number of control cells. HER2 amplified SKBR3 breast cancer cell line cells were captured and released in a similar fashion, cytospun, and then immunostained for the HER2 protein using a primary (Dako rabbit α-Erb2 A0485) secondary (Alexa Fluor 488 donkey α-rabbit, Life Technologies) antibody staining approach. Released SKBR3 cells were also probed with HER2 and centromere FISH probes using standard methods. In brief, released cells were cytospun and fixed with methanol-acetic acid (3:1), washed with 2X

SSC, dehydrated in an ascending series of ethanol, and a HER2/CEP-17 probe mix was added. DNA was then denatured at 75oC, hybridized at 37oC for 20 hours, and post-hybridization washes were performed in 0.4X SSC / 0.3% NP-40 at 72°C for 2 min and 2X SSC / 0.1% NP-40 at room temp for 30 seconds. The samples were counterstained with mounting medium containing DAPI and imaged at 60X.

3.5 Results and discussion

3.5.1 Biomaterial development and characterization

Carboxyl groups on pharmaceutical grade alginate were modified using standard carbodiimide chemistry to present both methacryl groups (65% theoretical derivitization) and biotin moieties. (0-12% theoretical derivitization). The methacryl groups covalently crosslink the alginate to form a stable hydrogel, and the biotin imparts the bulk material with a ligand for further biofunctionalization. (Figure 10) Methacryl conjugation was confirmed by conducting proton NMR using a similar analysis to that performed by Jeon.(*44*) (Figure 11)

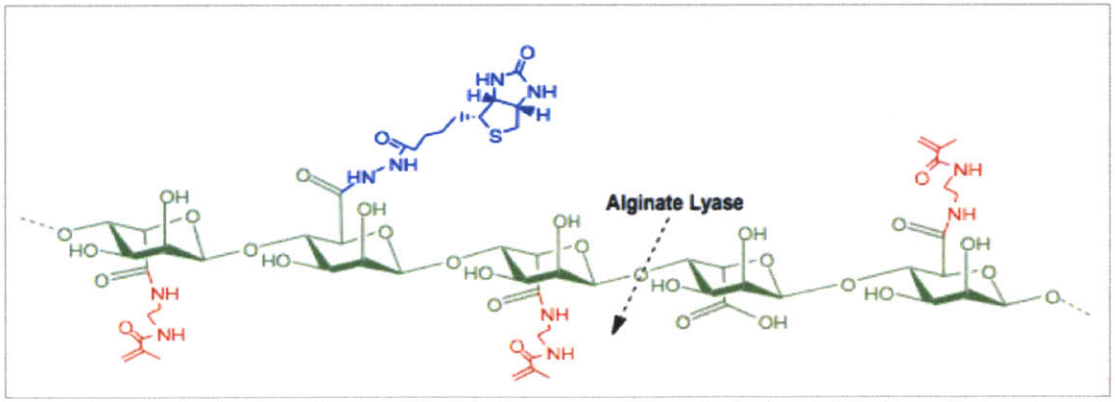

Figure 10. Here, we developed an alginate (green) biopolymer system which may be covalently crosslinked using methacryl groups (red) and biofunctionalized using biotin moeities incorporated in the base material (blue). The gel dissolution and subsequent cell release may be achieved by brief exposure to the bacterial enzyme alginate lyase which cleaves the backbone of the biopolymer.

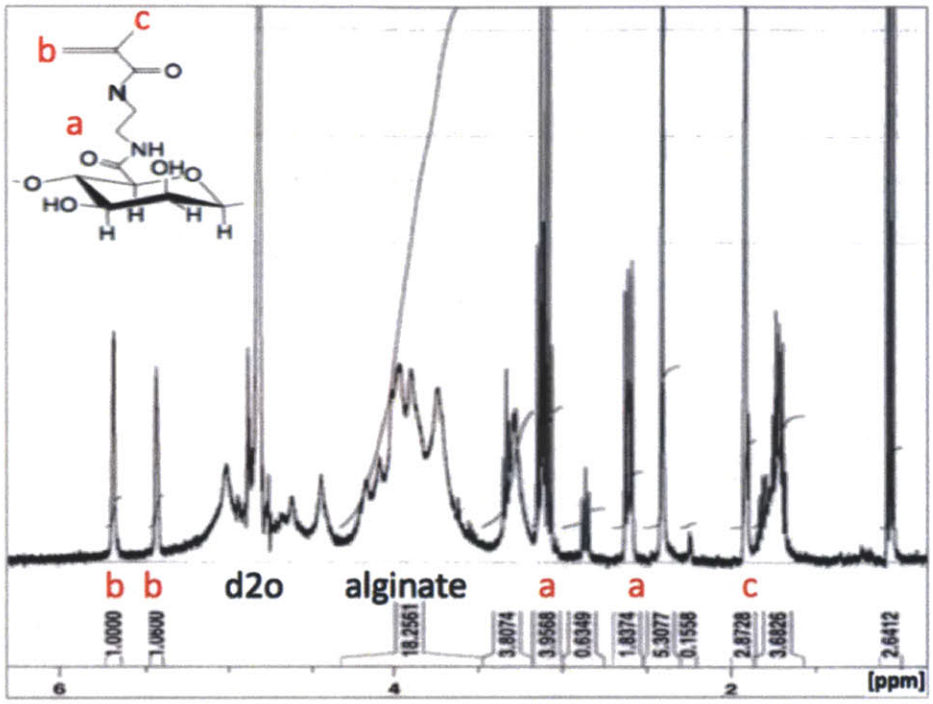

Figure 11. Proton NMR validation of alginate acrylation. The vinyl protons marked 'b' indicate the acrylation of the alginate polymer backbone.

Biotinylation was measured using a modified HABA assay. Alginate was degraded using alginate lyase (1 mg/ mL) for one hour before proceeding. This degradation enabled standardization and reproducibility of the assay; samples assayed without degradation formed visible aggregates in the wells. Figure 12 shows the correlation between theoretical modification (as a % of carboxyl groups on the alginate backbone potentially derivitized if the reaction went to completion) and resulting biotinylation as measured using the HABA assay. At 10% theoretical modification, the measured modification is 5.24%, representing a 52.4% reaction efficiency.

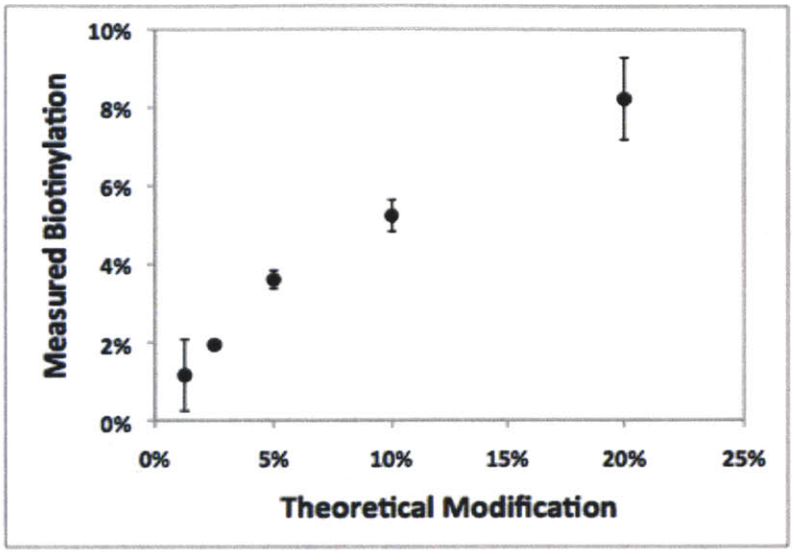

Figure 12. HABA analysis of biotinylation as a function of theoretical modification.

To characterize the swelling properties of the derivitized bipolymer, macroscale hydrogels were formed by photocrosslinking 200uL of 2% alginate solutions with a range of methacryl substitution (25-75%). As demonstrated in Figure 13, solutions with 25-35% theoretical derivitization did not fully photocrosslink and did not form stable gels. The equilibrium swelling ratio was measured for gels formed with alginates with 45-75% acryl substitution by measuring the weight of the gel after crosslinking, and after immersion in PBS for 24 hours, similar to approaches used by others.(*45*) As expected, gels with lower crosslinking had higher swelling ratios.(*46*)

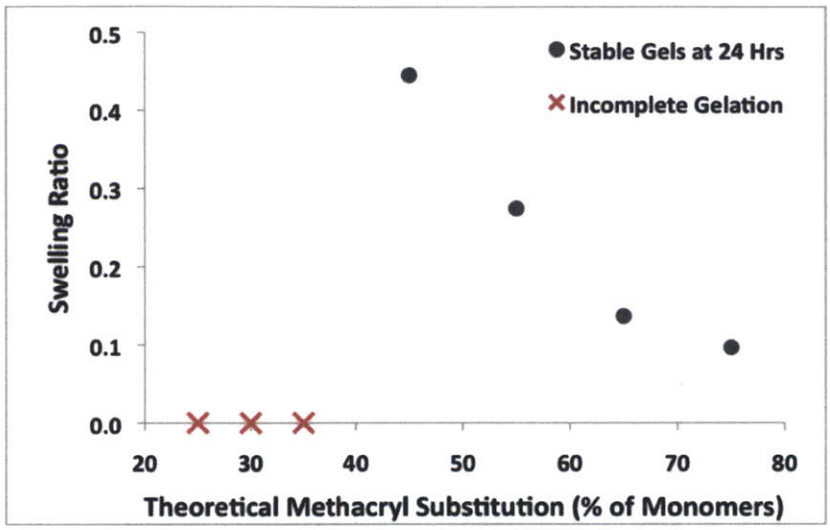

Figure 13. Swelling ratio of alginate gels formed with various degrees of methacrylation.

3.5.2 Hydrogel integration for microfluidic cell capture

As the microfluidic geometry of the channel is critical to maintaining the appropriate shear stress for cell capture, the thickness and roughness of the alginate layer was carefully controlled using spin-coating techniques to produce films in the sub-micron regime that would not affect overall channel fluidics. (Figure 14) The films were photocrosslinked to form a hydrogel which was stable in the presence of calcium-chelating anticoagulants (i.e., EDTA) but could be rapidly degraded with the addition of alginate lyase (Figure 15).

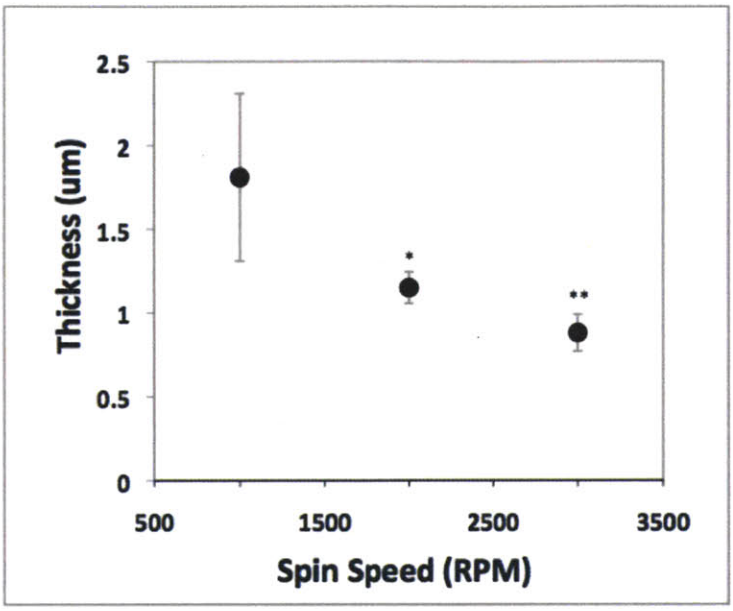

Figure 14. Alginate hydrogels were formed with micron-scale thickness using a spincoating process (* $p = 0.017$; ** $p < 0.001$).

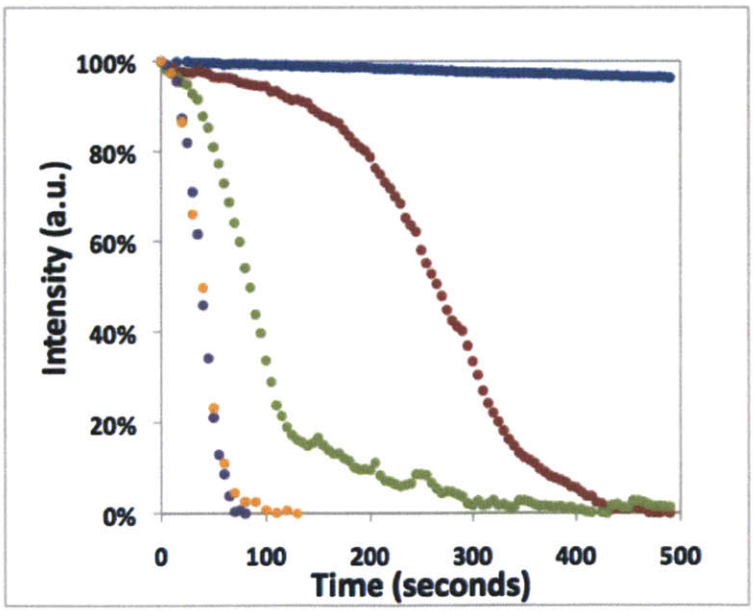

Figure 15. Upon treatment with alginate lyase at various concentrations (50 (red), 100 (green), 250 (purple), 1000 (orange) ug/ mL, control PBS (blue)), photocrosslinked hydrogels rapidly degraded in a dose-dependent fashion.

To ensure optimal ligand accessibility, a nanopatterning approach was employed similar to that developed by Comisar et. al.(*47, 48*) Here, highly biotinylated alginates (86 biotins per chain) were mixed in solution with non-biotinylated ('blank') alginates. These biotinylated alginate chains coil in solution to form nano-islands of functionality spaced apart by blank alginates.(*47*) Optimal island density was studied by varying the ratio of biotinylated chains to blank chains in the copolymer preparation; neutravidin was used to crosslink the gel bound biotins with a biotinylated capture ligand, thereby presenting the capture ligand on the surface. (Figure 16)

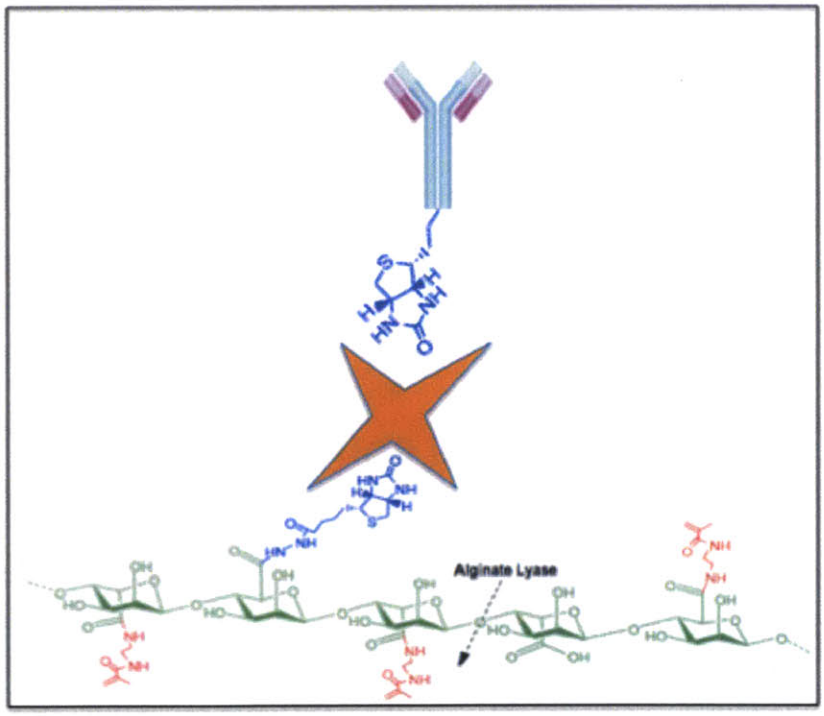

Figure 16. Schematic of 'sandwich' modification approach using neutravidin (orange) to crosslink a biotinylated antibody to the biotinylated alginate backbone.

This approach demonstrated an inverse trend in which lower bulk average biotin density in the gel correlated with higher ligand presentation. (Figure 17) Ligand presentation equivalent to that achieved with the silane-based chemistry commonly employed within microfluidic devices (*16,*

23) ("standard chemistry") was realized with 5 to 10 bulk average biotins. (Figure 17) Static cell capture experiments validated the ligand presentation results; gels functionalized with an anti-EpCAM antibody captured EpCAM expressing prostate cancer cells at a comparable efficiency to that of the standard chemistry. (Figure 18)

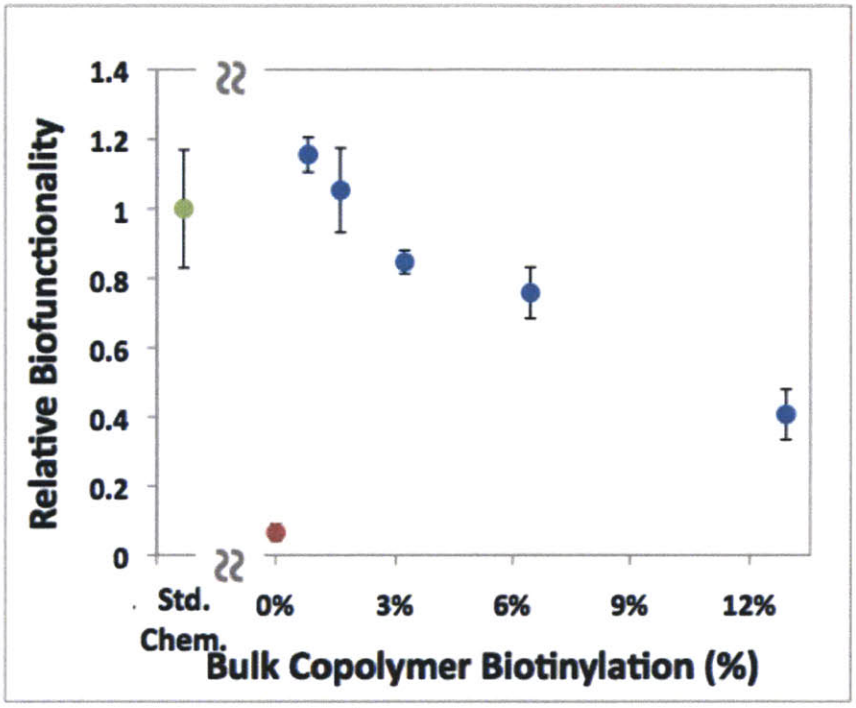

Figure 17. Gels were functionalized using gel-bound biotins, and an inverse trend between bulk biotin density and functionality was observed.

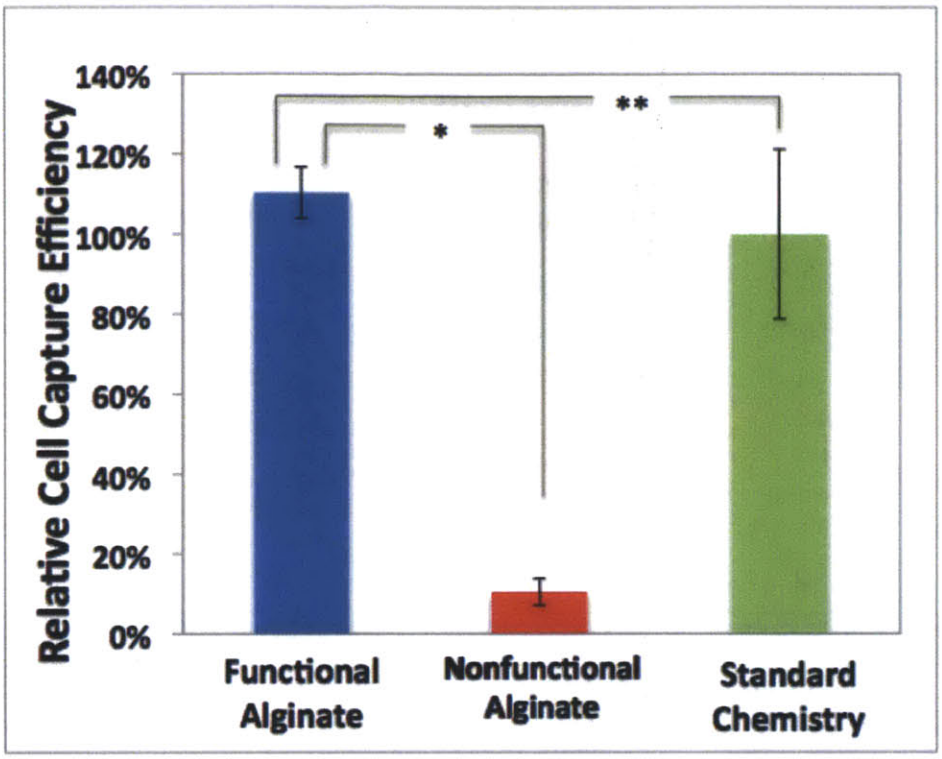

Figure 18. A static cell capture assay (D) demonstrated that the functional material (blue) captured cells with an efficiency comparable (* indicates $p = 0.45$) to standard surface modification approaches (green), while non-functional gels (red) resisted physisorbtion of capture molecules and non-specific cell binding (** indicates $p < 0.001$).

3.5.3 Release and characterization of isolated cells

To convey the gentle nature of the cell release process, a typical captured cell was imaged during the release process and the position of the cell was tracked over time. (Figure 19) This data demonstrates how, as the gel is degraded, a captured cell (A) first gradually detaches from the substrate, (B) then moves slowly along the surface (C) before being caught up in the flow stream which moves it downstream at the bulk fluid velocity. The efficiency of this cell release process was evaluated by directly quantifying cell capture, release, and recovery. This study demonstrated a 99% ± 1% release efficiency.

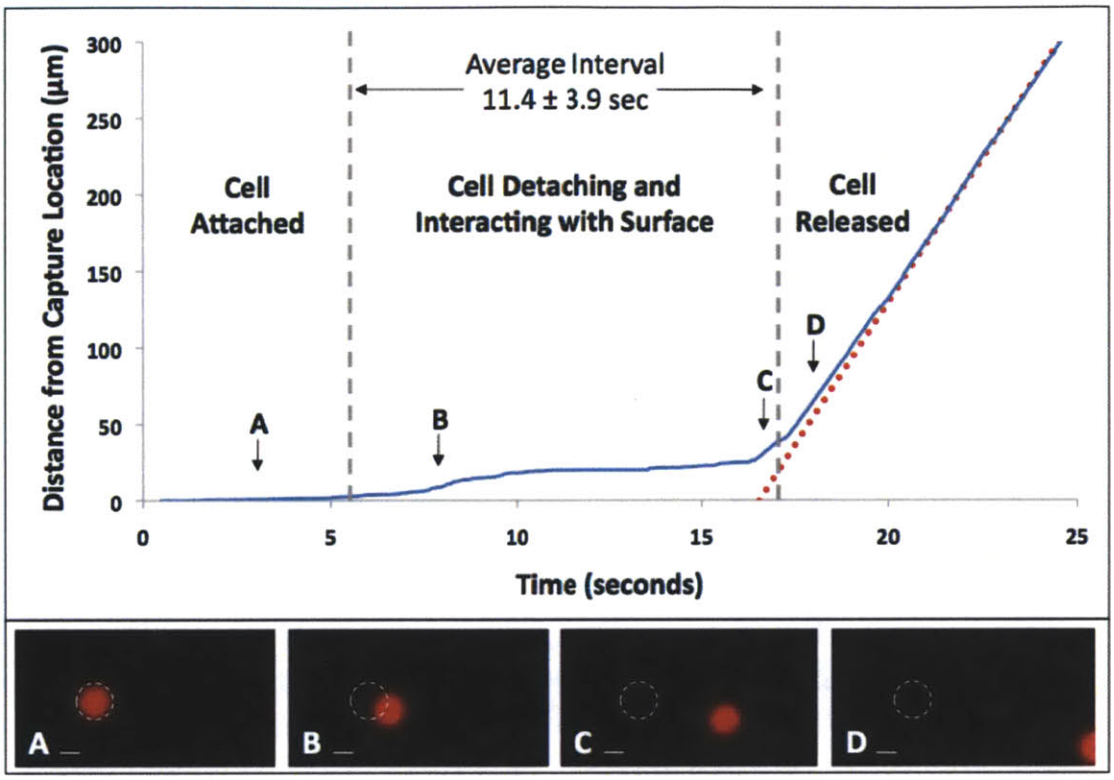

Figure 19. Cells from a prostate cancer cell line were spiked into whole blood, captured on an anti-EpCAM functionalized alginate gel, and released by dissolving the gel with alginate lyase. The progression of a typical cell during the release process (blue) was tracked using automated image processing software. Images A-D show the cell at various stages of the release process and mark the initial location of the cell with a white dashed circle. This series demonstrates the gentle nature of the release process as the cell starts (A) attached, then (B) slowly detaches and (C) travels along the surface until (D) it enters the free flow stream, now traveling at the average bulk velocity of the fluid in the channel (red dotted line). Scale bars are 10 microns. Cells (n=15) from 3 different gels were tracked during release to determine the average interval between initial movement to final release.

Released cells were characterized for their viability (98.9% ± 0.3%) compared to control cells simply spiked into whole blood (99.4% ± 0.6%) and found to be unaffected. (Figure 20A,E) Similarly, effects of the capture and release process on cell proliferation was studied by diluting released cells in culture medium and measuring the extent of single cell colony formation after

96 hours (69.3% ± 3.4%) as compared to similar control cells (68.8% ± 2.2%). (Figure 20B,E) As an initial demonstration of the compatibility of the release technology with downstream biological assays, breast cancer cells harboring amplified HER2 genes were spiked into blood, captured, released, and evaluated using standard immunostaining and fluorescence in situ hybridization (FISH) techniques. Expression of the HER2 surface receptor was found to be comparable to control cells (113% ± 21.2% relative intensity). (Figure 20C,E) Furthermore, HER2 gene amplification is readily evident by FISH, illustrating the potential broad applicability of this cell release technology to enable standard molecular diagnostic applications in a variety of clinical specimens. (Figure 20D)

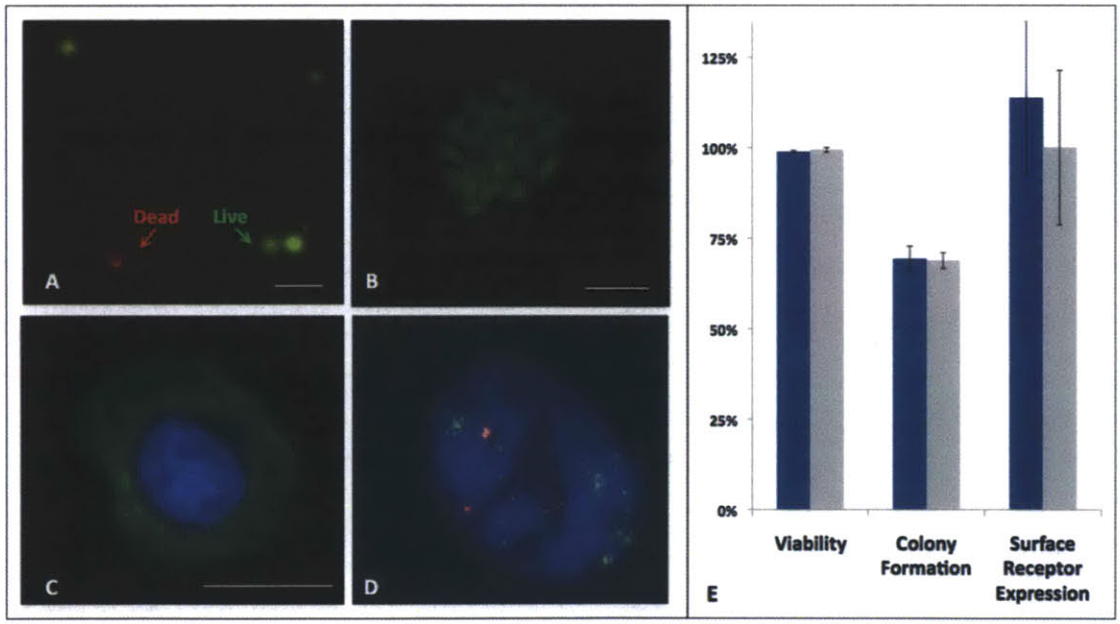

Figure 20. Released cells were evaluated for (A) viability and (B) colony formation; scale bars are 50 um. Released cells were compatible with downstream (C) immunostaining of cell surface receptors (HER2 expression in a released cell shown in green, counterstained with DAPI nuclear staining in blue; 20 um scale bar). (D) FISH analysis in a released HER2 (green probe) amplified breast cancer cell is shown (control probe in red). (E) Released cells (blue bars) were found to have comparable viability, rates of colony formation from single cells, and relative surface receptor expression when compared to control cells (gray bars) ($p > 0.05$).

3.6 Conclusions

The alginate biopolymer system presented here represents an important step forward in developing affinity-based cell capture surfaces as it enables gentle, efficient recovery of isolated cells without compromising their viability or proliferative potential. The critical followup of this work is the development of precisely controlled coating techniques for the integration of this materials approach with the complex microfluidic architectures used for rare cell isolation.(*16, 17, 19, 29*) While existing technologies have demonstrated their clinical relevance, recovering these cells with high efficiency and in an unadulterated fashion will place them in the hands of molecular and cell biologists in a manner that is readily compatible with their arsenal of sophisticated tools, so that we may begin to further elucidate the roles of these cells in human biology.(*1, 4, 49*)

Chapter 4: Whole Blood Magnetophoresis for Circulating Tumor Cell (CTC) Isolation

4.1 Introduction

Over the past 30 years, numerous technologies have been developed to address the CTC enrichment challenge, including bulk immunomagnetic approaches, density-gradient isolation, and size-based separation methods. (*8, 13, 14, 50, 51*) Although these technologies have established the potential prognostic utility of CTCs, albeit with poor sensitivity, the bulk handling and manipulation techniques (including RBC lysis) required pose an inherent danger of losing rare and fragile tumor cells. (*1, 52*) Furthermore, mixed reports on the physical size and morphology of CTCs reduces confidence in size-based filtration methods for enrichment. (*8, 17, 53*) More recently, microfluidic surface-based techniques have grown in prominence as they facilitate lossless cell handling; these approaches have enabled CTC isolation from whole blood without any pre-processing, resulting in increased efficiencies. (*16, 17, 25*) Isolated cells, however, often remain bound to the substrate and are not directly compatible with downstream analyses. While this limitation may be potentially addressed using the technological approach presented in the previous chapter, microfluidic surface capture techniques are fundamentally limited to positive enrichment modalities, as the area required to capture all contaminating RBCs and WBCs makes operating in a 'negative-depletion' mode impractical. Non-enrichment based strategies have the potential to identify interesting rare cell populations, however the lack of purification severely limits molecular analyses. (*7*)

Advancement in our understanding of CTCs has been limited, chiefly due to the lack of a robust, highly sensitive, universal CTC enrichment technology that is compatible with the needs of cell biologists, molecular geneticists, and classical pathologists. This requires a high-throughput (> mLs / hour) system with a high degree of sensitivity (efficiency) and specificity (purity) as CTCs represent only 1 in 10^8 cells in whole blood. The central biological hurdle facing development is that the limited understanding of this heterogeneous cell population results in a poorly defined "target" to isolate – creating the need for a universal system that can be rapidly tuned to sort various cell populations; such a system could sort cells in a "positive enrichment" fashion to answer defined questions about particular populations, while also enabling a "negative depletion" mode in which hematogenous cells are depleted, exposing the underlying rare cell biology. Finally, enriched CTCs must be presented in a manner that is conducive to application in defined *in vitro* and *in vivo* culture models, the analytical techniques employed in modern molecular biology, as well as conventional cytopathology.

4.2 Approach

Here we present Magnetophoretic Inertial Microfluidcs for Integrated Cell Sorting (MIMICS) - a cell sorting system that interrogates over 10 million individual events each second, resulting in a high throughput, ultra-efficient rare cell sorter that delivers enriched cells in a vial, readily compatible with any downstream assay. This is the first system combining the high sensitivity and single cell resolution that is characteristic of FACS with the practicality of MACS at a throughput and specificity afforded by inertial focusing, enabling operation in both 'positive selection' and 'negative depletion' modes. Whole blood is loaded into the three-component integrated system which enables (1) lossless sample debulking, (2) specific cell positioning and (3) highly sensitive magnetophoretic separation of target cells. (Figure 21) Whole blood is mixed

with immunomagnetic beads and first processed through a post array which deflects nucleated cells into a buffer stream; the cells are then precisely aligned and ordered in the center of a second microchannel using inertial focusing techniques, and the magnetically tagged cells are displaced to the channel wall using an external magnetic field.

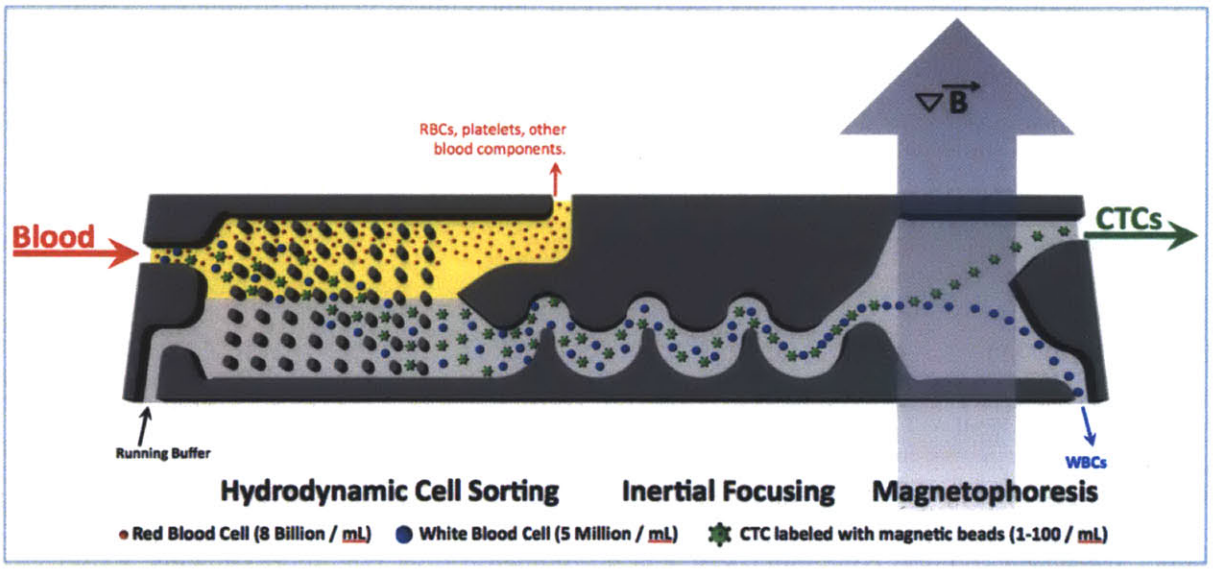

Figure 21. The overall process flow for the integrated cell enrichment system is described. (left) Immunomagnetic beads are mixed with whole blood to tag cells intended for deflection. The HCS array isolates nucleated cells from smaller blood components such as RBCs, platelets, and free magnetic beads. These nucleated cells enter the inertial focusing and magnetophoresis channels where they are focused to a central stream and then magnetically labeled cells are separated. The two system inputs are whole blood and a running buffer; system outputs include the waste of HCS array, non-deflected cells, and deflected cells. The system runs in an integrated modality wherein the HCS product is connected directly to the focusing channels. This continuous cell separation mode improves both the throughput and system reliability while minimizing parasitic cell losses.

Using EpCAM-based positive selection, low expressing cells were enriched with exceedingly high efficiency (> 90%) and purity (~ 5 log removal of contaminating cells); lossless enrichment

of ultra low EpCAM expressing cell lines from whole blood was achieved through negative depletion of WBCs. High-speed microfluidics allow bulk-scale throughput (~8ml whole blood / hour), while precise localization of cells to a center streamline enables single cell resolution sorting, resulting in exquisite sensitivity and specificity. Continuous, sheath-less operation enables large volumes (>15ml) to be processed without hindering system performance. Using this system, we demonstrate that CTCs may be isolated from patient blood samples and analyzed using both advanced molecular approaches and traditional cytopathological techniques.

4.3 Methods

4.3.1 System design

The overall system is driven by a pressure source which pushes the running buffer and whole blood into the HCS array. (Figure 22) The waste outlet is connected to a syringe pump which withdraws the waste solution containing RBCs at a volumetric flow rate approximately 3 fold greater than the HCS product flow rate. This ratio, as well as the driving pressure selected (18-21 PSI), is used to ensure the purity of the HCS array product and maintain the flow rate needed to achieve optimal function. The HCS array product, containing leukocytes and putative CTCs, is connected to the magnetophoresis channel, which deflects cells above the magnetic threshold to a single outlet. Undeflected cells are collected via another outlet.

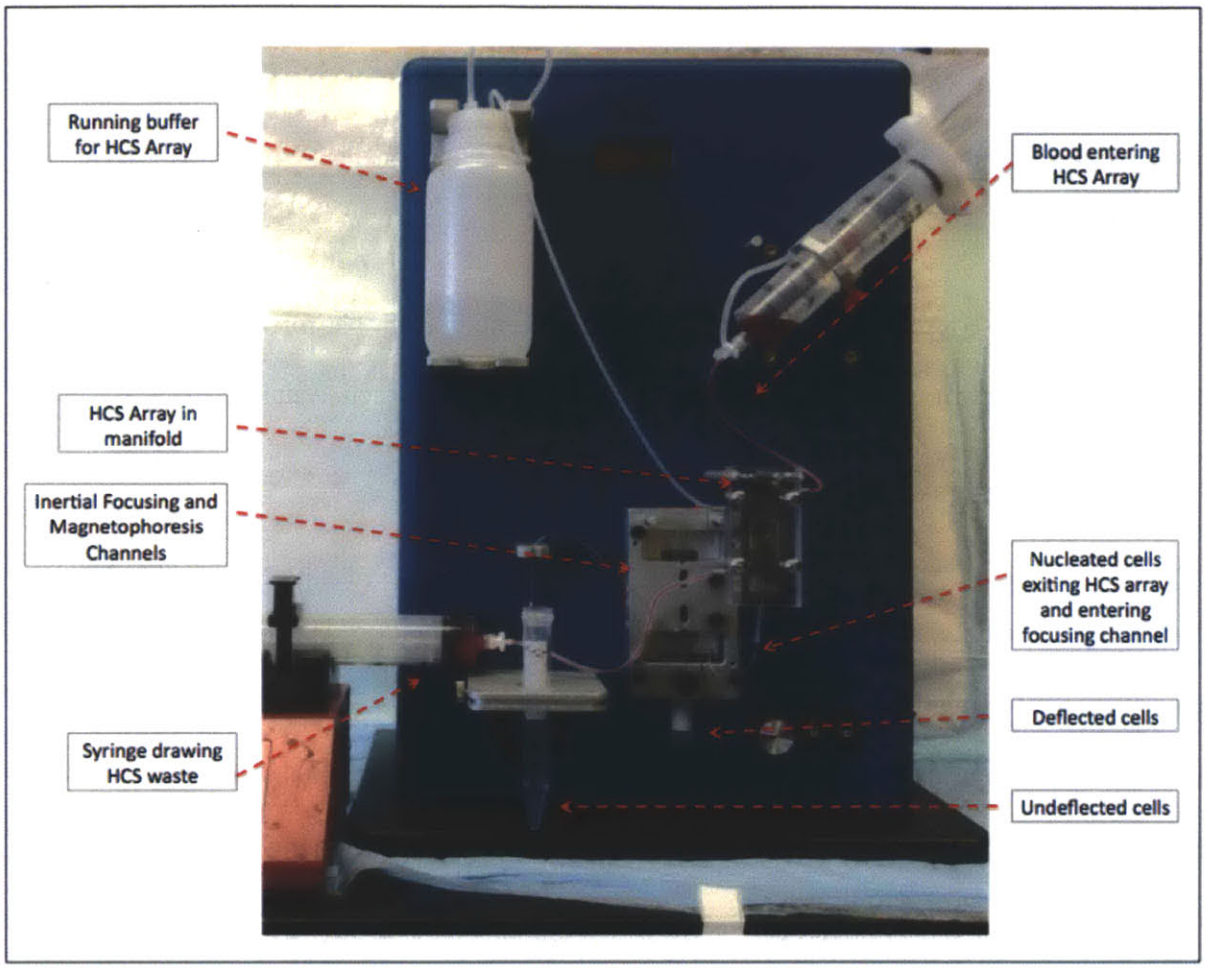

Figure 22. Overview of the entire MIMICS system and processor.

4.3.2 Cell culture

MDA-MB-231, SKBR3, and MCF10A cell lines were obtained from ATCC (Manassas, VA), PC3-9 cells were a gift from Veridex, LLC, and LBX1-expressing MCF10A cells were derived from a stable cell line previously developed and published by our laboratory.(*54*) All cells were cultured and propagated in accordance with providers recommendations and maintained in humid, 37°C, 5% CO_2 cell culture incubators. As noted for specific experiments, cells were prelabeled with a fluorescent tracer dye (CellTracker Red or CellTracker Green, Life Technologies, USA) following the manufacturer's recommended protocol.

4.3.3 Whole blood

Fresh whole blood was collected from healthy volunteers under an approved Institutional Revew Board protocol or commercially sourced from Research Blood Components (Watertown, MA).

4.3.4 Microscopy

All fluorescent microscopy was conducted using either inverted or upright microscopes (TiE or Eclipse 90i, Nikon, Japan) with the appropriate filter cubes for the respective stains.

4.3.5 HCS array design and fabrication

The hydrodynamic cell sorting (HCS) array is designed to efficiently separate nucleated cells from other blood contents, in a high-throughput and continuous operation. The array relies on the deterministic lateral displacement principles previously described.(*55-57*) Each of the 20 parallel channels has two input streams that run side-by-side in laminar flow, one consisting of the running buffer (1% F68 Pluronic in PBS, Sigma P1300), and consisting of the whole blood to be separated. The blood is introduced into an array of microposts (active area: 500 um wide by 22 mm long by 150 um high per channel; single post diameter of 150 um; 24 channels per chip) and enters at a small angle (~1°) relative to the array, such that the leukocytes, which are large with respect to the flow streamlines, are displaced out of the streamline when they encounter a post. By contrast, the enucleated components of the blood (RBCs, platelets, plasma) follow the streamlines predicted by laminar flow theory, unperturbed by the array. By the end of the array, nucleated cells have been sufficiently deflected into the buffer stream, separating them from the rest of the blood. Two different array configurations were designed at MGH and fabricated by Silex (Norway) using deep reactive ion etching (DRIE), HCS_{leuko} and HCS_{cancer}. The gaps between posts (g) are 20 and 32 um respectively, the center to center distances between the posts (λ) are 35 and 56 um respectively, and the row shift fraction (ε) is 0.16 for both designs. (Figure

23) The chip is sealed with an anodically bonded glass cover and mounted in a custom polycarbonate manifold to connect the macroscale tubing to the microscale channels.

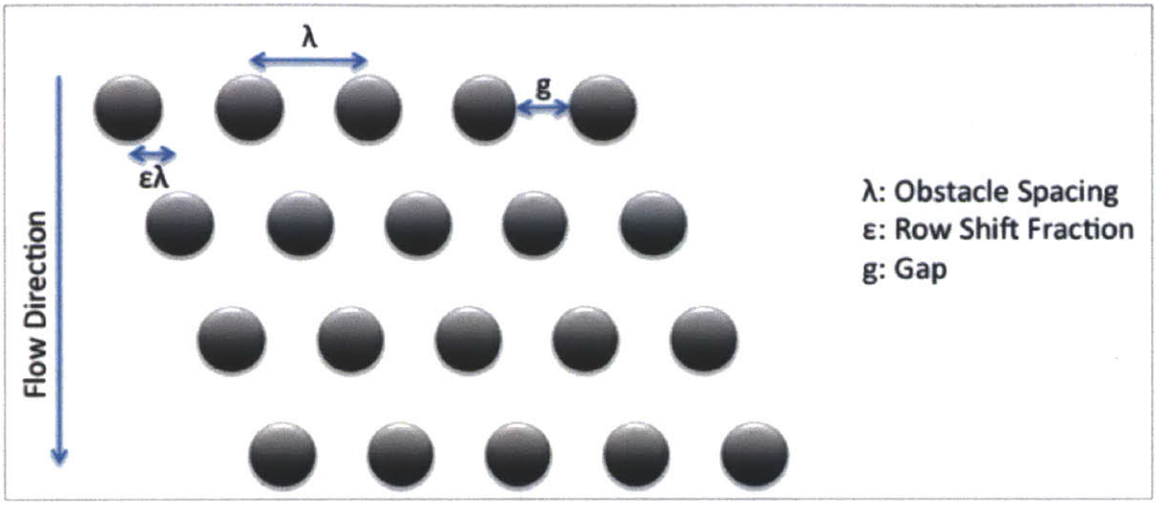

Figure 23. Schematic of an HCS array depicting key parameters

4.3.6 Magnetophoresis chip design and fabrication

The chip relies on inertial focusing of cells in a microfluidic channel, followed by magnetic deflection of magnetically labeled cells from the focus stream to a stream at the edge of the channel. The chip was designed and fabricated at MGH using standard soft lithography techniques. (*43*) The channels are 50 um high and consist of 3 distinct regions: an inlet region with filters, a focusing region and a deflection region. The inlet filters are needed to prevent downstream clogging of the focusing channels and have a gap size of 30 um. The focusing region consists of 60 asymmetric serpentine curves with a width of 50 um and a connecting curve with maximum width of 95 um. (Figure 24, left) In the deflection region, the channel expands to a 500 um width, to reduce the flow speed of cells in the channel, therefore increasing the residence time of cells in the magnetic field. The chip splits into either 2 outlets (positive selection) or 3 outlets (negative depletion) that separates the deflected and undeflected cells.

(Figure 24, center and right) The chip is placed within a custom stainless steel manifold that holds 4 magnets in a quadrapole configuration to create a magnetic circuit enabling cell deflection. (Figure 25)

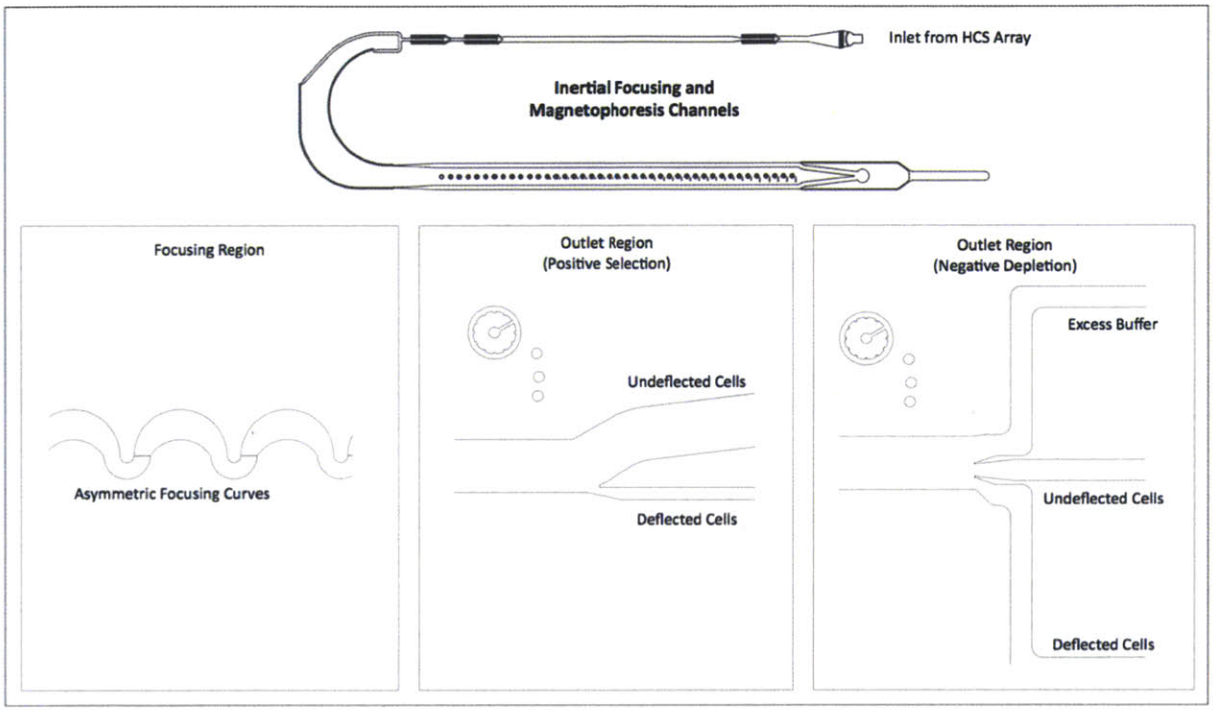

Figure 24. Schematic of the inertial focusing and magetophoresis channels, depicting (top) overview, (left) focusing region, (center) outlet configuration for postive selection, and (right) outlet configuration for negative depletion.

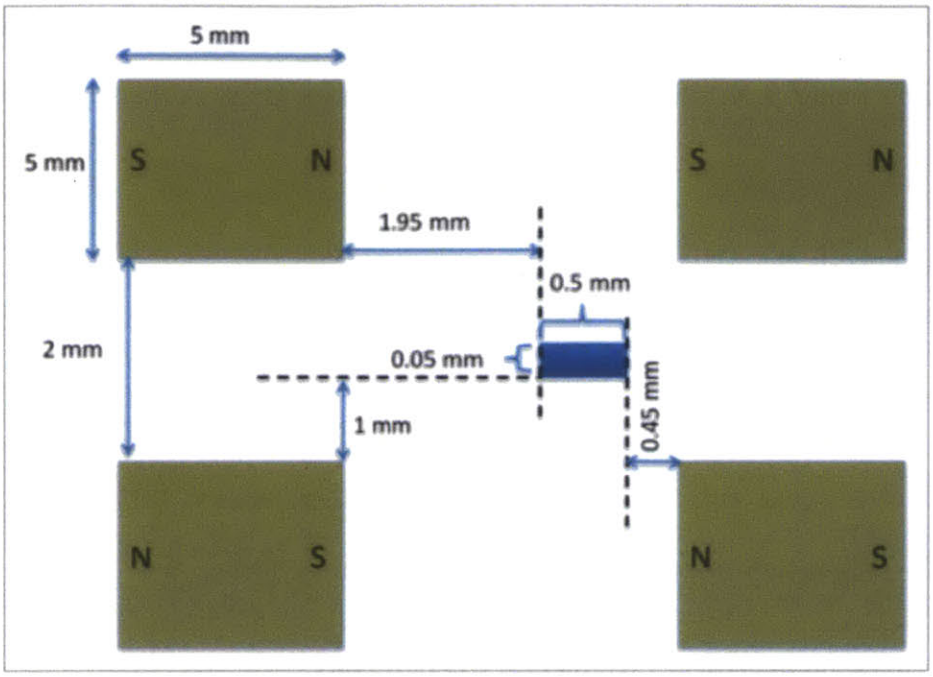

Figure 25. Schematic indicating the position of the 4 permanent magnets placed in a manifold to create a quadrapole magnetic circuit, relative to the magnetophoresis channel.

4.3.7 HCS array characterization

To demonstrate the size-based separation principle, 2μm (red) and 10μm (green) polystyrene microspheres were combined into a single solution and flowed through the 'blood' inlet of an HCS chip. The chip was imaged in four distinct locations from the inlet to the exit of the chip. To characterize the performance of the two HCS arary designs, whole blood samples (n > 10) were processed through each chip, and the starting blood as well as outlet product and waste solutions were analyzed to quantify nucleated cell retention, RBC removal and platelet removal. Analysis was conducted using a Sysmex KX blood analyzer, or for dilute solutions, by staining nucleated cells with Hoescht dye and determining their concentration using a Nageotte chamber. Dilute RBC concentrations were determined by counting all events in brightfield and subtracting the number of nucleated events detected using the Hoescht stain. Additionally, product and waste

collected from whole blood processed through an HCS_{cancer} array was analyzed using a coulter counter (Beckman Coulter X-X, USA) to illustrate the size-based nature of the separation from whole blood.

4.3.8 Magnetophoresis characterization

4.3.8.1 Characterization with magnetically tagged and untagged Cells

To demonstrate magnetic cell sorting, red fluorescent SKBR3 cells labeled with EpCAM coated magnetic beads were mixed with non-labeled green fluorescent stained PC3-9 cells. This mixture was flowed through the IFM chip and imaged at various locations.

4.3.8.2 Evaluation of critical variables on streak quality

To characterize the effects of critical variables on cell focusing, solutions with various concentrations of WBCs and RBCs were prepared by processing whole blood through an HCS chip and labeling the WBCs with calcein AM (1 uM, Life Technologies, USA). Samples were then diluted to achieve the desired concentration and RBCs were added as needed to achieve the desired hematocrit. They were then processed through the IFM chip and imaged at 10x using long exposure times (~ 5 seconds) to collect a fluorescent streak image that represents the position of >1000 individual events at the end of the deflection region. A line-cut across the image is taken and signal intensity across the channel was measured. (Figure 26) Commercially available curve fitting tools were used to determine the full-width-half-maximum (FWHM) of the streak image, and streak quality was defined as (Channel Width / FWHM); the tighter the focus stream, the smaller the FWHM, the greater the streak quality.

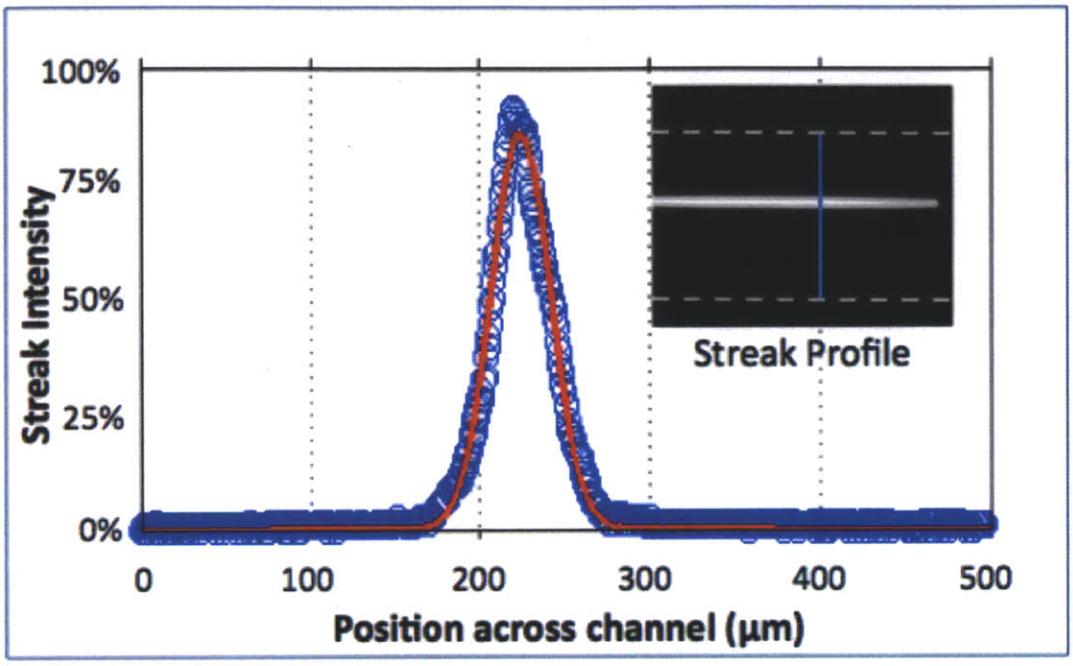

Figure 26. Performance of the inertial focusing components was assessed by analyzing a (inset) long exposure fluorescence image. A linecut was taken across the image, and the (panel) signal intensity was plotted and fit to a Gaussian distribution.

4.3.9 Quantitative modeling of cell deflection

Finite element modeling (FEM) was conducted using commercially available software (COMSOL) to calculate the magnetic gradient created in the deflection channel by the quadrapole magnetic circuit depicted in Figure 25. Second order effects due to position in the z-dimension or edge effects at the beginning or end of the deflection region (y-dimension) were not considered. The fluid velocity profile in the deflection region was also determined using FEM based on 2D modeling, given the bulk-average flow rate and channel dimensions.

The results of the FEM modeling of the magnetic gradient and fluid velocity profile, the empirical measurement of cell position based on streak imaging, estimates of CTC size, and the properties of Dynal MyOne beads as reported in the literature were integrated to develop a

quantitative model of cell deflection. (*58*) Briefly, cells were considered to be in the center of the focused stream upon entering the deflection region, and their position was iteratively calculated based on the assumed bead loading, resulting deflection in the x-direction and travel down the channel in the y-direction (due to fluid velocity). This model was then used to determine the minimum magnetic load needed to deflect a cell into the 50um region by the channel wall, as a function of the bulk flow rate; an expected range was calculated based on the distribution in cell size as well as initial focus position.

The model's outcome was experimentally validated by preparing samples spiked with PC3-9 cells with a spectrum of bead labeling; these samples were then processed through the chip at various flow rates and bead loading on PC3-9 cells recovered in the deflected and undeflected solutions was quantified. Curve fits were applied to these distributions, and the intersection of the deflected and undeflected distributions was taken to represent the 'minimum magnetic load needed for deflection'.

4.3.10 Labeling target cells in whole blood

Target cells were labeled in whole blood using Dynal MyOne streptavidin magnetic beads (656-01, Life Technologies, USA) coupled with biotinylated antibodies per the manufacturers recommendations.

Beads were added in whole blood and mixed using either passive or active approaches. In passive mixing, the samples underwent end-over-end rotation for 15 minutes (positive selection) or 60 minutes (negative depletion). For positive selection, active mixing was employed by bringing the sample tube in contact with a magnet for 30 seconds, removing the magnet, rotating

the tube 180° around its long axis, and bringing it back in contact with the magnet; this cycle was repeated continuously for 7 cycles. (Figure 27)

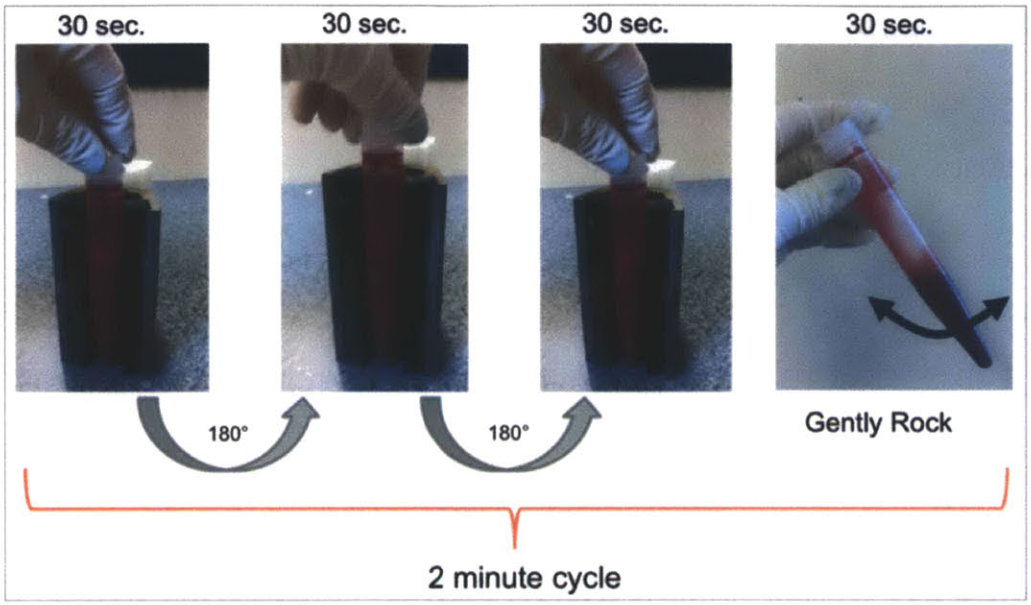

Figure 27. Depiction of the Active Magnetic Mixing (AMM) procedure

Labeling of target cells was determined as a function of beads added per WBC. For positive selection, pre-labeled cell lines with low and high EpCAM expression (MB-231 and SKBR3) were doped into whole blood, incubated with various amounts of anti-EpCAM (BAF960, R&D Systems, USA) coated beads, and samples were mixed using either active or passive mixing. Following mixing, samples were processed through an HCS chip to remove RBCs and collected in a 24 well plate; target cells were identified based on their fluorescence and bead loading was evaluated. For negative depletion, whole blood samples were incubated with various combinations of anti-CD45 and anti-CD15 (BAM1430, MAB7368 (biotinylated in house), R&D Systems, USA) coated beads and passively incubated for 60 minutes. Samples were then RBC lysed (BioLegend 420301, used per manufacturer's protocols) and stained with Hoescht dye to

accurately identify nucleated cells. Bead loading was evaluated on > 100 nucleated events in each sample.

4.3.11 Evaluation of integrated system

Five cell lines with a wide range of EpCAM expression were used to evaluate rare cell enrichment efficiency in the integrated system. EpCAM expression levels were measured using flow cytometry. Briefly, pure populations of each cell line were prepared in suspension, stained with either the biotinylated goat anti-EpCAM antibody used for cell isolation or a biotinylated irrelevant IgG (BAF108, R&D Systems, USA), rinsed, and labeled with a fluorescent avidin secondary stain. After labeling, the samples were rinsed, fixed, and evaluated using standard single-color flow cytometry. (MACSQuant, Miltenyi Biotec, USA) Analysis was conducting using commercial flow cytometry software (FlowJo, USA) and the median fluorescence value for each EpCAM-stained cell population was compared to the respective IgG control.

Performance of the integrated system was evaluated by pre-labeling the cell lines described with a fluorescent marker and spiking them into whole blood at low concentrations (~ 1000 / mL whole blood). The samples were then incubated with magnetic beads, processed through the integrated system, and rare cell yield was quantified using a mass balance approach. The depletion of nucleated cells was quantified by measuring the initial WBC concentration (Sysmex KX Analyzer, Sysmex, USA) and comparing to the final WBC concentration, measured by staining nucleated cells using Hoescht and counting in a nageotte chamber. For positive selection, anti-EpCAM beads were added at a concentration of 300 ug beads / mL whole blood (~ Y beads / WBC, assuming 5M WBC/mL), and incubated with whole blood using active magnetic mixing for 15 minutes. For negative depletion, anti-CD45 and anti-CD15 beads were

added at a 100:50 ratio per WBC, and incubated using end-over-end passive mixing for 60 minutes.

4.4 Results and discussion

4.4.1 Hydrodynamic cell sorting (HCS) array

Building on established design principles, we developed two HCS arrays: HCS_{leuko} deflects virtually all (99.7% ± 0.4%; D_c=2.6 um) nucleated cells into the product stream with minimal contaminating RBCs (< 0.1%), as well as HCS_{cancer} which has a larger hydrodynamic size cutoff (D_c=3.8um), deflecting ~60% of nucleated WBCs (Figure 28, Figure 29). (*55-57*)

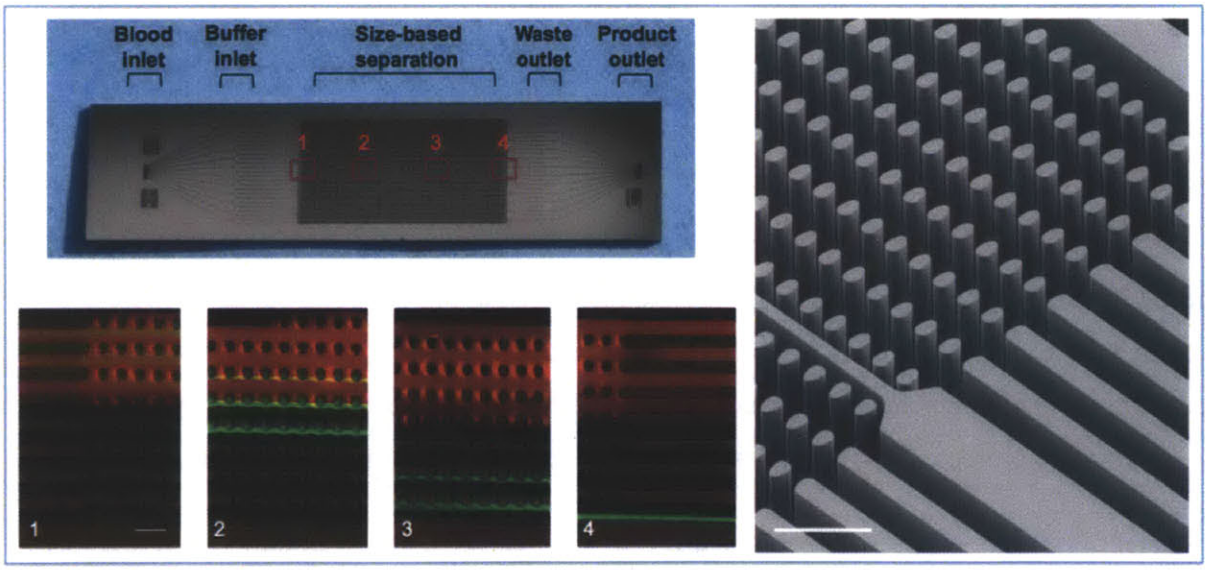

Figure 28. The hydrodynamic size based sorting that occurs in the HCS array is demonstrated here. A mixture of fluorescent 2 μm (red) and 10 μm (green) beads enter the channel (1) and while the 2 μm beads remain in laminar flow in the top channels, the 10 μm spheres interact with the post array (2-3) shown in the SEM and are fully deflected into the adjacent buffer stream by the end of the array (4)

HCS Array Type	HCS_{cancer}	HCS_{leuko}
Nucleated Cell Retention	59 ± 9.0 %	99.7 ± 0.4 %
RBC Removal	99.97 ± 0.03 %	99.94 ± 0.03 %
Platelet Removal	100 ± 0 %	100 ± 0 %

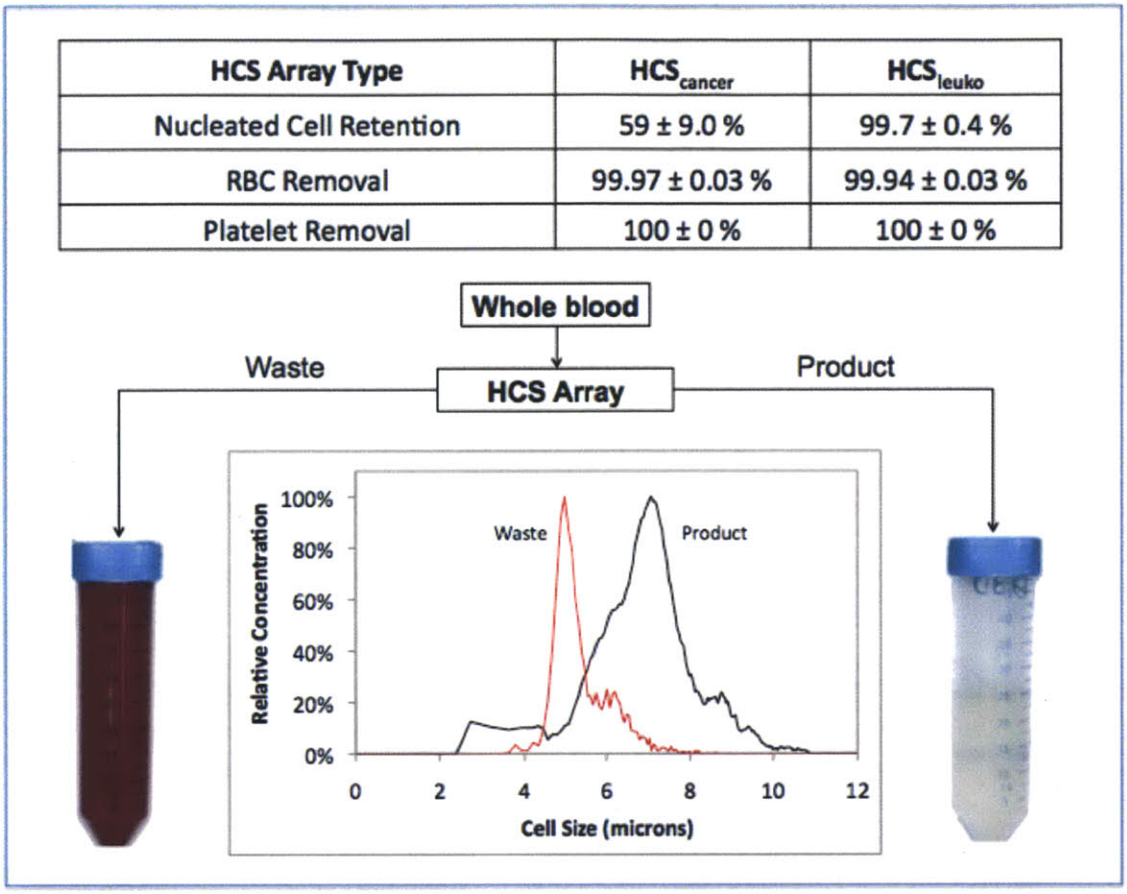

Figure 29. Both the HCS_{cancer} and HCS_{leuko} designs demonstrate the ability to separate nucleated cells from RBCs in whole blood. Although a crude approximation of hydrodynamic cell size, coulter counter measurements of product and waste from a sample processed through the HCS_{cancer} array are presented to demonstrate the size-based nature of the deterministic separation process.

Granulocytes, with their lobular flexible nuclei, have a notably smaller hydrodynamic radius than mononuclear WBCs; standard flow cytometry characterization confirms that the WBCs being removed by our HCS_{cancer} array are principally granulocytes and small lymphocytes. (*55*) (Figure 30) Importantly, the chip retains all nucleated cells above 8 um in size as well as 100% of each of the 5 different tumor cell lines we evaluated.

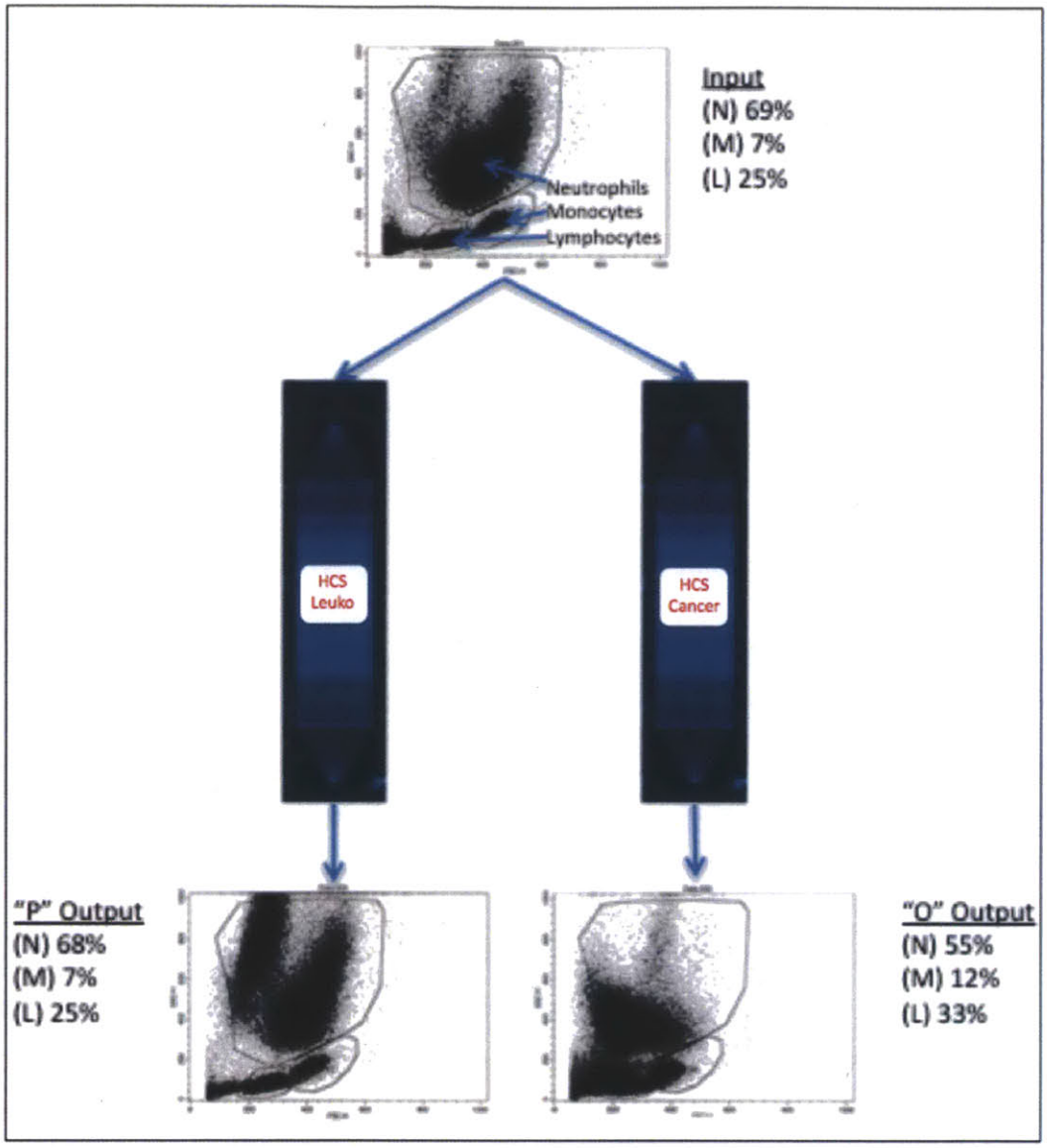

Figure 30. A whole blood sample (input) was processed in parallel through both versions of the HCS array, and the resulting products were collected. These samples were then compared to the input sample (after RBC lysis) using standard flow cytometry; gating based on accepted forward/side scatter characteristics was used to approximate the fraction of neutrophils, monocytes, and lymphocytes in each sample. As demonstrated, the HCS_{cancer} array retains fewer neutrophils and lymphocytes than the HCS_{leuko} array.

4.4.2 Inertial focusing to control cell position

The system relies on both the inertial ordering of cells within a microfluidic channel, as well as their magnetic loading to enable cell sorting via magnetophoretic deflection of tagged cells to the channel wall. (Figure 31)

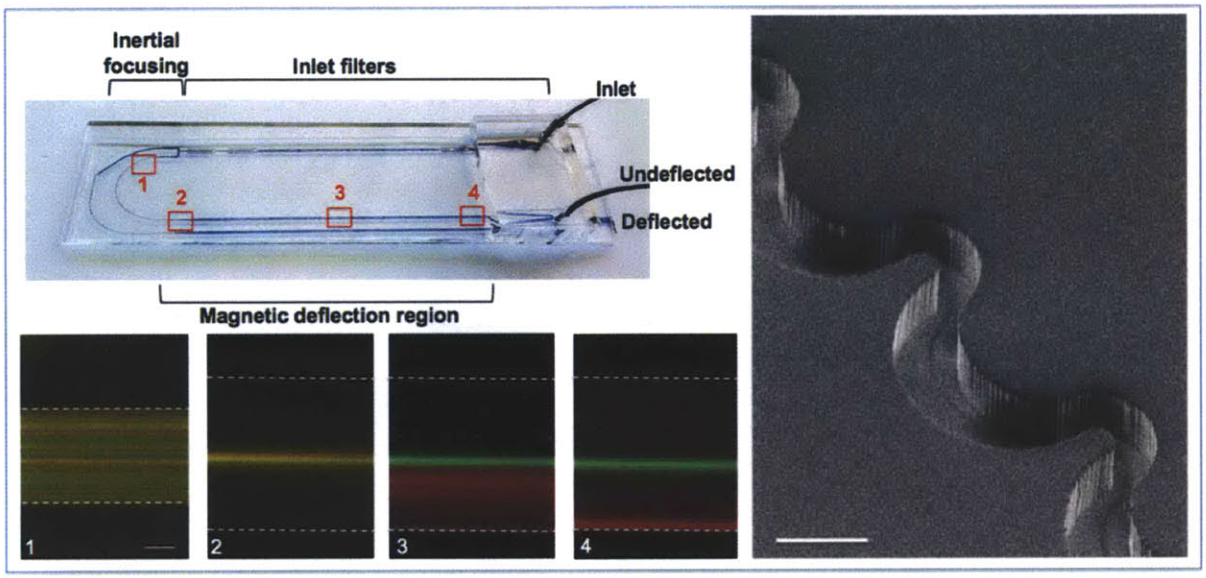

Figure 31. The cell focusing and magnetophoretic sorting features are demonstrated here. Magnetically labeled (red) and unlabeled (green) cell poulations were mixed and enter the channel at random (1). After passing through 60 asymmetric focusing units (pictured in the SEM), the cells are aligned in a single central stream (2). Magnetically tagged cells are then deflected (3) using an external magnetic field, and full separation is achieved by the end of the channel (4).

To control the position of cells in the X-Z plane, we rely on inertial focusing principles previously discovered in our laboratory. (*59*) Here, we characterized the operating regime to understand the effects of flow rate, cell concentration and background RBC concentration on nucleated cell focusing in the deflection region as inter-particle interactions increase when the fluid slows upon entering. As presented below, the optimal flow rate was determined to be 100

uL / minute. (Figure 32) Streak quality was determined to be acceptable for solutions with nucleated cell concentrations below 3M / mL and an effective hematocrit below 0.5%. (Figure 33, Figure 34)

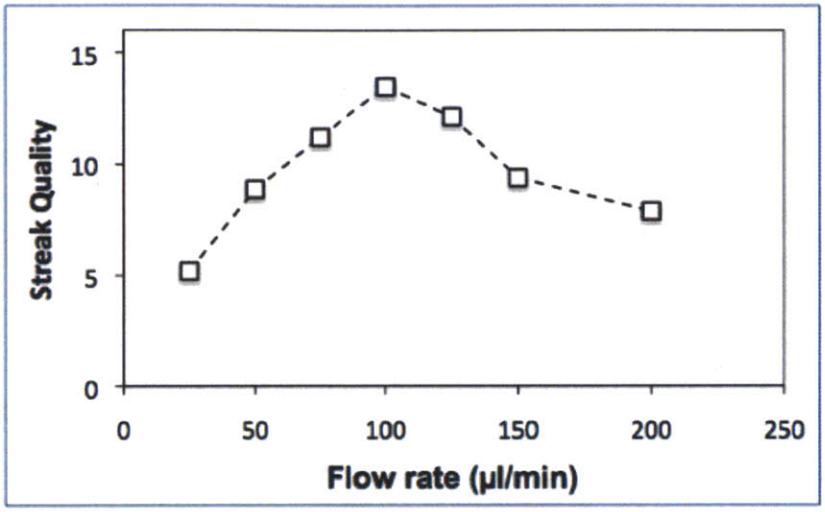

Figure 32. Observed streak quality as a function of flow rate. Below 100 uL / min, streak quality decreases as inertial forces are not sufficient for optimal focusing. Above this rate, streak splitting begins to occur and so the focused stream does not maintain a central position.

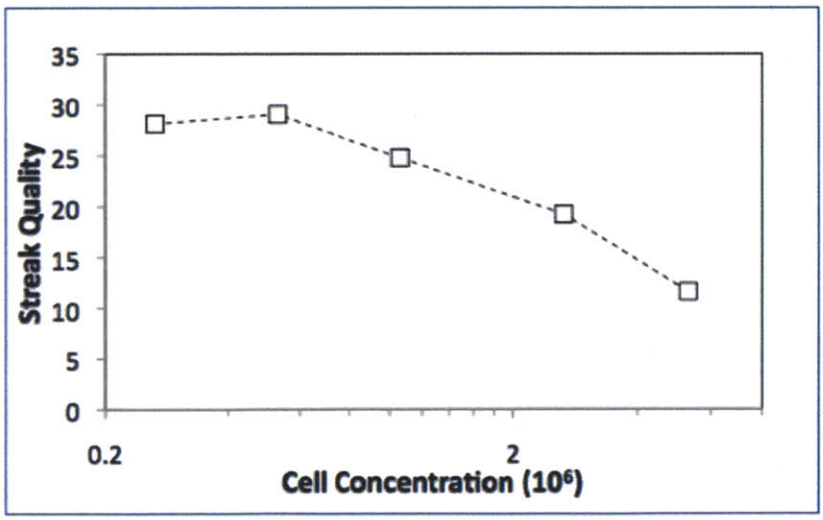

Figure 33. Streak quality decreases with increasing cell concentration as inter-particle interactions increase, causing defocusing.

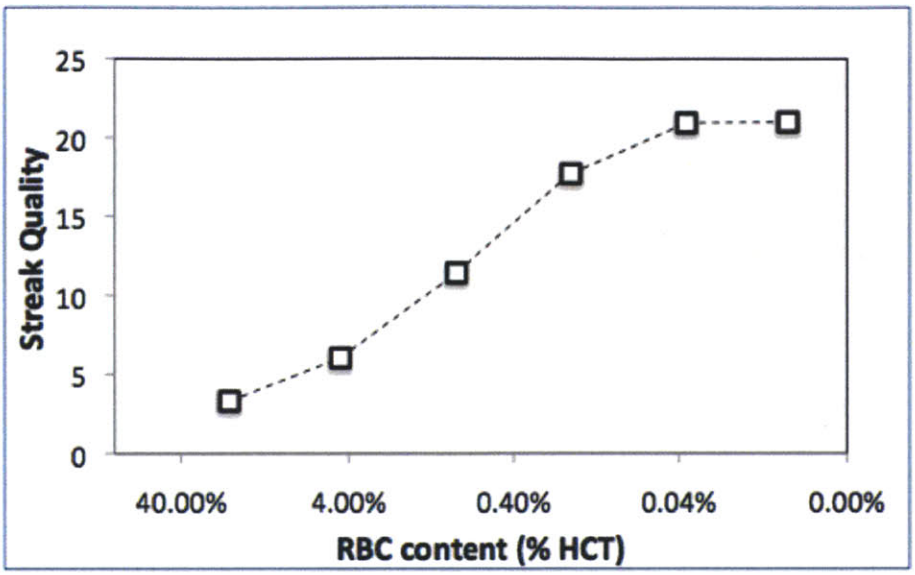

Figure 34. RBC contamination of the HCS array product has the potential to cause defocusing of otherwise focused nucleated cells by increasing inter-particle interactions.

4.4.3 Highly sensitive magnetophoresis

As demonstrated, inertial focusing enables precise control over cell position, here centering all nucleated cells in the middle of the channel. This in turn enables highly sensitive microfluidic magnetophoresis, as magnetically tagged cells start in the center of the channel and only need to deflect ~ 200 um to reach the cell-free zone at the channel wall. (Figure 35) Based on the bulk flow rate, we are able to determine the residence time of a cell in the deflection region to be τ_r ~ 600 ms. Finite element modeling of the quadrapole magnetic circuit used here yields an estimate of the magnetic gradient (dB/dx) across the channel to be 150 T/m; combining this information with the actual fluid velocity profile in channel, we calculate the magnetic payload needed to successfully deflect labeled cells (assuming a maximum cell diameter of 30 um) to within 50 um of the channel wall. Based on the magnetic moment of Dynal MyOne beads, we predict that cells with 15 or more beads will be reliably deflected into the collection stream. (Figure 36)

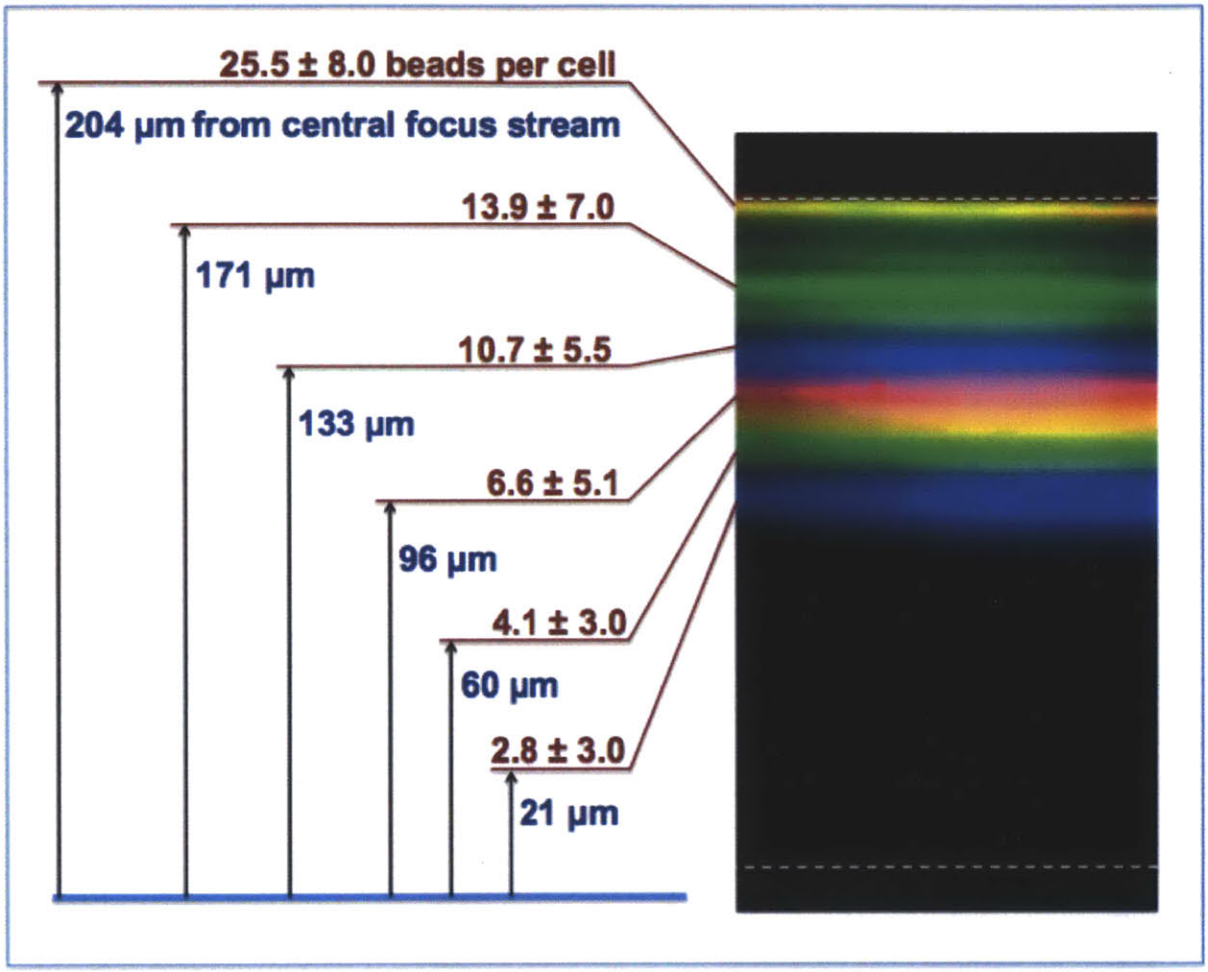

Figure 35. Here, the highly sensitive nature of the microfluidic magnetophoresis is depicted. Cell populations with characterized bead loading were serially processed through the inertial focusing and magnetophoresis channels, and imaged part of the way down the deflection channel. As demonstrated, cells with increasing bead loading deflected further towards the side wall.

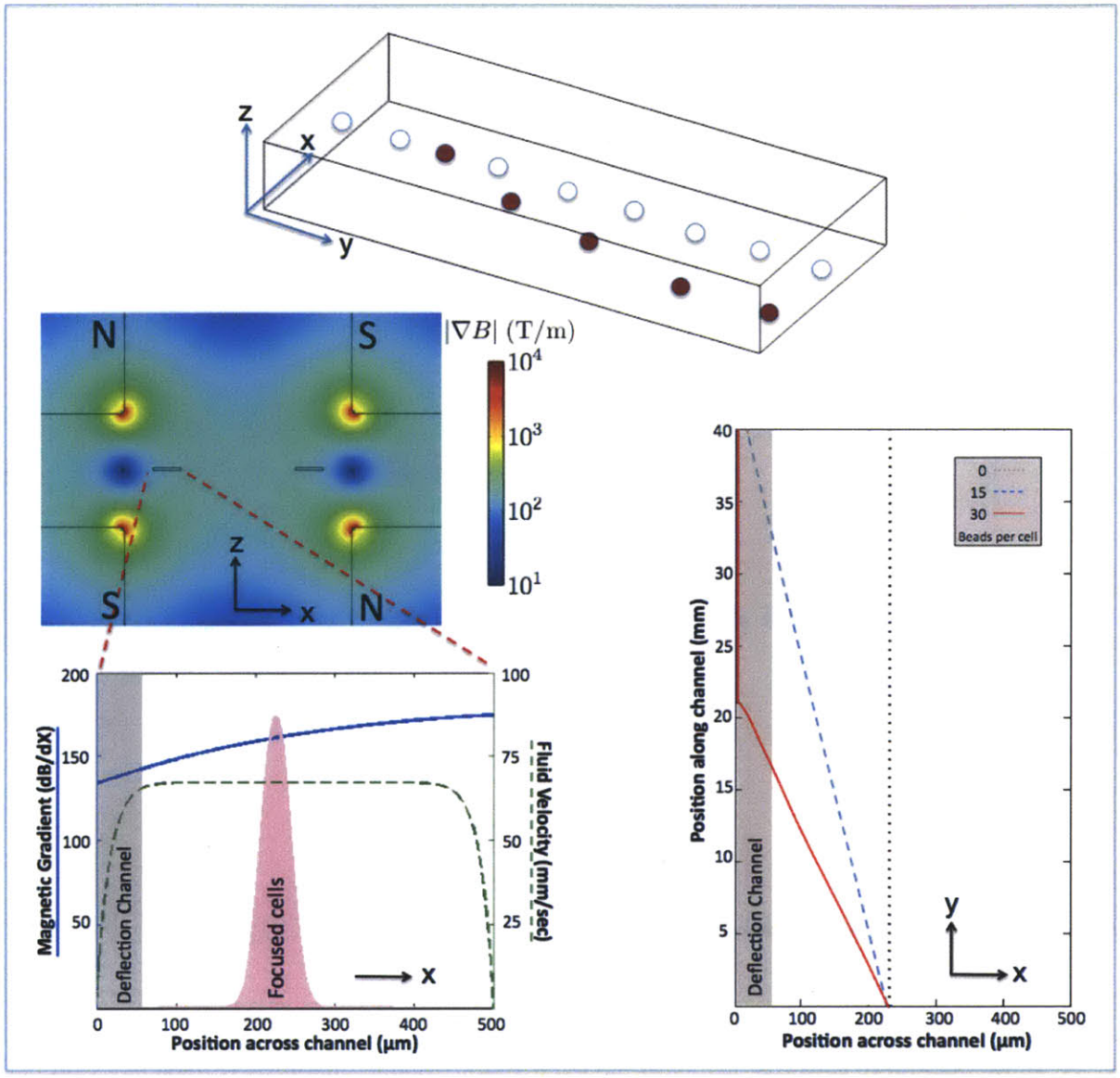

Figure 36. A mathematical model was built to understand the deflection of labeled cells (red) from a focused stream of particles (white). FEM analysis of the quadrapole magnetic circuit (center left) and fluid flow in the channel provided estimates of the magnetic gradient (blue) and flow rate (green) across the deflection channel (bottom left). This information, in conjunction with our experimental understanding of cell position in the focused stream (pink) was used to construct an overall model to predict the trajectories of focused cells with varying magnetic payloads (right).

Given the spread in both cell size and initial position with the focus stream, we are further able to establish expected cutoff values to define the minimum calculated magnetic load (and variability) as a function of flow rate. Importantly, this analysis is validated by experimental measurements. Briefly, cell solutions with varying levels of bead labeling were prepared and processed at various flow rates (τ_r from 300 to 600 ms); the distribution of bead number on cells collected in the deflection stream versus the non-deflected stream was analyzed and mirrors expected results, as the magnetic payload needed to deflect increases with increasing flow rate (decreased residence time) in accordance with the model. (Figure 37, Figure 38)

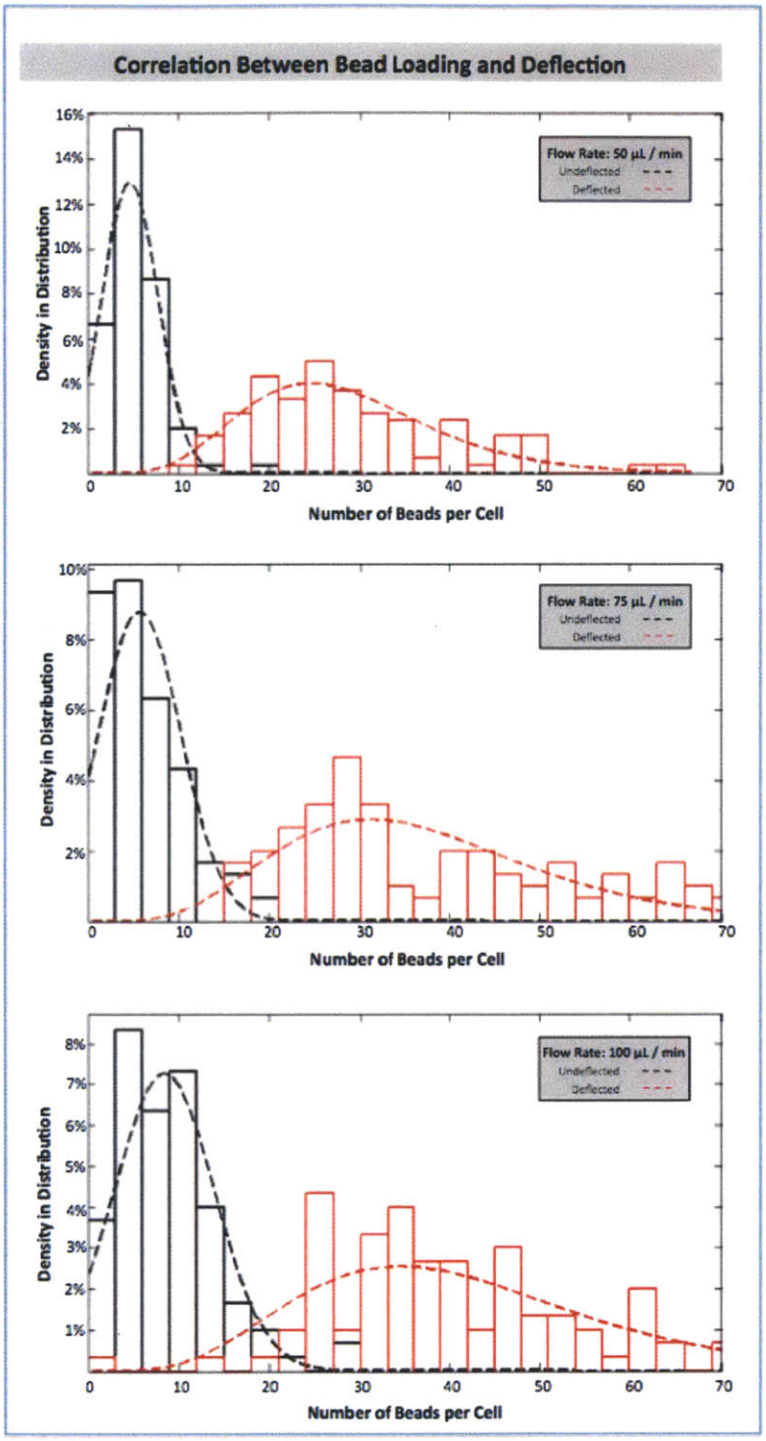

Figure 37. The experimental 'mimimum payload to deflect' was determined by plotting histograms of bead loading density for deflected and undeflected cells; the intersection of curve fits of this data was taken to represent this minimum value.

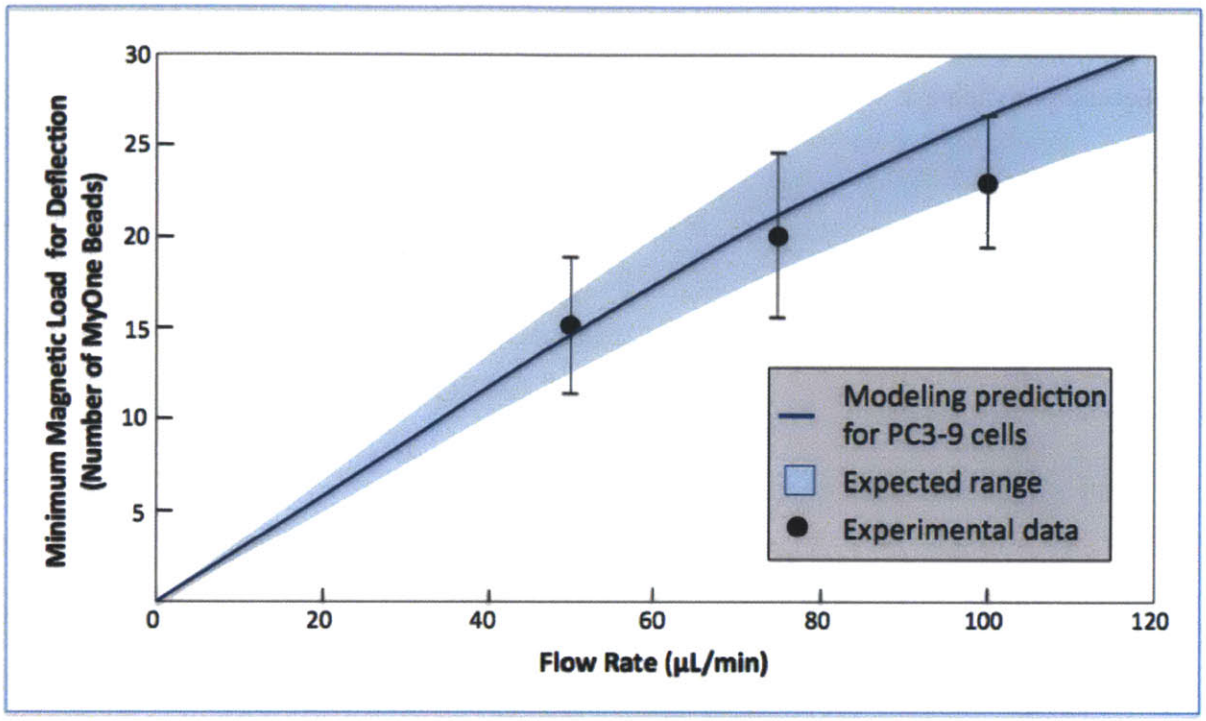

Figure 38. The analytical model presented in Figure 36 was used to determine the minimum magnetic load needed to deflect PC3-9 cells as a function flow rate, given the measured variability in cell size. Importantly, the experimental data presented in Figure 37 concurs with the predictions.

4.4.4 Multi-modal sorting of CTCs

We used the MIMICS system to explore two modes of immnomagnetic sorting to isolate CTCs using this system: a positive selection mode wherein target CTCs were identified and tagged based on their expression of the surface marker EPCAM, and a negative selection mode wherein the sample was depleted of leukocytes tagged with surface markers CD45 (otherwise known as common leukocyte antigen) and CD15 (a broadly expressed granulocyte marker).

4.4.5 Immunomagnetic labeling of target cells in whole blood

For positive selection, while simple mixing of anti-EpCAM magnetic beads in whole blood enabled sufficient labeling of high EpCAM expressing cells (SKBR3), the addition of Active

Magnetic Mixing (AMM) was found to dramatically increase the extent of bead-cell interactions and was necessary to achieve sufficient magnetic labeling of low EpCAM expressors (MB-231). (Figure 39)

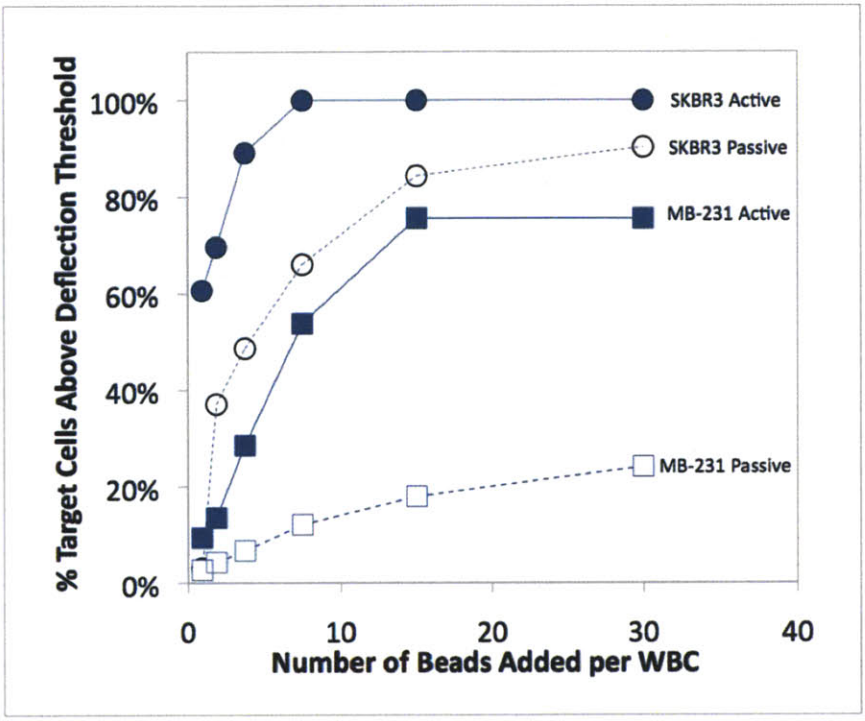

Figure 39. For immunomagnetic positive selection, anti-EpCAM magnetic beads were mixed with whole blood spiked with either MB-231s (square) or SKBR3s (circle). The use of active magnetic mixing (filled symbols) was necessary to achieve optimal labeling of very low EpCAM expressing MB-231 cells.

For negative depletion, while CD45 is the gold-standard leukocyte marker, a combination of beads targeted against CD45 and CD15 was needed to achieve sufficient labeling of the sample. Given the heterogeneity of CD45 expression on leukocytes, and the known low expression of CD45 on granulocytes, this was determined to be the appropriate secondary marker. (Figure 40)

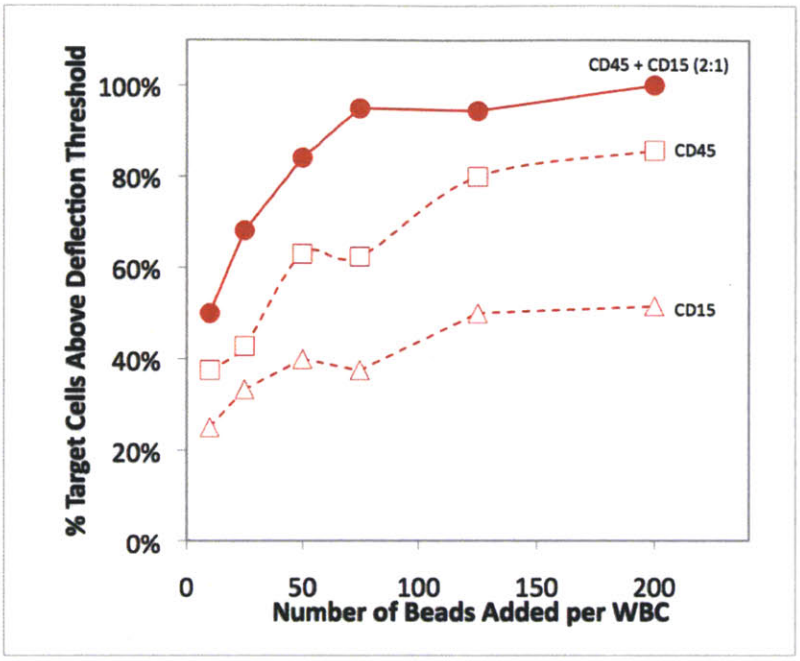

Figure 40. For immunomagnetic negative depletion, a combination of anti-CD45 (targeting all WBCs) and anti-CD15 (targeting granulocytes) beads is necessary to label ~ 100% of the target WBCs.

4.4.6 Performance of integrated system for rare cell isolation from whole blood

To evaluate the efficiency of CTC purification, 5 cell lines with dramatically varying EpCAM expression were spiked into whole blood isolated using positive or negative selection modes. (Figure 41)

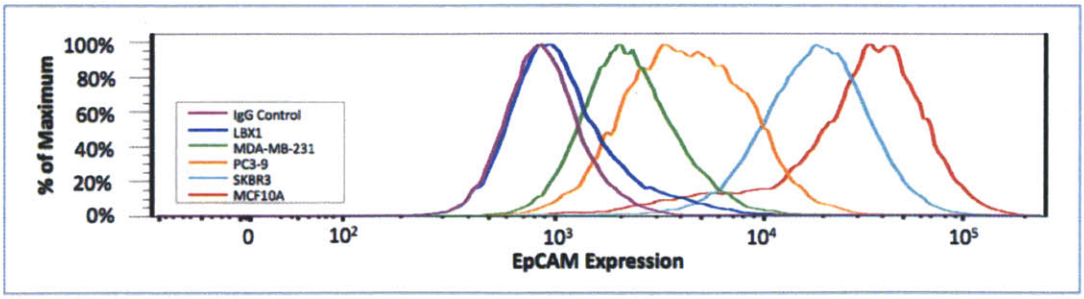

Figure 41. EpCAM expression of five model cell lines.

With the advent of AMM and the high sensitivity of the MIMICS technology, very low EpCAM expressing cells (MB231) could be isolated with greater than 70% efficiency, and low expressing EpCAM cells commonly used as model CTCs (PC3-9s) were isolated with greater than 90% efficiency. A model of EMT induction in traditionally high EpCAM expressing MCF10A cells previously developed in our group resulted in a cell line (LBX1) with ultra-low EpCAM expression; in the negative depletion mode, we were able to isolate both these cells and the parental MCF10As with high efficiency, demonstrating the benefits of an EpCAM-independent sorting mode. (*54*) (Figure 42)

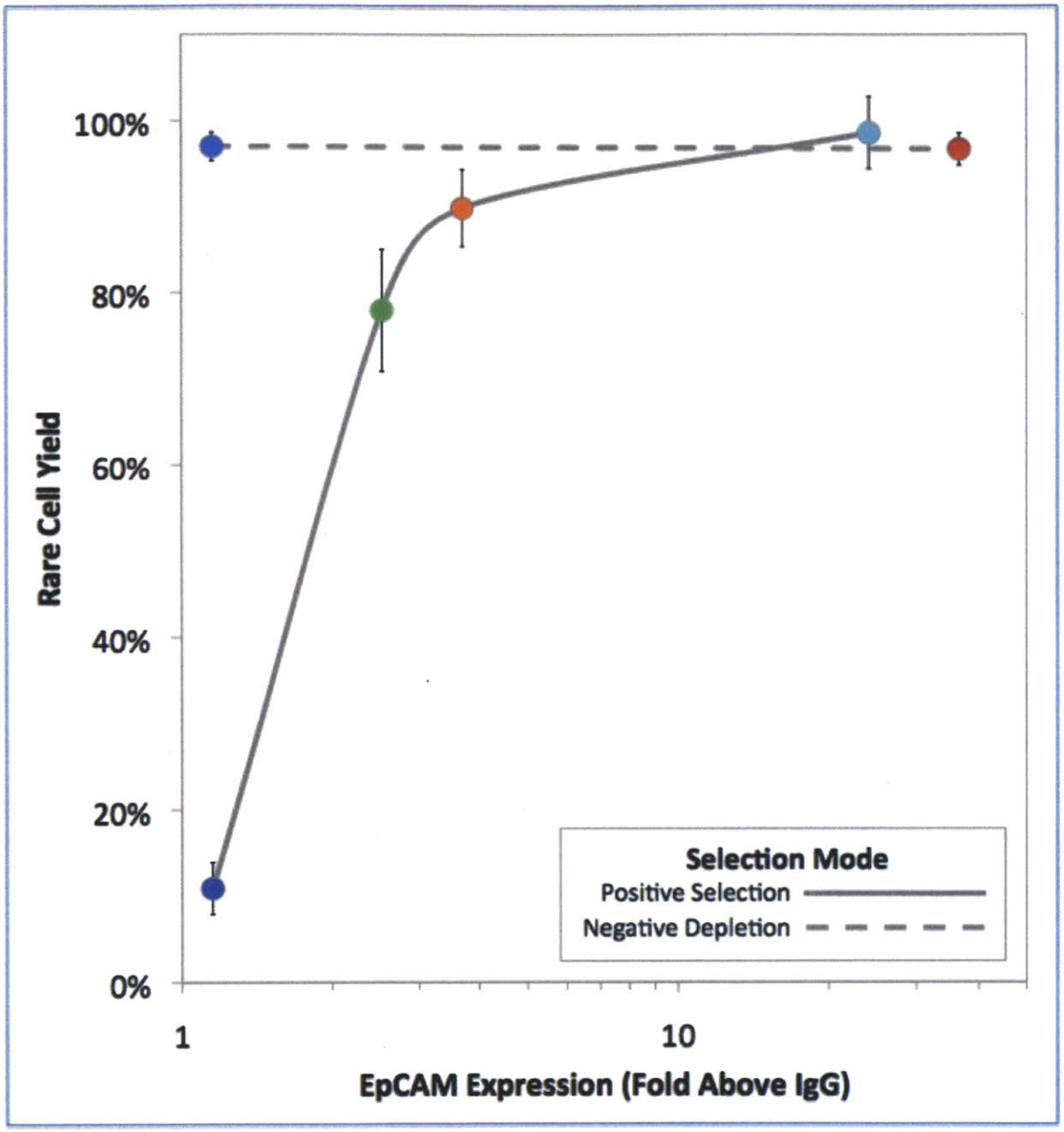

Figure 42. Overall system performance was evaluated using 5 cell lines of varying EpCAM expression (Figure 41). As expected, EpCAM based positive isolation efficiency was dependent on EpCAM expression level, however PC3-9 cells (orange) traditionally considered low EpCAM expressors are isolated with an efficiency greater than 90%. Encrichment through negative depletion was independent of EpCAM expression.

Sample purity varied notably between operating modes – in positive EpCAM based selection, a purification of over 3.5 log was achieved (1495 average contaminating WBCs/mL input); in negative selection, a purification of 2.5 log was achieved (31,838 average contaminating WBCs/mL). (Figure 43) Importantly, the isolated cells are presented in suspension, enabling direct compatibility with virtually all downstream analytical techniques.

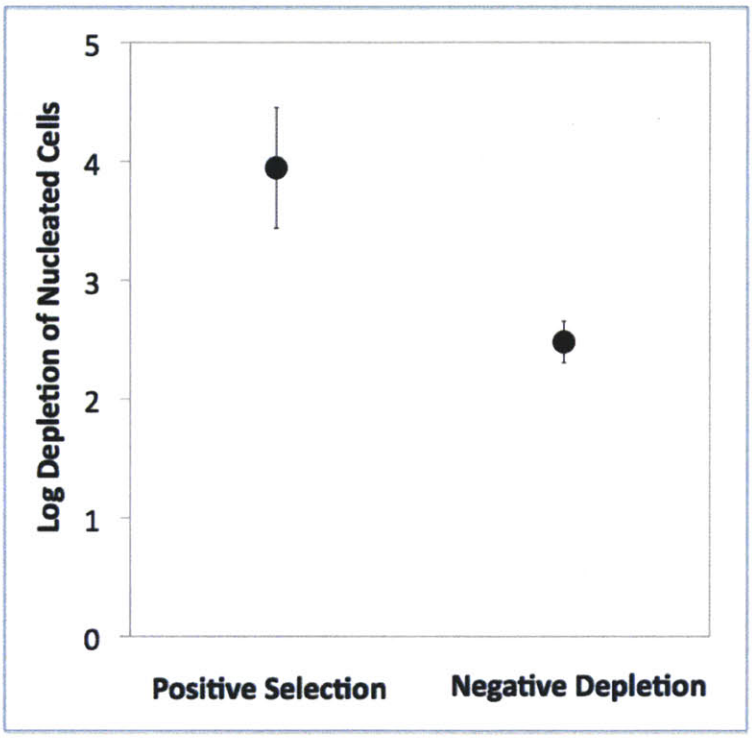

Figure 43. While enrichment through negative depletion was independent of EpCAM expression, this approach has an order of magnitude lower purification when compared to positive selection, demonstrating the tradeoff between these complementary approaches.

4.4.7 Isolation and characterization of CTCs from patient samples

In an initial cohort of breast, prostate, and lung cancer patients, we demonstrate the clinical application of the MIMICS technology to enable isolation of patient CTCs. In the following series of figures we demonstrate the use of 'positive selection' for isolation of PSA+ PSMA+

CTCs and for the identification of the EML4-ALK translocation CTCs enriched from known mutant lung cancer patients. (Figure 44, Figure 45) We further demonstrate the use of 'negative depletion' for the isolation of cytokeratin expressing CTCs from a series of ER+/PR+ and triple negative (TN) breast cancer patients as well as traditional Papanicalaou staining of enriched cells from these samples; using this classical staining approach, a board certified cytopathologist was able to identify certain 'suspicious' cells in these samples. (Figure 46 - Figure 54) Finally, we demonstrate that bulk qPCR analysis of cells isolated using negative depletion from a prostate cancer patient demonstrates the presence of putative CTC markers at the RNA level when compared to a similarly processed healthy donor; PSA+ , PSMA+ and dual PSA+PSMA+ CTCs were identified in this sample by standard immunofluoresence. (Figure 55, Figure 56)

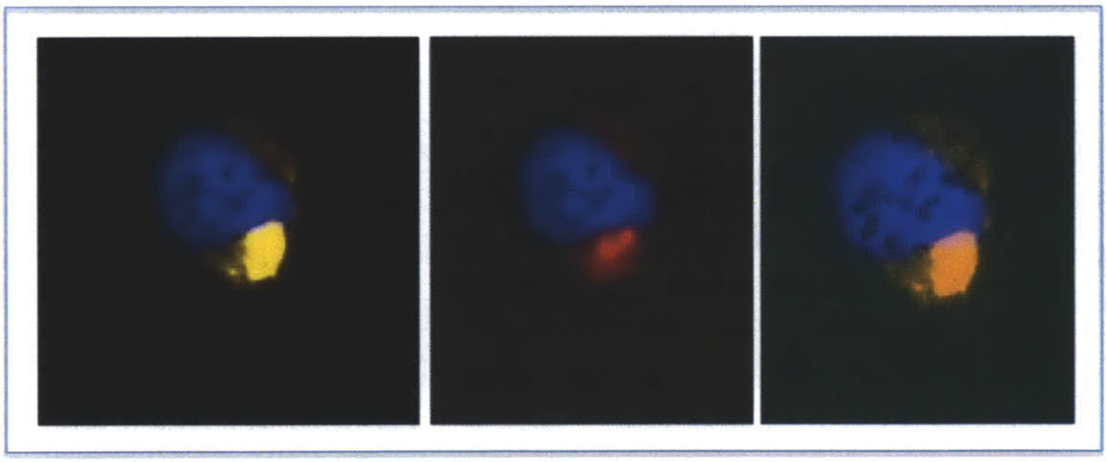

Figure 44. Example of a PSA+/PSMA+ CTC isolated using positive selection from a patient with metastatic prostate cancer. The sample was stained for DAPI (blue, all panels), PSMA (yellow, left) and PSA (red, center). The right panel shows co-localization of the PSA and PSMA signals in the cytoplasm, as well as demonstrating the presence of the EpCAM beads used for cell isolation.

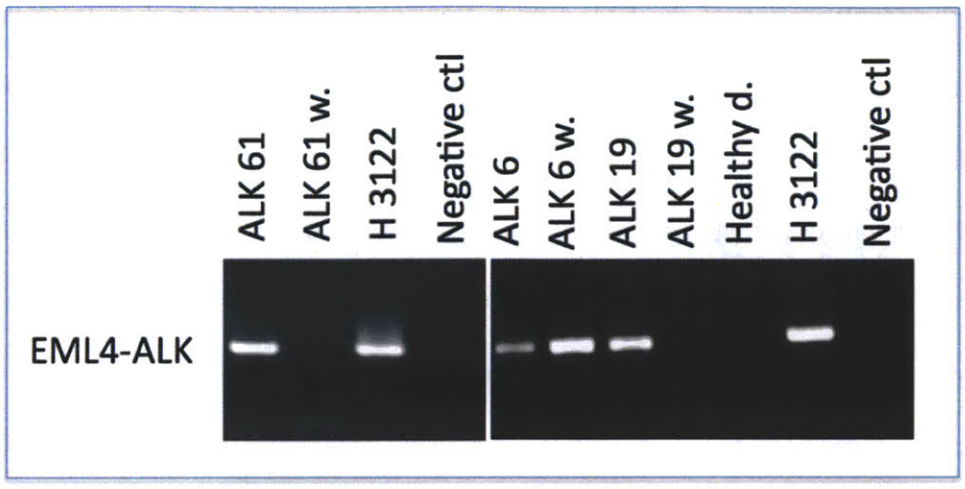

Figure 45. The positive selection approach is compatible with sensitive molecular characterization of enriched CTCs. Here, blood samples from 3 non-small cell lung cancer (NSCLC) patients with known EML4-ALK translocations was processed using positive selection; both the 'product' and 'waste' samples were magnetically enriched and DNA was extracted and probed for the EML4-ALK translocation. As demonstrated, a positive signal was found in all 3 CTC fractions (ALK61, ALK6, ALK19) and in cell line controls (H3122). Negative controls and healthy donors were negative. Interestingly, the undeflected 'waste' from ALK61 and ALK19 were also negative, but the waste from ALK6 (ALK6 w.) was positive, indicating that there were likely CTCs in this sample with magnetic labeling below the deflection threshold.

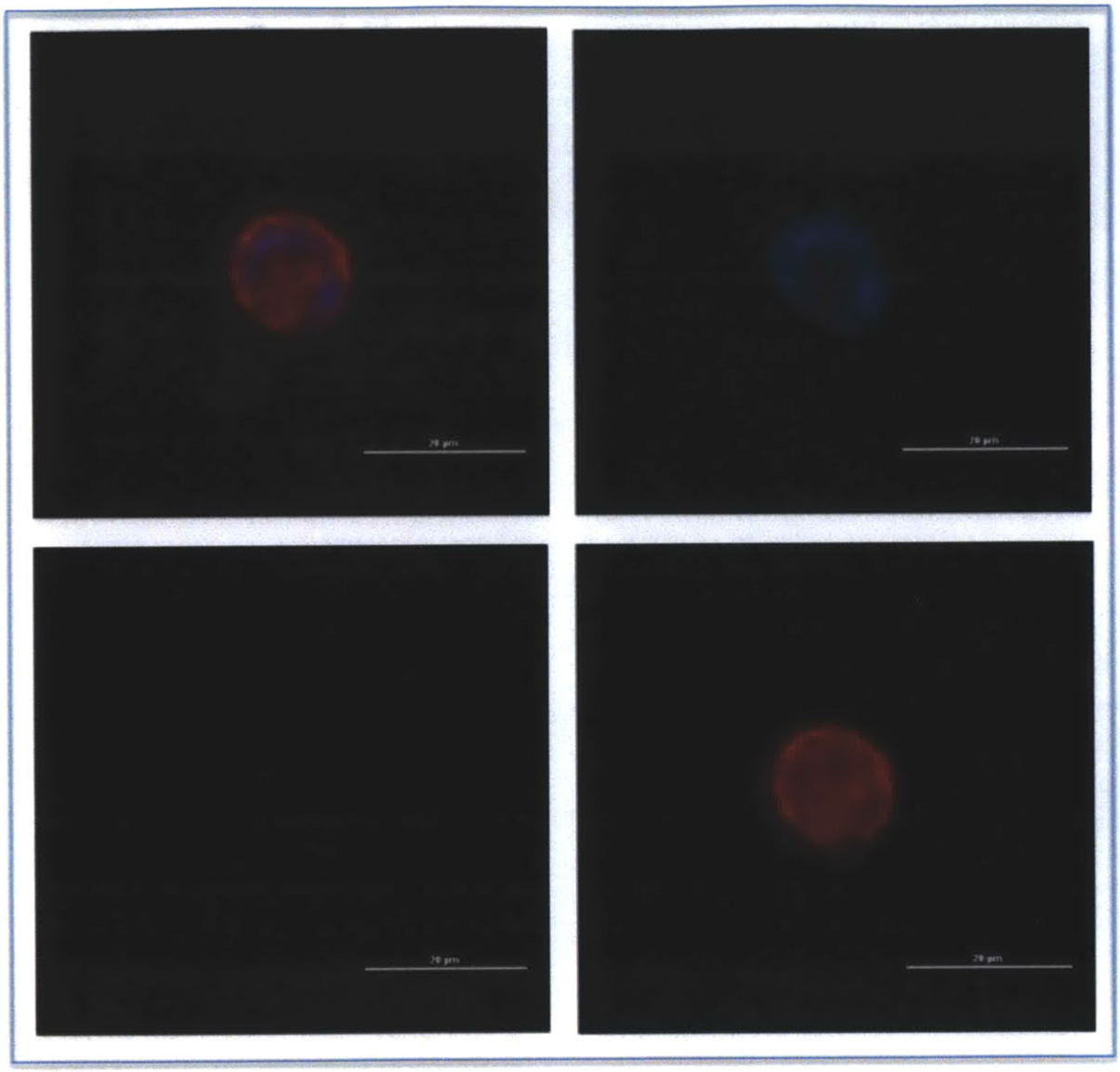

Figure 46. Identification of a cytokeratin positive (CK+) CTC from a patient with metastatic breast cancer, enriched using negative depletion. Clockwise from top right, DAPI (blue), cytokeratin (red), CD45 (green), and merged image.

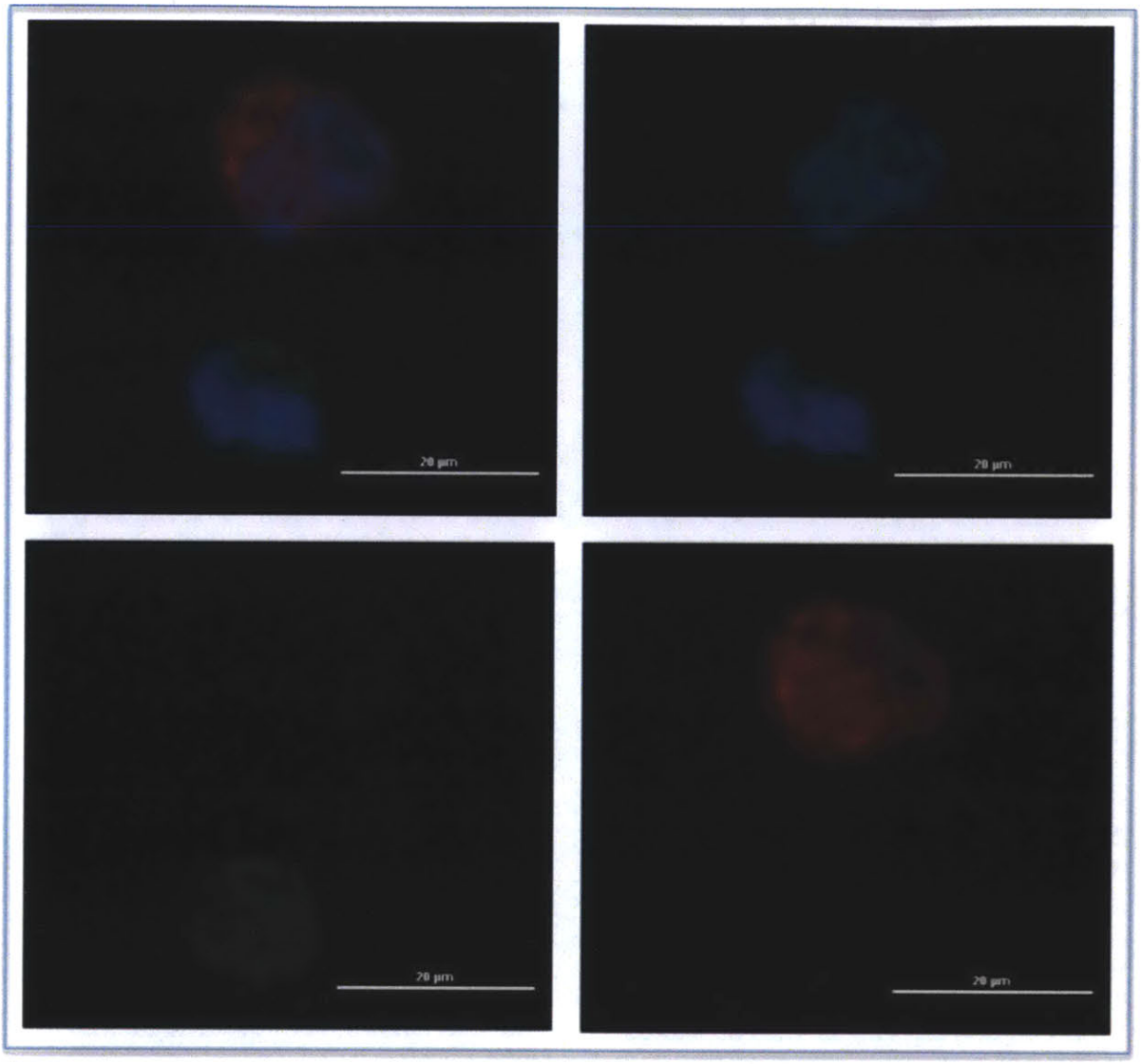

Figure 47. CK+ CTC from a patient with metastatic breast cancer, , enriched using negative depletion. Stained as in Figure 46.

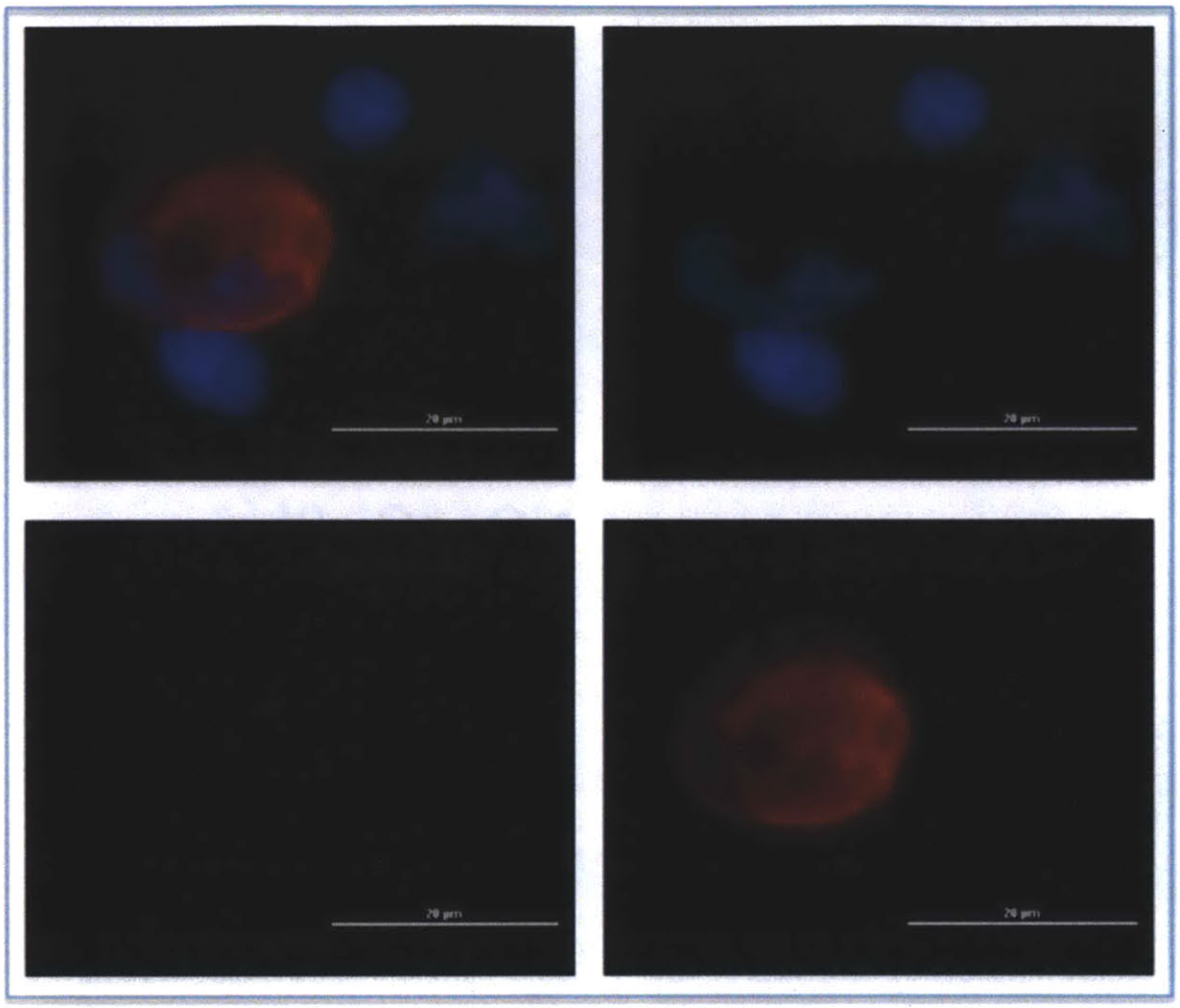

Figure 48. CK+ CTC from a patient with metastatic breast cancer, , enriched using negative depletion. Stained as in Figure 46.

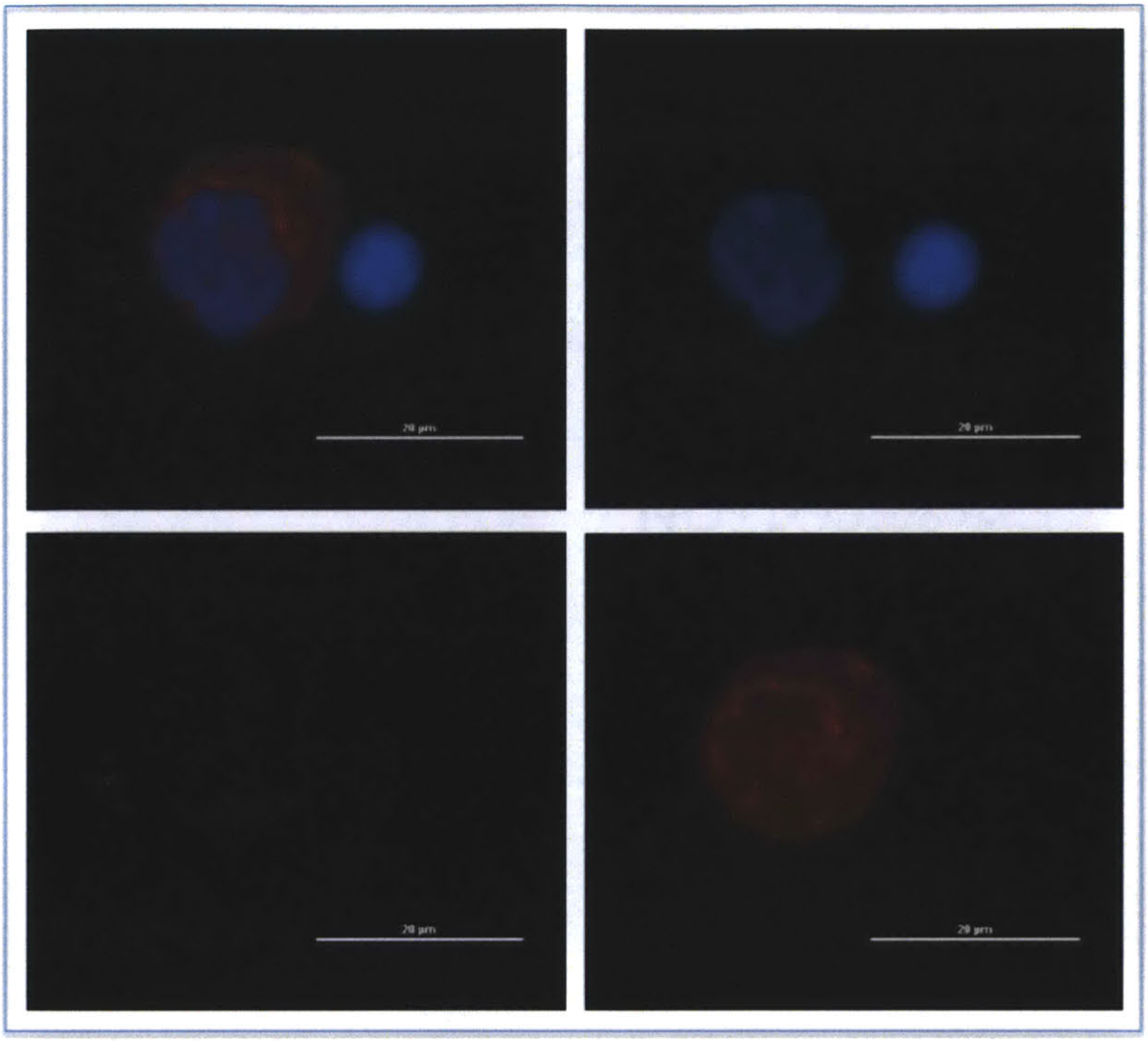

Figure 49. CK+ CTC from a patient with metastatic breast cancer, , enriched using negative depletion. Stained as in Figure 46.

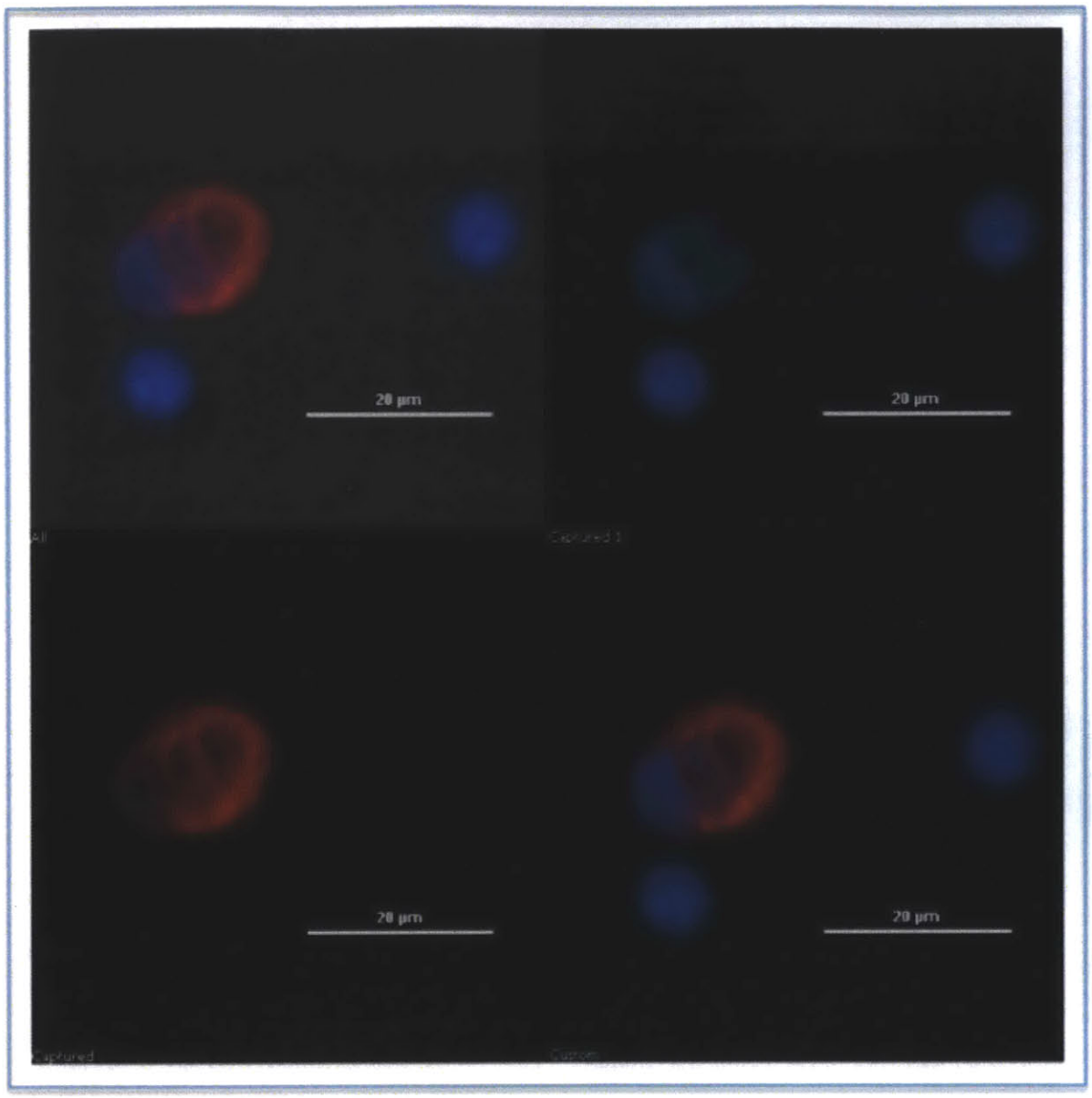

Figure 50. CK+ CTC from a patient with metastatic breast cancer, enriched using negative depletion and stained for DAPI (top right panel), cytokeratin (bottom left panel), and CD45. Bottom right panel shows all 3 immunofluoresence stains (DAPI, CK, CD45) merged together, and top left panel incorporates a brightfield image.

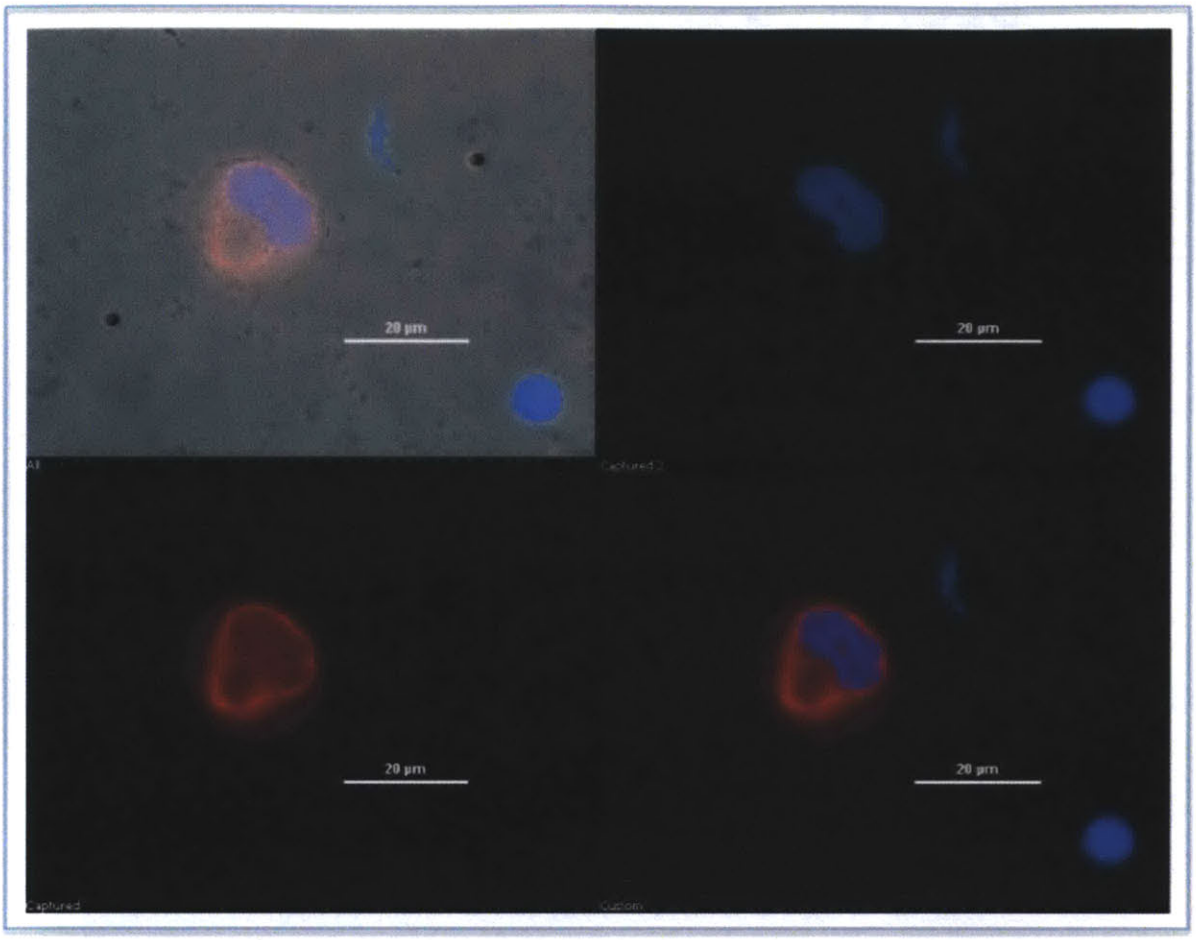

Figure 51. CK+ CTC from a patient with metastatic breast cancer, enriched using negative depletion and stained for DAPI (top right panel), cytokeratin (bottom left panel), and CD45. Bottom right panel shows all 3 immunofluoresence stains (DAPI, CK, CD45) merged together, and top left panel incorporates a brightfield image.

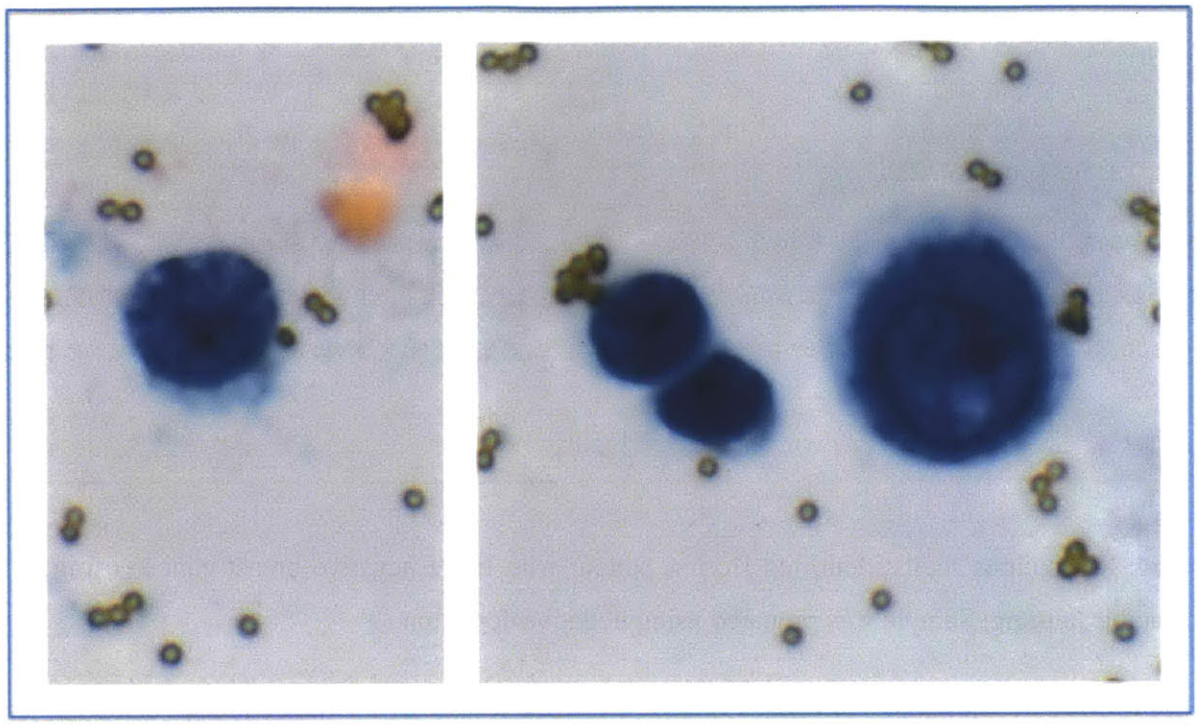

Figure 52. CTCs were isolated from the blood an ER/PR+ breast cancer patient using negative depletion and stained using traditional papanicalaou staining. These cells were identified as 'suspicious' and 'consistent with lobular carcinoma' by a board-certified cytopathologist. (60X)

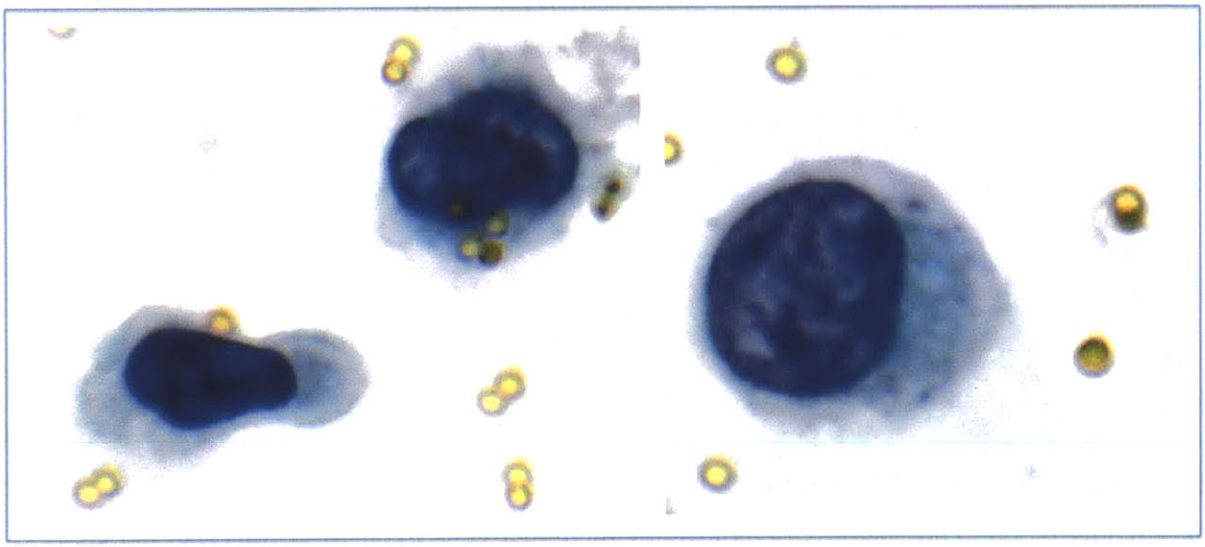

Figure 53. Similarly identified cells from the sample shown in Figure 52, here at 100X.

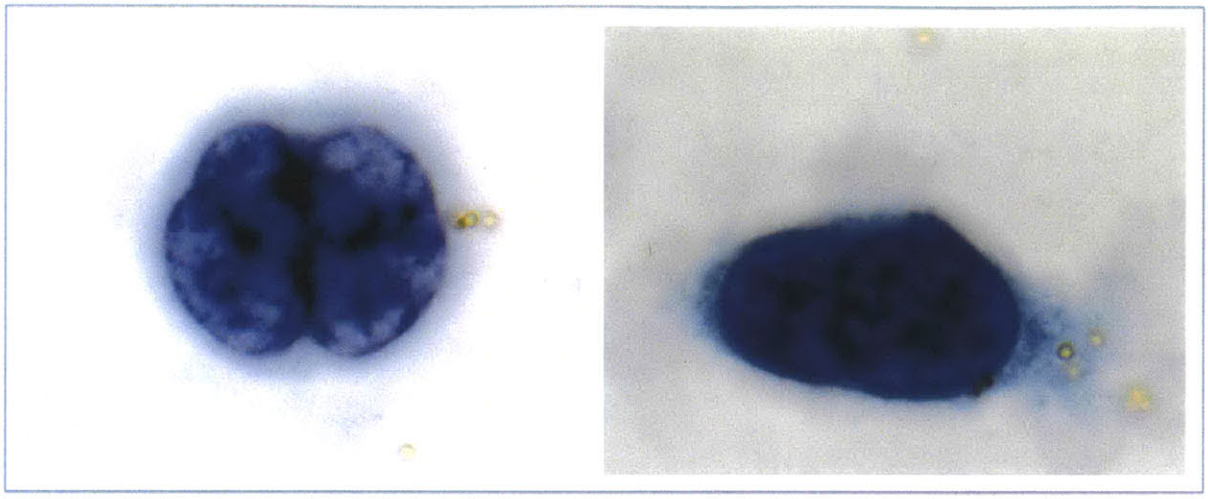

Figure 54. 'Suspicious' cells identified from a patient with triple negative breast cancer using papanicalaou staining. Sample was prepared using negative depletion.

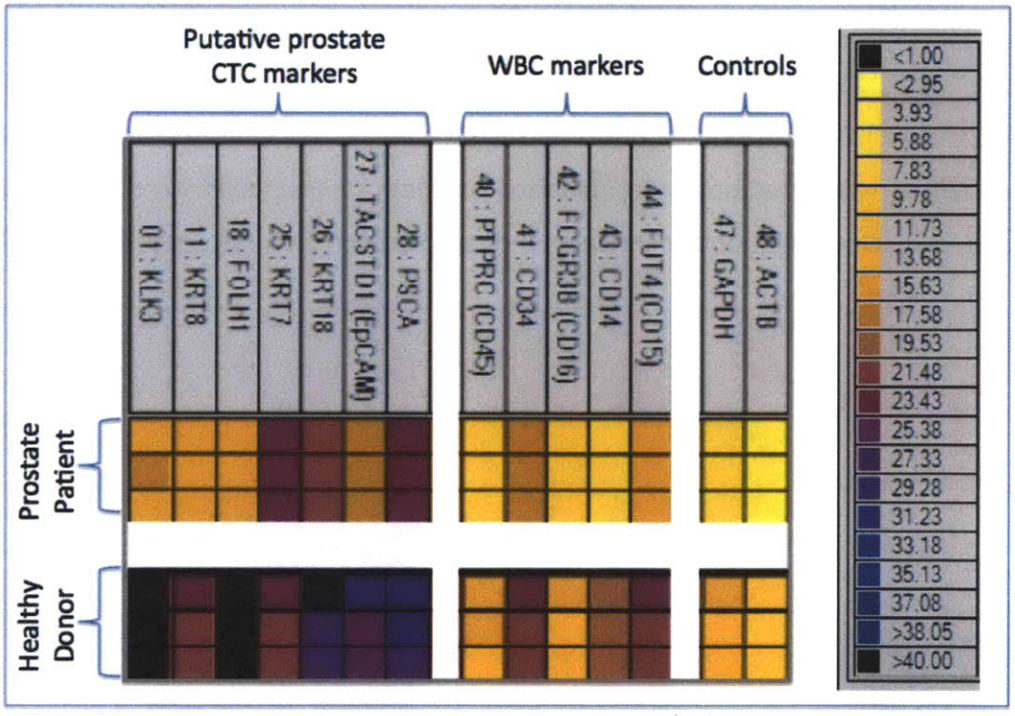

Figure 55. Fluidigm bulk qPCR analysis of negative depletion product enriched from a prostate patient's whole blood. This analysis demonstrates increased gene expression for CTC markers when compared to a similarly processed healthy donor, particularly for PSA (KLK3) and PSMA (FOLH1).

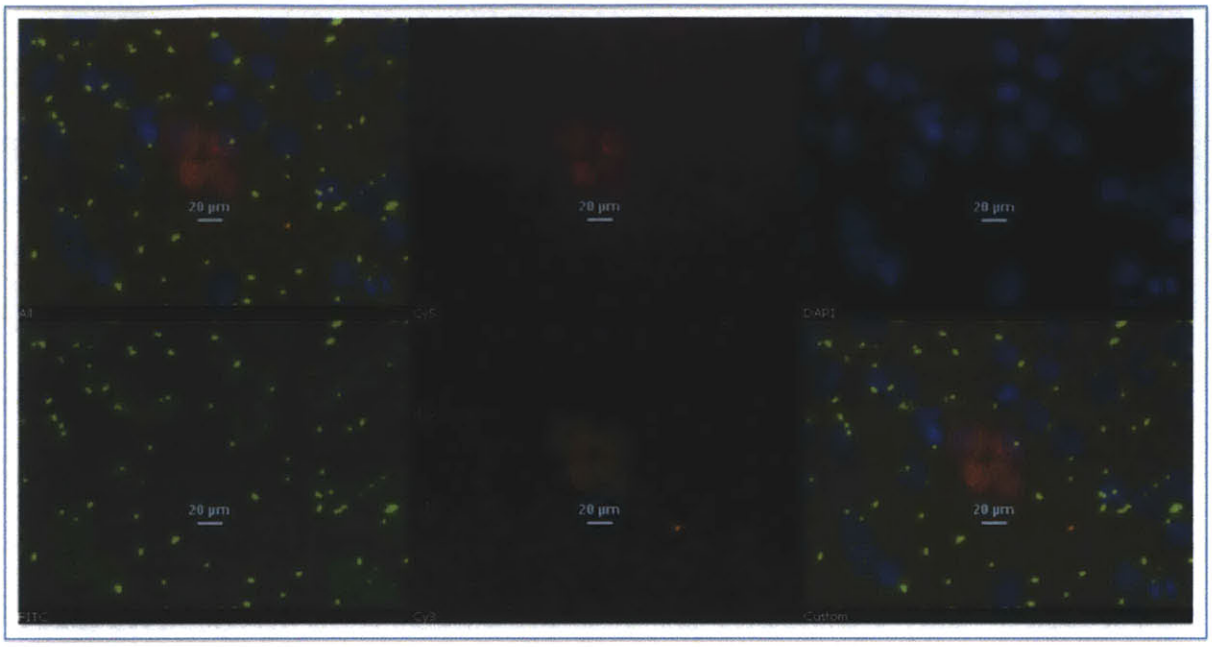

Figure 56. Immunoflourescent confirmation of prostate CTCs from the patient sample presented in Figure 55. Stains include DAPI (blue), PSA (Cy5), PSMA (Cy3), CD45 (FITC). Note that the punctate FITC staining is due to inadvertent labeling of free magnetic beads with the fluorescent secondary antibody.

4.5 Conclusions

We have demonstrated that the MIMICS system is a powerful cell isolation technology. Operable in both positive selection and negative depletion modes, the system is able to process whole blood at over 8 mL per hour. By harnessing multiple microfluidic technologies, we couple lossless sample debulking with highly sensitive magnetophoresis, resulting in in-line CTC sorting from whole blood at a rate of over 10 million events per second with high efficiency and specificity. Furthermore, using clinical samples, we demonstrate that putative CTCs may be analyzed using both standard Papanicalaou staining and bulk transcriptome analysis. The ability to study CTCs in such detail with classic morphological stains and sophisticated molecular approaches has the potential to greatly further our understanding of these rare cells.

Chapter 5: Single Cell Analysis of CTCs from an Endogenous Pancreatic Mouse Model

5.1 Introduction

Pancreatic cancer is the fourth leading cause of cancer-related death in the United States estimated to be 34,000 deaths for 2008. Moreover, median survival of metastatic pancreatic cancer patients is only 3-6 months at present. Most patients present with surgically unresectable disease on diagnosis, and although many different systemic therapies have been tried, their efficacy has been limited. Therefore, it is essential that the mechanisms of pancreatic cancer metastasis are more clearly understood so that better therapies may be developed. To further elucidate these mechanisms, here we apply the MIMICS system presented in the previous chapter to isolate putative CTCs from an endogenous pancreatic mouse model; target cells are enriched in an unbiased fashion using the negative depletion approach and presented for single cell transcriptome analysis and characterization.

5.2 Background

5.2.1 Pancreatic cancer biology

Pancreatic ductal adenocarcinoma (PDAC) comprises the majority of all pancreatic cancers and appears to progress from three precursor lesions: pancreatic intraepithelial neoplasias (PanIN), mucinous cystic neoplasm (MCN), and intraductal papillary mucinous neoplasm (IPMN). (*60*) (Figure 57) PanIN is the most common precursor lesion and in humans it undergoes multiple molecular events to develop into PDAC. A very early event in PDAC initiation is the development of an activating mutation in the oncogene *K-RAS*. The *K-RAS* oncogene is a GTP-

binding protein that is involved with a number of cellular processes including differentiation, proliferation, and survival. Activating mutations occur at codon 12 and can be found in nearly all advanced PDAC (*61*). PDAC malignant progression is further modulated by inactivating mutations or deletions of the tumor suppressors $p16^{Ink4a}$, $p14^{ARF}$, *p53*, and/or *SMAD4*. The tumor suppressor *p53* is mutated in a number of different malignancies and occurs in 50-75% of PDAC through point mutation and loss of heterozygosity (*61*). Importantly, mutation of *p53* has been linked with both genetic instability and metastasis in PDAC in the mouse models (*62*).

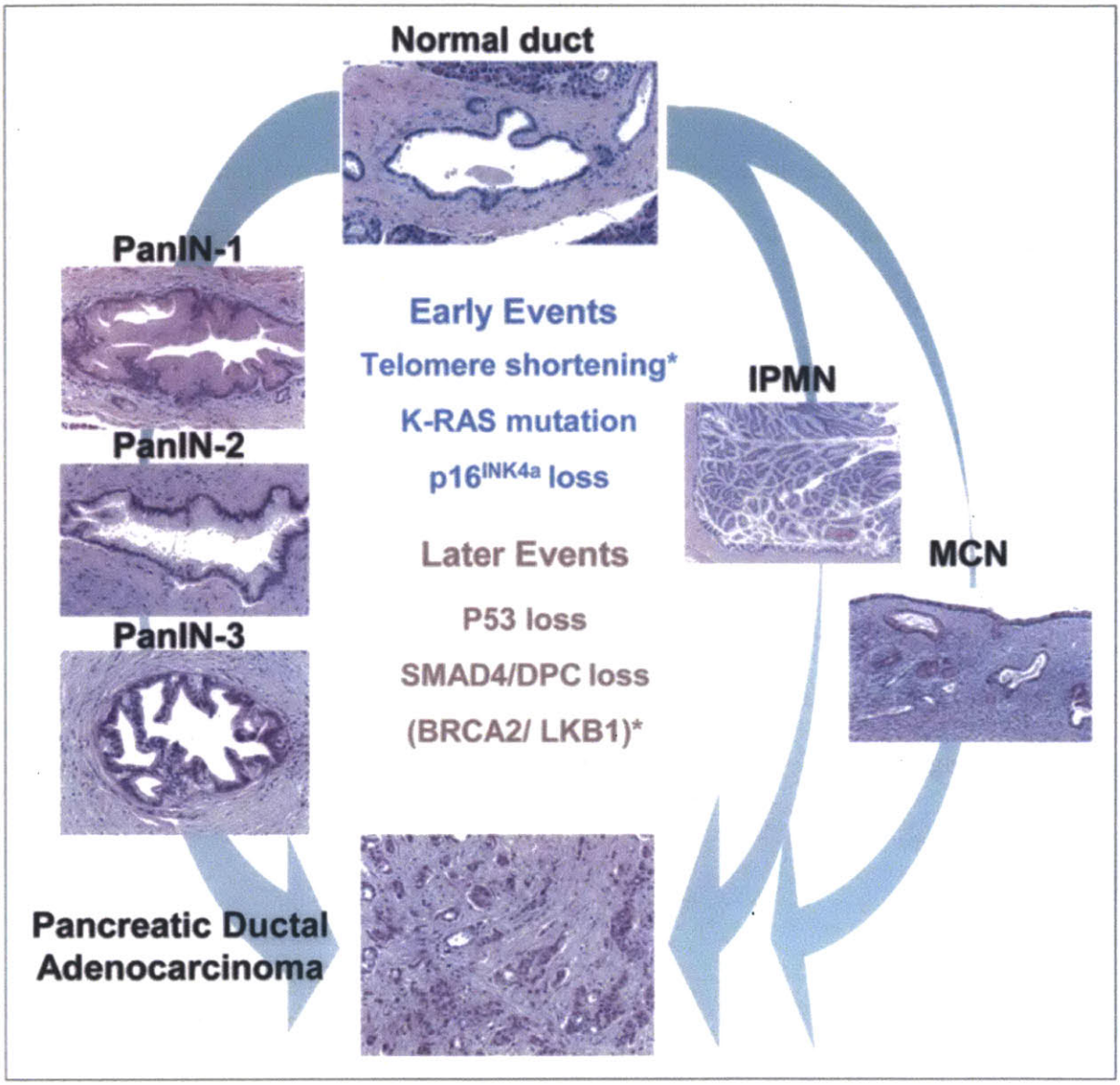

Figure 57. Development of Pancreatic Ductal Adenocarcinoma (PDAC). Adapted from (*60*)

5.2.2 Mouse models of pancreatic cancer

All of these genetic alterations have been engineered into mouse models developed through the conditional mutation of *Kras* and concurrent knockout of each of the above tumor suppressors using a Cre-lox system (*63-65*). These established systems harbor common genetic aberrations

found in human PDACs and provide a robust system to evaluate the effects of tumor genetics to the phenotype of the primary tumor, metastases, and CTCs.

Comparative analyses between these sites of tumor cells can reveal features unique to CTCs. This type of analysis is not possible in humans since primary and metastatic lesions are not often removed in patients as part of therapy. Differences found in genetic or molecular profiles between these tumor cells may provide unique insights into the pathogenesis of metastasis, provide a foundation for human pancreatic CTC investigations, and expose new strategies to develop therapies against this otherwise incurable disease. In fact, such studies recently conducted within our group using a murine analog of the HB-Chip implicated non-canconical Wnt signaling in pancreatic cancer metastasis. (*66*) Briefly, an endogenous $Kras^{G12D}/Tp53^{lox/+or\ lox}$ driven PDAC murine model was studied, and found to produce CK+ CTCs in 7/8 tumor-bearing mice. (Figure 58, Figure 59)

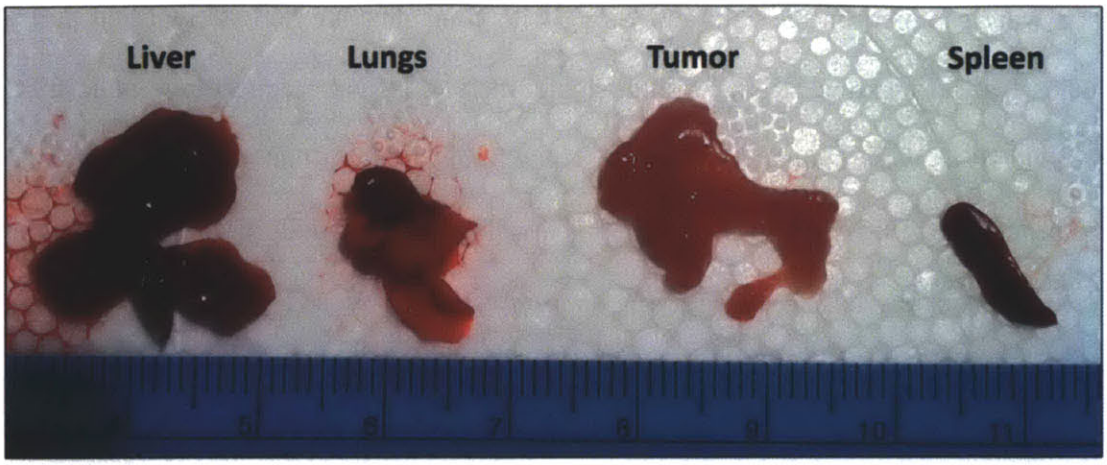

Figure 58. Representative image of tumor size observed in a $Kras^{G12D}/Tp53^{lox/+or\ lox}$ driven PDAC mouse model at approximately 6 weeks of age.

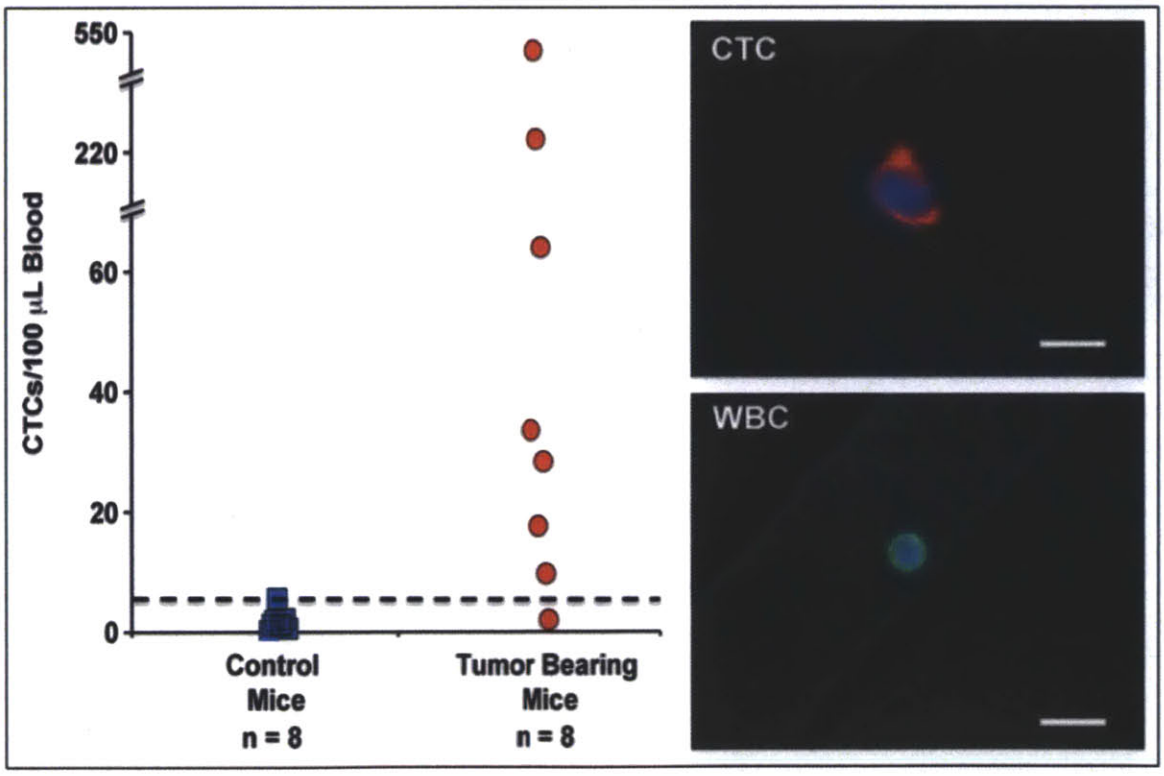

Figure 59. CTCs isolated from endogenous tumor-bearing mice using a modified HB-Chip. Immunostaining was used to identify CK+, CD45- cells as CTCs. Adapted from (*66*)

These CTCs were captured on the chip and, along with contaminating WBCs (reported purity 0.1% – 6%), lysed to extract RNA. Using single molecule RNA sequencing, bulk CTC transcriptome analysis was conducted by splitting blood samples from tumor bearing mice and processing through anti-EpCAM and sham IgG functionalized chips and digitally subtracting the matched NSB leukocyte reads. By identifying transcripts overexpressed in the CTC-enriched samples and comparing to mouse and human primary tumors, *Wnt2* was identified as a prototype CTC-enriched transcript. A detailed study of the role of *Wnt2* in pancreatic cancer indicated that expression suppresses anoikis, enhances anchorage-independent sphere formation, and increases metastatic propensity *in vivo*. Importantly, Yu and Ting also demonstrate that it may be suppressed by inhibition of the Map3k7 (Tak1) kinase either with short hairpin RNAi or with a small molecule inhibitor 5-Z-oxozeanol. (*66*) This study demonstrates the potential for molecular analysis of CTCs to unearth novel therapeutic targets to address metastasis.

5.2.3 Heterogeneity in CTCs

Recent work in our group and others has revealed a significant heterogeneity within circulating tumor cells isolated from a single patient. (*4, 7, 18, 67*) At a coarse level, this is demonstrated by the presence of both proliferative (Ki67+) and apoptotic (M30+) CTCs in prostate cancer patients. (*4*) (Figure 60) Moreover, in a small cohort of prostate patients, an elevated fraction of Ki67+ CTCs appeared to correlate with castration resistant disease, whereas a depressed fraction of Ki67+ CTCs appeared to correlate with a castration-sensitive phenotype. (*18*)

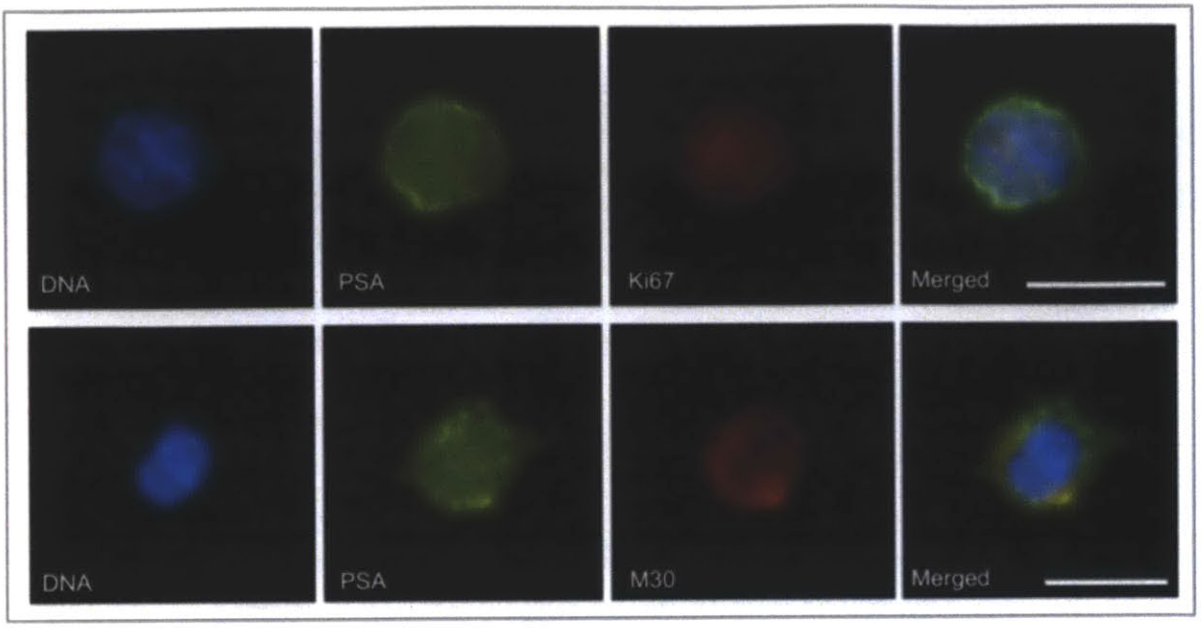

Figure 60. Demonstration of CTC heterogeneity as a mixture of proliferative (Ki67+) and apoptotic (M30+) CTCs were found in prostate cancer patients. Adapted from (*4*)

Heterogeneity may also be seen along a different axis. In malignancies of epithelial origin, there is strong evidence linking an Epithelial-to-Mesenchymal Transition (EMT) to the metastatic cascade and the development of cancer stem cell (CSC) like features. (*67, 68*) It has been further suggested that CTCs may contain subsets of such cells undergoing EMT and potentially responsible for forming metastases. In fact, in a study being conducted by our group focused on breast cancer CTCs isolated using the HB-Chip, RNA-ISH analysis has revealed the presence of CTCs with a range of epithelial and mesenchymal properties. (*68*) (Figure 61) Together, this evidence supports the assumption that CTCs in fact are a heterogeneous cell population.

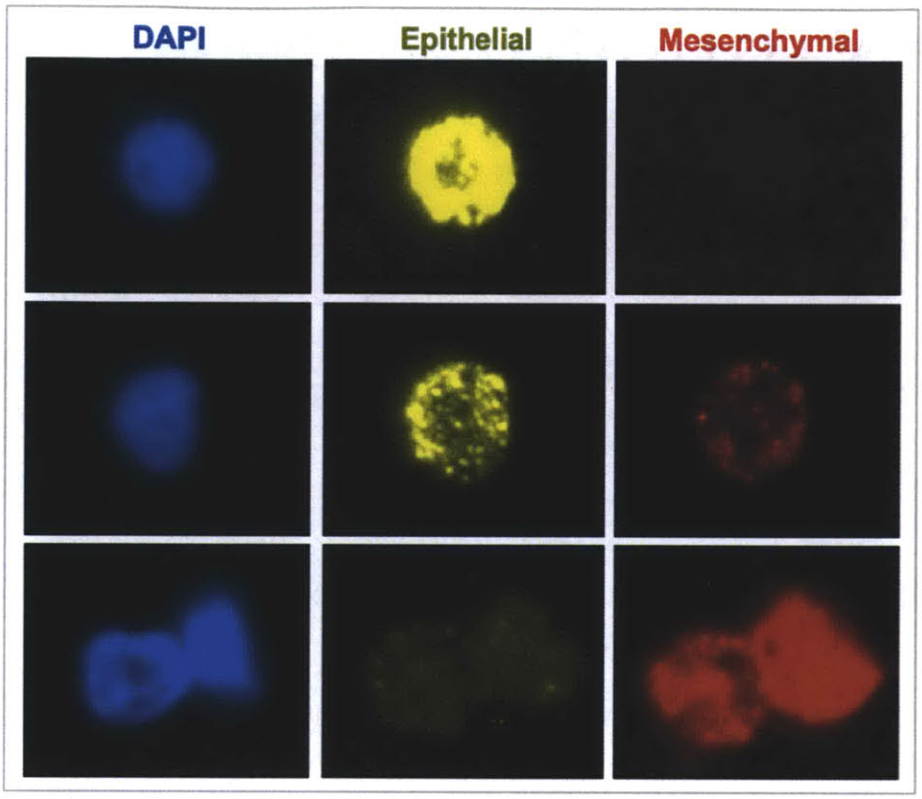

Figure 61. Demonstration of CTCs (identified based on the presence of epithelial markers) with varying epithelial and mesenchymal marker expression. (*68*)

5.3 Motivation

The identification of *Wnt2* as a potential tumor-associated marker by bulk analysis of CTC enriched transcriptomes, and the subsequent validation of this target demonstrates the potential for CTCs to be highly informative with regards to metastasis. However, the current platform utilized by Yu and Ting is limited not only by a bias towards EpCAM expressing CTCs as a result of the positive-selection nature of the technology, but also because it depends on a pooled analysis of all CTCs. (*66*) This potentially masks the presence of exquisitely unique cells in the CTC population that may express high levels of important transcripts (i.e., stem cell or EMT markers) that are more biologically relevant to metastasis. Therefore, in order to be able to fully

explore the range of CTC transcriptomes, a platform that allows for unbiased CTC enrichment and subsequent single cell analysis is needed.

5.4 Approach

This project is focused on applying the MIMICS enrichment technology described in the previous chapter to enable unbiased CTC isolation from endogenous PDAC models and subsequent single cell transcriptome analysis, with the goal of more clearly revealing CTC heterogeneity and potential novel CTC-associated transcripts. (Figure 62) The negative depletion technology described in the previous chapter is modified here to work with mouse blood samples, and the approach has been validated using both a murine PDAC cell line, as well as an orthotopic model. CTCs were isolated from endogenous tumor-bearing mice and immunostained for cytokeratin and CD45 to further validate the application of this enrichment system in the murine model. A portion of each enriched sample was also plated in a dish and potential CTCs were individually selected using a micromanipulator, and subsequently underwent RNA-extraction and cDNA amplification. Each single cell product was then screened using qPCR for putative CTC markers, including the pancreatic specific transcript PDX1 as well as a number of cytokeratins and CD45 (a leukocyte marker) as a negative control. At this stage, a profile of CTC heterogeneity began to emerge, validating the technological approach undertaken. Selected samples will now be sequenced and analyzed to further reveal CTC heterogeneity, however the results of this complex analysis is beyond the scope of the thesis presented here.

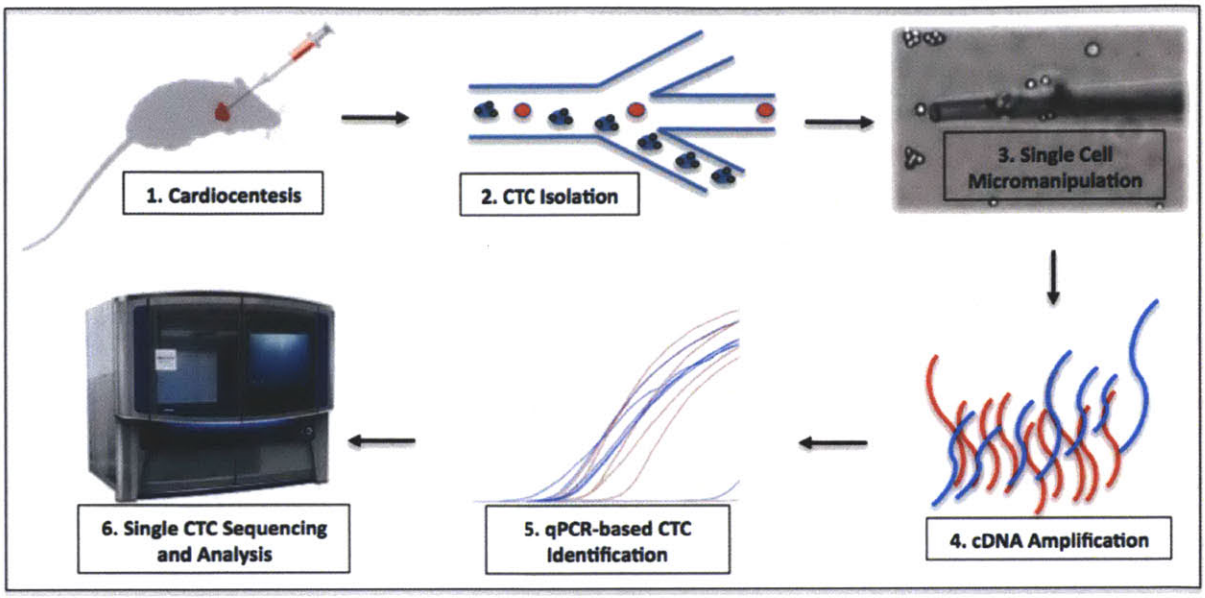

Figure 62. Project Overview. Following CTC enrichment using negative depletion, single putative CTCs were isolated using a micromanipulator, RNA was extracted, cDNA amplified, and qPCR was conducted to aid in target identification for downstream transcriptome sequencing.

5.5 Methods

5.5.1 Mice and cell lines

Mice with pancreatic cancer used in these experiments express Cre driven by *Pdx1*, *LSL-Kras*^{G12D}, and *Tp53*$^{lox/+}$ or *Tp53*$^{lox/lox}$ as previously described (*64*). Normal FVB mice were purchased from Jackson Laboratory. For cardiocentesis, animals were sedated with isofluorane, the chest wall was sterilized with ethanol and a skin incision was made above the rib cage. A 23-gauge needle was used to draw approximately 1 mL of blood into a syringe primed with 100 μL of PBS-10mM EDTA pH 7.4 (Gibco). Blood EDTA concentration was raised to 5mM by either the addition of a concentrated bolus of 500mM EDTA or 1:1 dilution with 10 mM EDTA. Animals were then euthanized per animal protocol guidelines.

A mouse pancreatic cell line (NB508, $Kras^{G12D}/Tp53^{lox/+}$) previously generated from primary tumors developed in this endogenous model was used for spiked cell experiments. For orthotopic experiments, a GFP-transfected line of NB508 cells was injected into the pancreas of healthy FVB mice. Both lines were maintained in standard culture conditions using RPMI-1640 medium + 10% FBS + 1% Pen/Strep (Gibco/Invitrogen).

5.5.2 Adaptation of CTC enrichment technology

Given the desire for an unbiased enrichment system, the previously presented negative depletion technology was selected for this application. All processing protocols were identical to those previously identified, except a rat anti-mouse CD45 antibody (BAM114, R&D Systems, USA) was conjugated to MyOne beads.

Spiked cell experiments were conducted to validate the system by spiking ~ 1000 GFP expressing NB508 cells into 1 mL of healthy mouse blood and processing to determine recovery efficiency. Orthotopic models were used to validate recovery efficiency as well as initially determine expected depletion efficiency from tumor-bearing mice. In these experiments, enriched samples were evaluated for the number of GFP+ cells observed in the product using the quantitative methods described in the previous chapter.

5.5.3 Immunostaining of CTCs isolated from the endogenous model

Isolated CTCs were spun onto glass slides and immunostained using a primary-secondary approach. Primary antibodies were rabbit anti-wide spectrum cytokeratin (1:50, Abcam ab9377), and goat anti-mouse CD45 (1:500, R&D systems AF114). Secondary immunofluorescent-tagged antibodies were used for signal amplification. These were donkey anti-rabbit Alexa Fluor 594 (1:500, Invitrogen A-21207), and donkey anti-goat Alexa Fluor 488 (1:500, Invitrogen A-

11055). Nuclei were then counterstained with DAPI and the slides were rinsed with PBS, coverslipped and stored at 4°C. They were imaged under 10x magnification using the BioView Ltd. automated imaging system (Billerica, MA) as well as an automated upright fluorescence microscope (Eclipse 90i, Nikon, Melville, NY). Positive staining for CK, without CD45 staining, was required for scoring potential CTCs, which were then manually reviewed. Threshold and baseline signals were established using specimens from non-tumor bearing mice.

5.5.4 Single cell micromanipulation and transcriptome amplification

After enrichment from whole blood, cells were collected in a petri dish and viewed using an inverted microscope (Nikon, Melville, NY) outfitted with a hoffman modulation contrast (HMC) system to improve viewing of live cells. Cells of interest were indentified based on lack of labeling with anti-CD45 beads, as immunofluoresence analysis indicated that cells with a high number of attached beads were contaiminating leukocytes. Target cells were individually isolated using a hydraulic micromanipulator (Eppendorf, Germany) and transferred to droplets containing RLT buffer and/or flash frozen in liquid nitrogen. Single cell amplification of individual transcriptomes was conducted using the protocol developed by Tang et. al. (*69*) (Figure 63) Following the initial PCR amplification, samples were screened using qPCR for leukocyte (CD45) and CTC (PDX1, CK8, CK18, CK19) markers to determine which samples were best suited for sequencing.

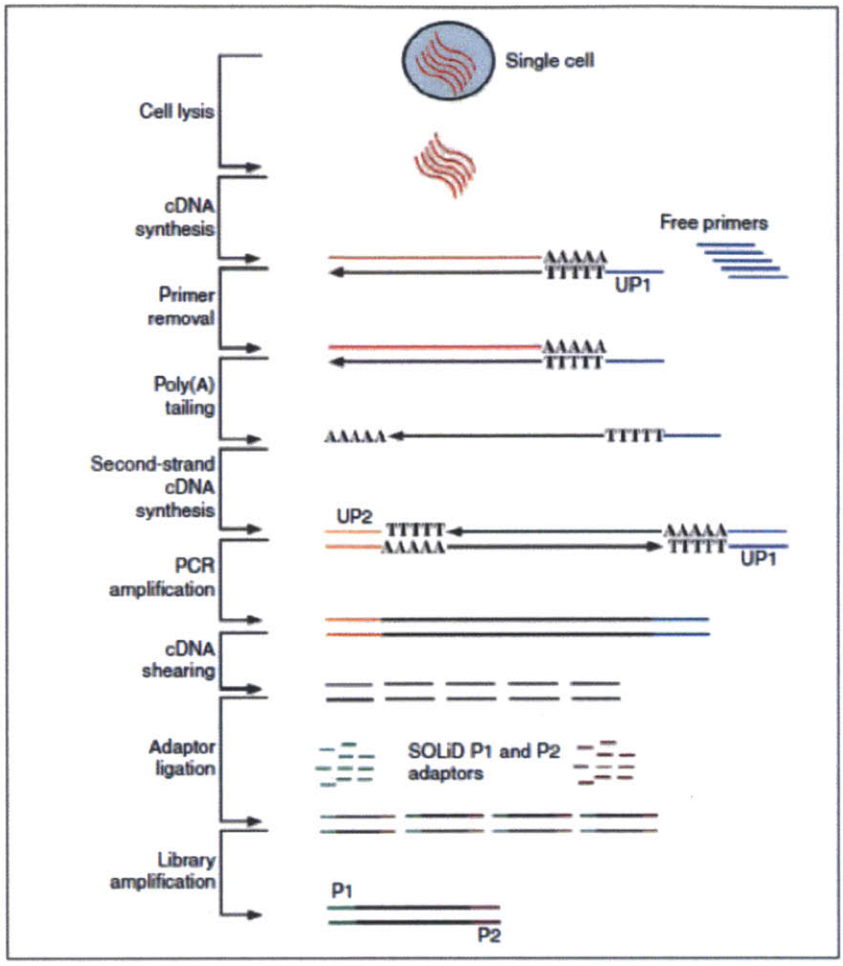

Figure 63. Single cell amplification protocol. Adapted from (*69*)

5.6 Results and discussion

5.6.1 System modifications to enrich CTCs from mouse blood using negative depletion

The inertial focusing based technology presented in the previous chapter was modified for application with the endogenous mouse model system. While mice have WBC concentrations comparable to humans (5-12 M / mL), the distribution amongst various subclasses of WBCs is notably different. Human hematology reveals a bi-modal distribution, with ~ 50% neutrophils and ~ 40% lymphocytes, whereas in the mouse, ~ 75% of all WBCs are lymphocytes. As

lymphocytes express high levels of the CD45 antigen, we evaluated WBC labeling using CD45 alone, rather than combined with a myeloid marker as was found to be needed in the human system. Additionally, 1:1 dilution of the blood with PBS prior to processing was compared to labeling in whole blood. As demonstrated in Figure 64, when labeling in whole blood we were able to achieve ~100% labeling efficiency with CD45 beads alone. The reduced performance observed with diluted samples is attributed to an increase in volume resulting in reduced bead-cell interactions. All future experiments were conducted with 100 anti-CD45 beads added per WBC to undiluted whole blood.

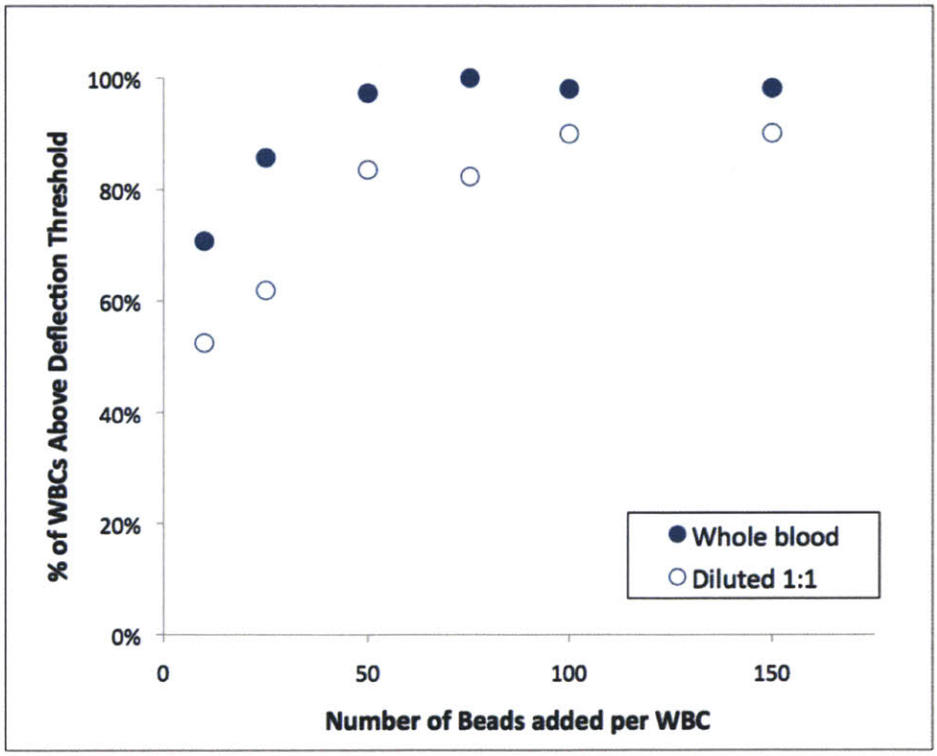

Figure 64. Labeling of mouse WBCs using anti-CD45 MyOne beads.

5.6.2 System validation using spiked cells

The enrichment approach performed as expected when modified. GFP labeled NB508 cells were spiked into healthy mouse whole blood, and were recovered with an efficiency of 97.5%. Importantly, when compared to the data presented by Yu and Ting on capture efficiency of NB508 cells using an anti-EpCAM approach (~ 35%), the unbiased method used here is a notable improvement. (*66*) This is suspected to be due to the variable expression of EpCAM on NB508 cells.

5.6.3 Enrichment of CTCs from orthotopic and endogenous tumor bearing mice.

Blood samples from orthotopic mice were collected and processed approximately 2 weeks post-injection and enriched products were analyzed for GFP+ cells. Blood from endogenous mice was similarly collected and processed; in these samples, CTCs were indentified based on immunostaining; healthy controls were also processed to control for artifacts due to staining. As presented in Figure 65 (left panel) CTCs were found in high numbers in both models. Importantly, low levels of contaminating WBCs were found in the products, as WBCs were depleted by over 3 log when compared to the initial blood samples. (Figure 65, right panel) The combination of relatively high CTC yields and low contamination resulted in sample purities that were feasible for downstream single cell selection. A selection of cytokeratin positive CTCs isolated from the blood of endogenous PDAC bearing mice is presented below (Figure 66 - 71).

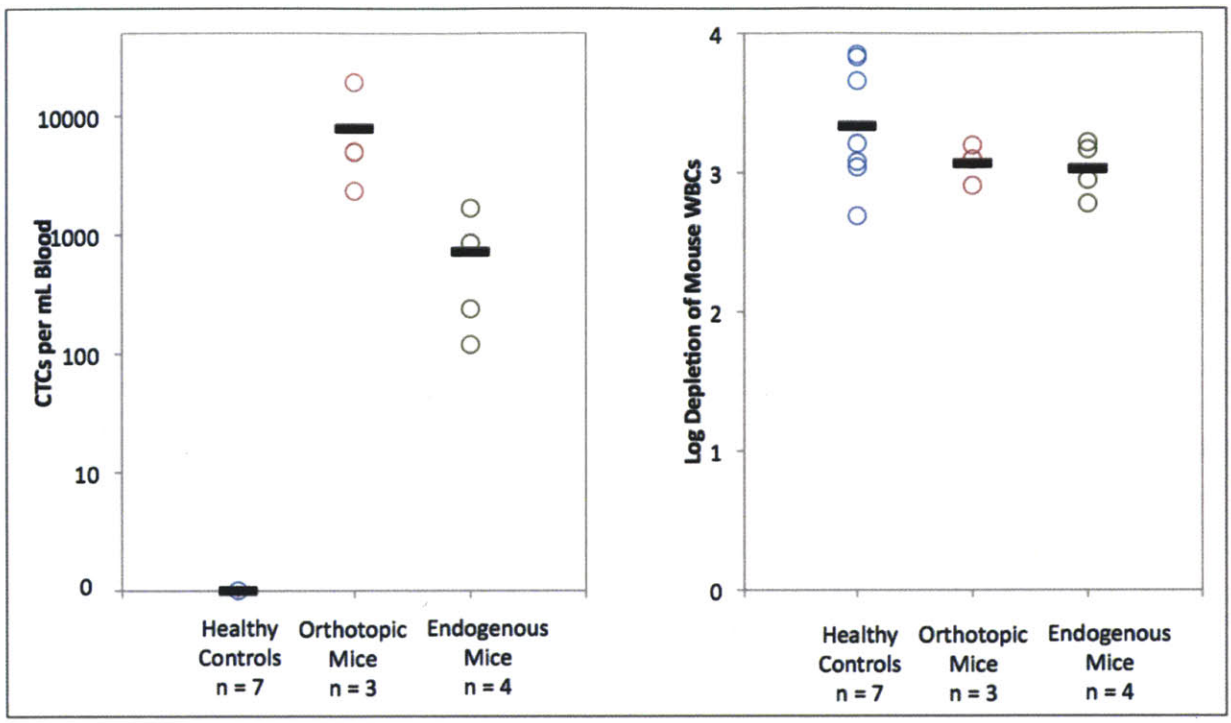

Figure 65. CTC enrichment from whole blood obtained from both orthotopic and endogenous mouse models. (left panel) Significant enrichment was achieved by ~ 3 log depletion of mouse WBCs. (right panel)

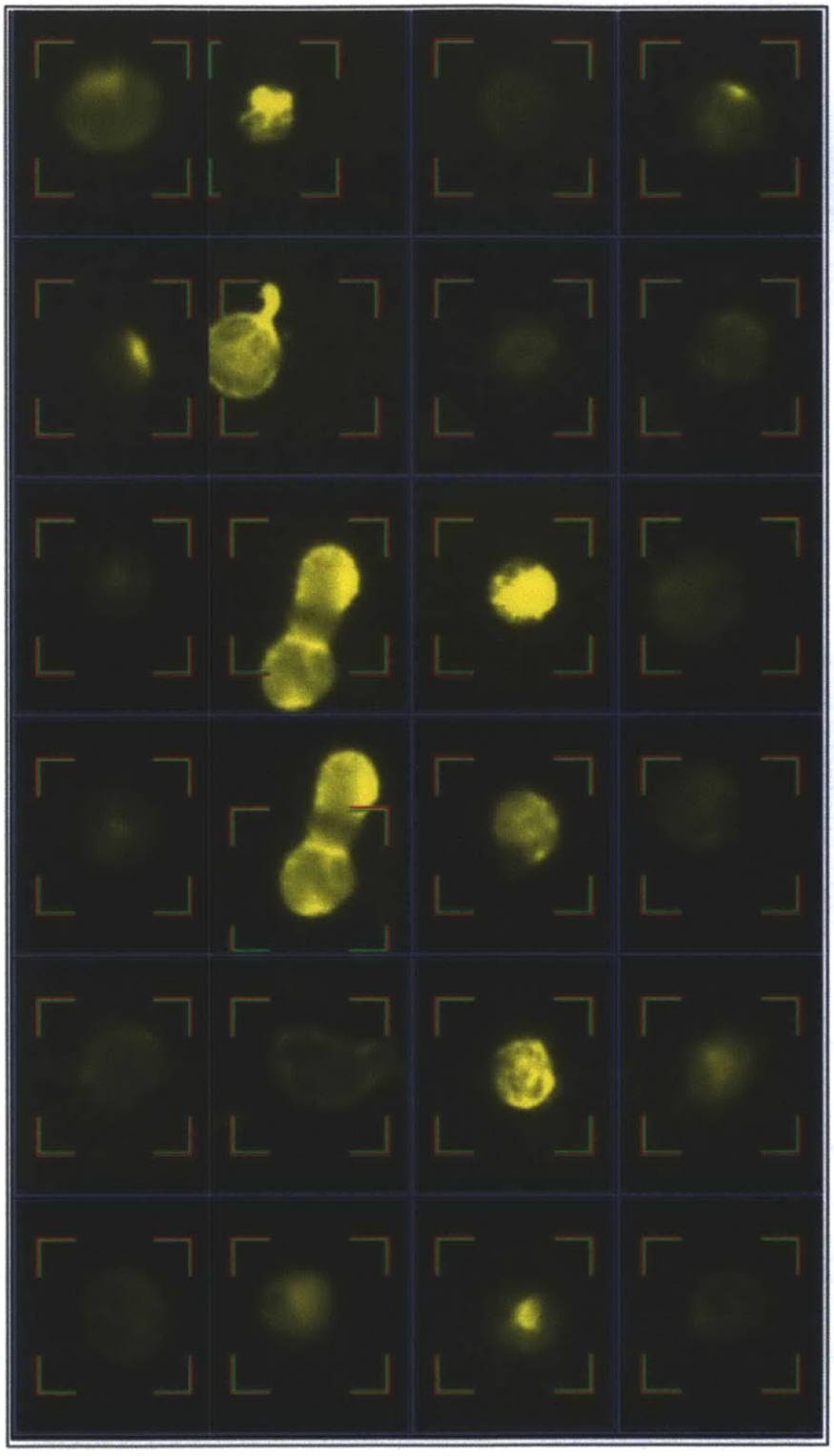

Figure 66. Representative gallery of CK+ cells identified by BioView imaging platform.

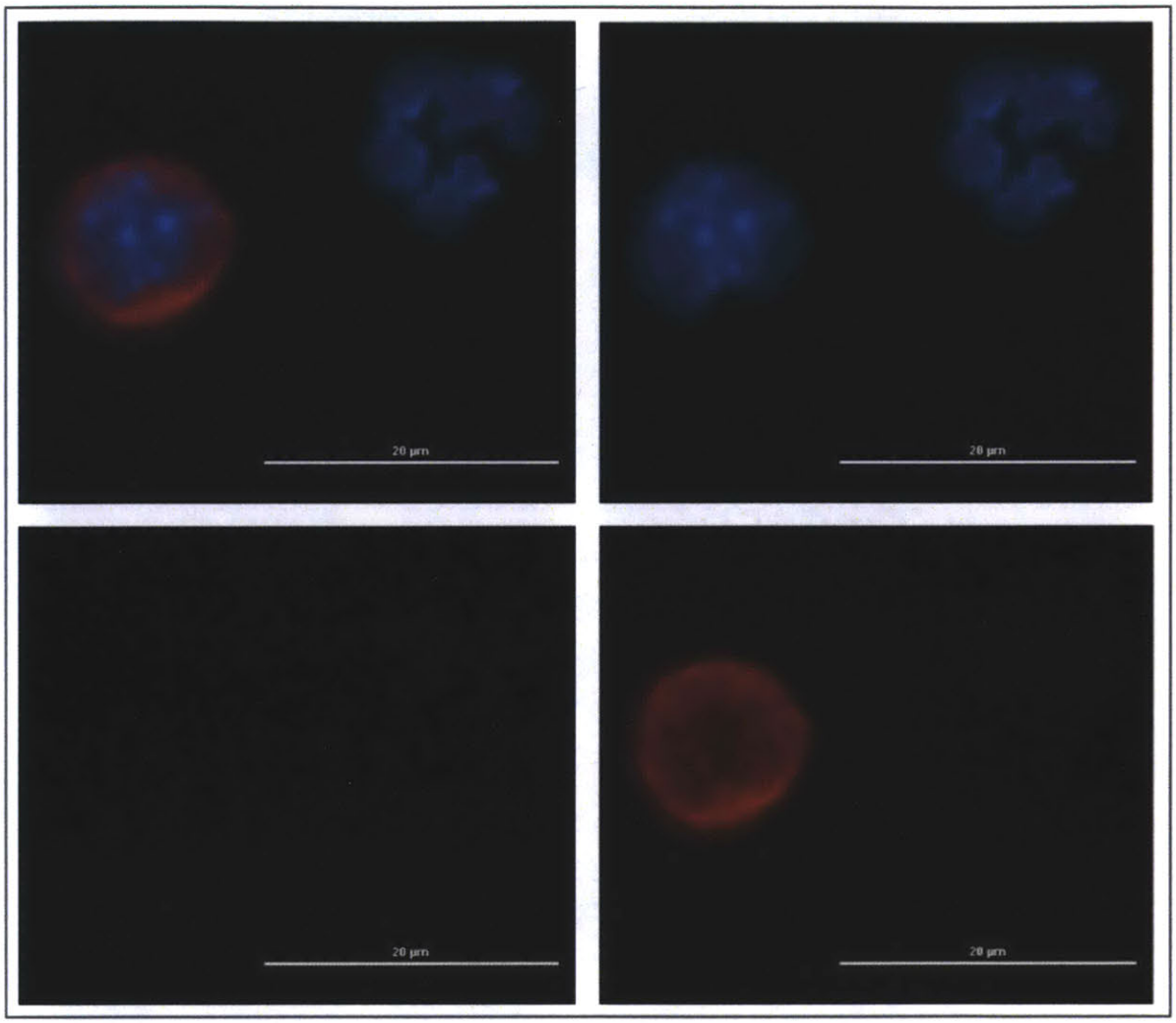

Figure 67. Cytokeratin positive CTC found in the blood of an endogenous PDAC bearing mouse stained with DAPI (blue), cytokeratin (red) and CD45 (green).

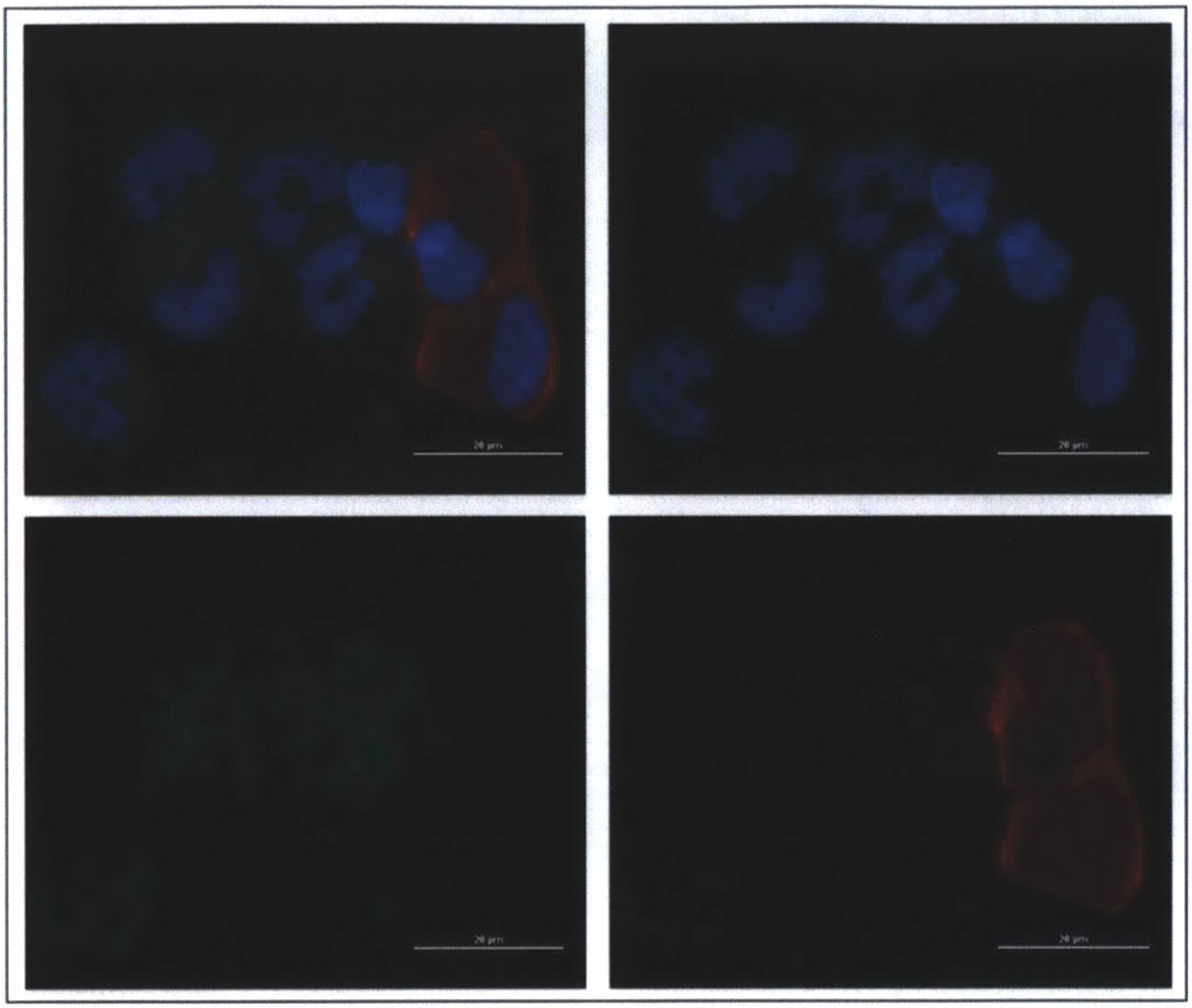

Figure 68. CTC identified from an endogenous mouse sample. Stained as in Figure 67.

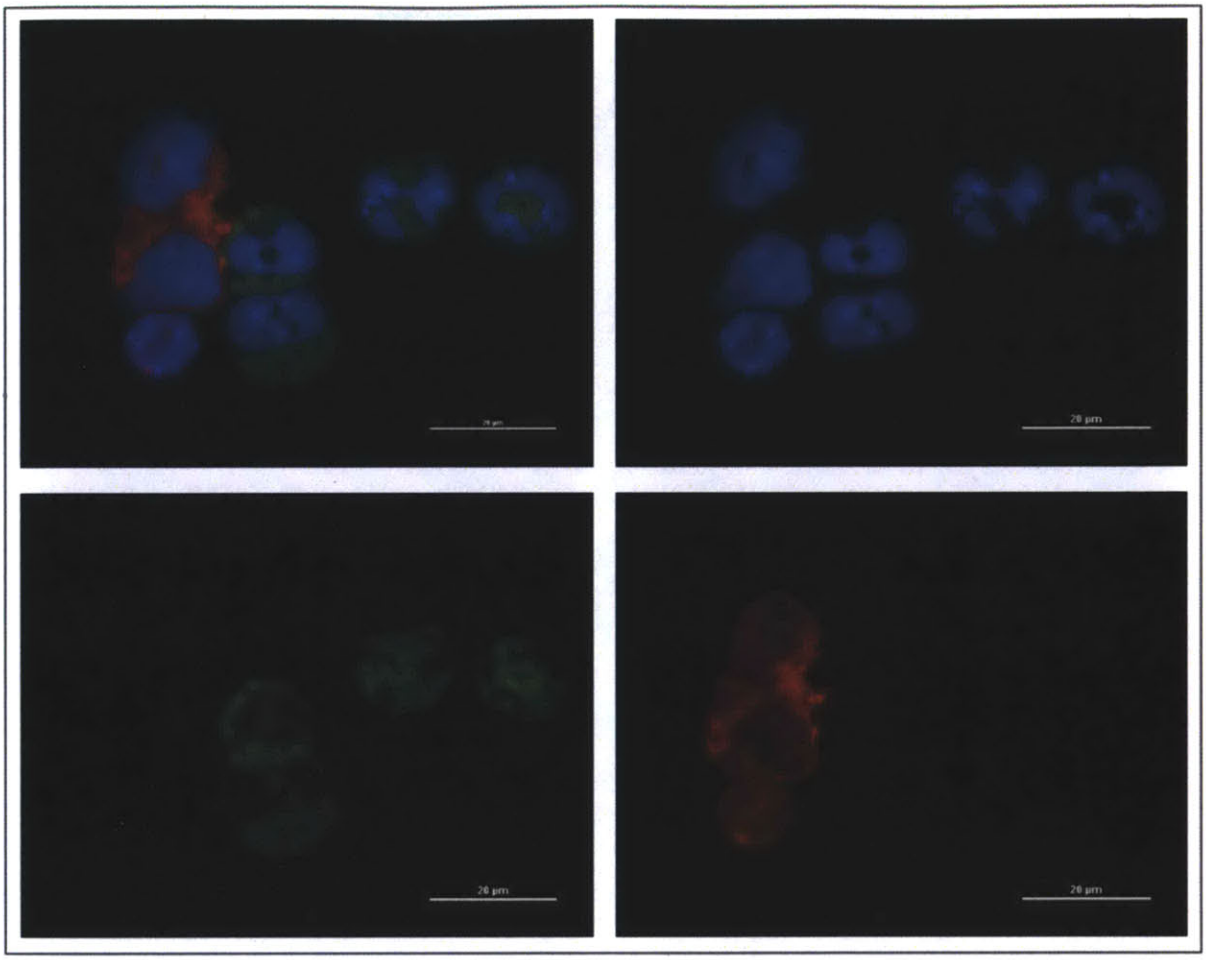

Figure 69. CTC identified from an endogenous mouse sample. Stained as in Figure 67.

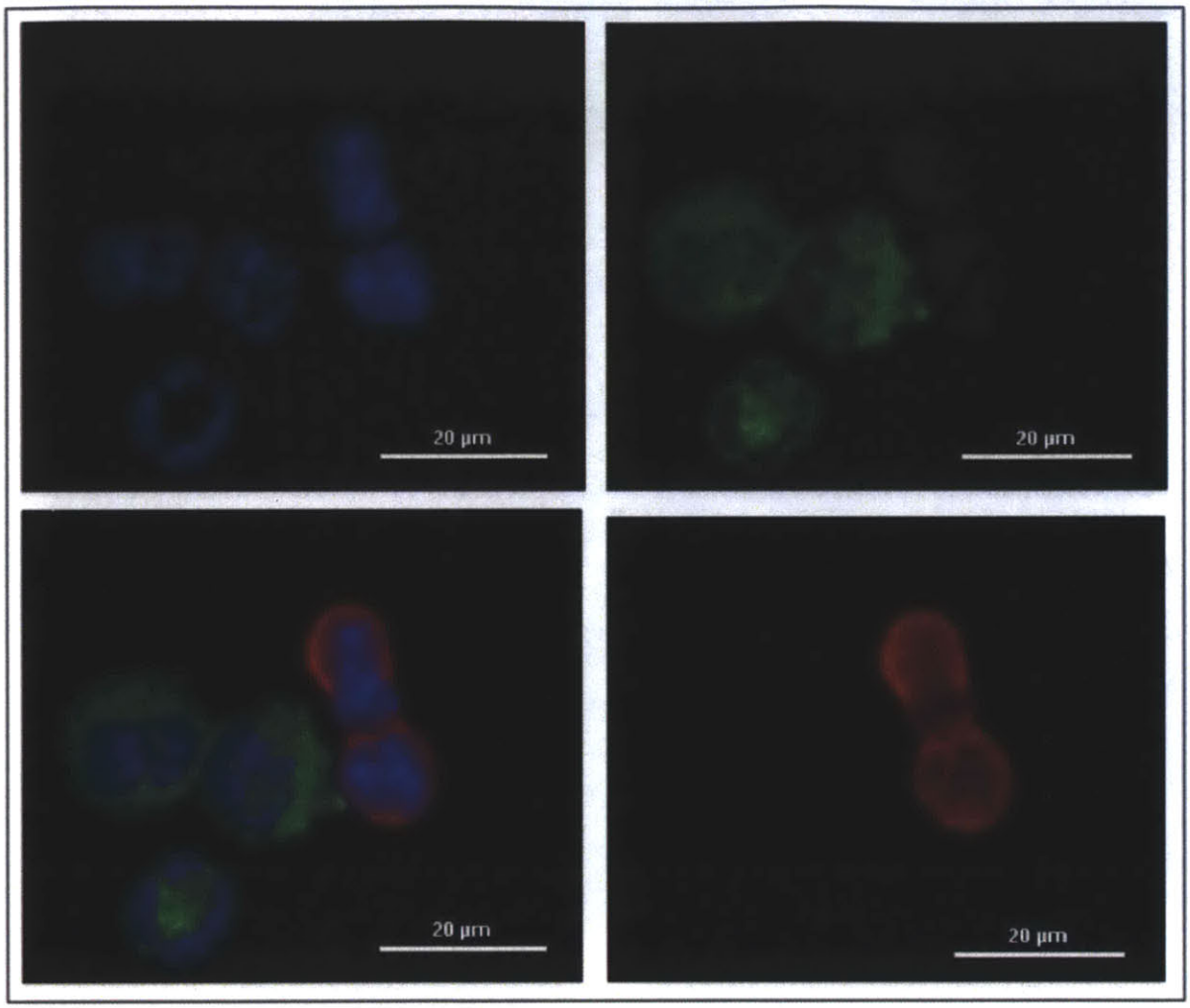

Figure 70. CTC identified from an endogenous mouse sample. Stained as in Figure 67.

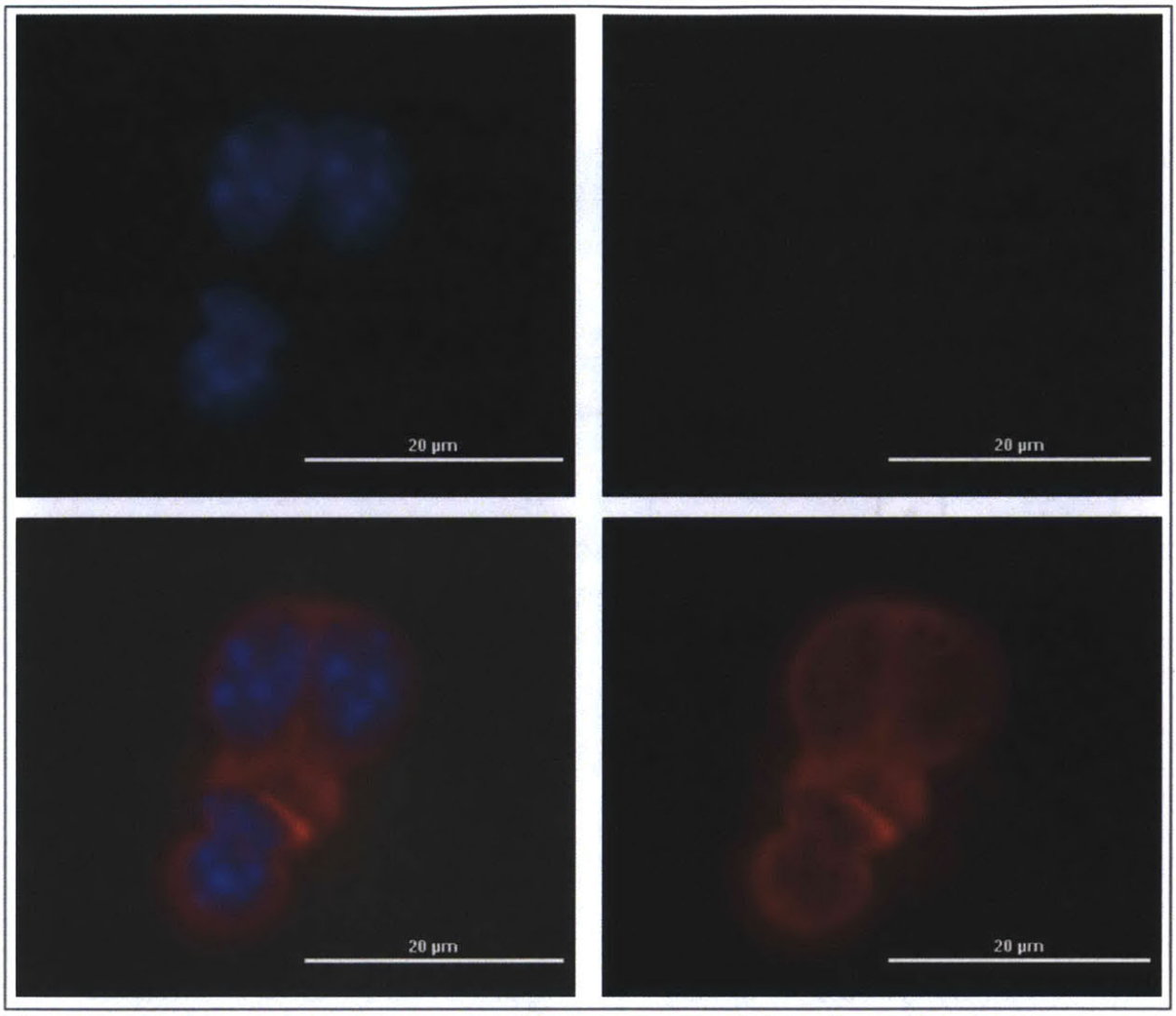

Figure 71. CTC identified from an endogenous mouse sample. Stained as in Figure 67.

5.6.4 Single cell transcriptome amplification

To validate the single cell amplification protocol developed by Tang, et. al. in our own hands, 6 single NB508 cells were selected using the micromanipulation techniques described and amplified. (*69*) As demonstrated, five of the six transcriptomes successfully amplified, and based on the qPCR data presented, a threshold Ct value was set at 25 cycles for further analysis. (Figure 72)

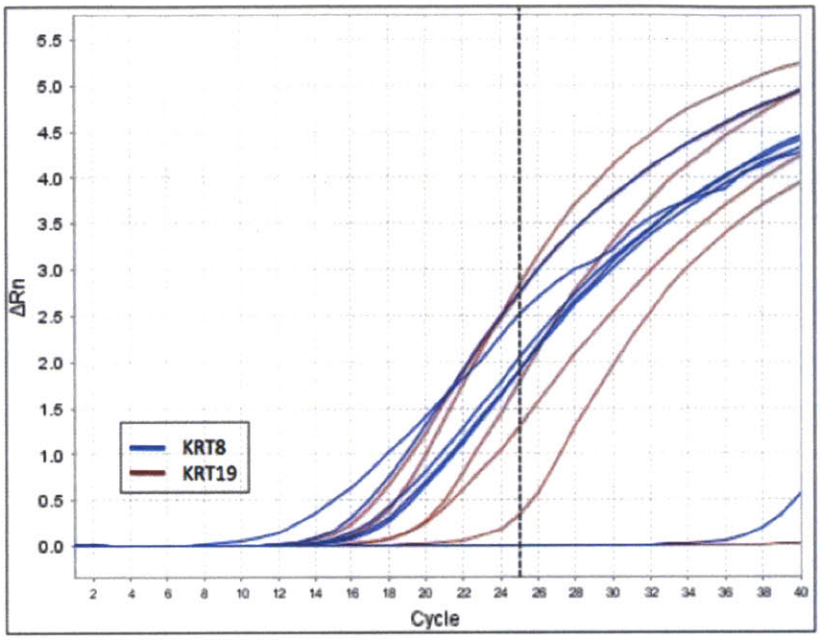

Figure 72. qPCR Analysis of 6 single NB508 cells indicates 5 of 6 single cells were successfully amplified. Dashed line at 25 cycles indicates threshold used for further analysis.

5.6.5 CTC Identification by qPCR and initial insight into heterogenity

60 single cells enriched from endogenous samples were analyzed in an initial cohort, and qPCR was conducted for GAPDH (sample quality), KRT8, KRT18, KRT19 (cytokeratins traditionally associated with CTCs), and PDX1 (a pancreatic specific marker). This analysis demonstrated that 49/60 single cells were successfully amplified, and 24/48 CD45- cells were positive for cytokeratins. Interestingly 5/48 cells were positive for PDX1, but no keratins, and 19/48 cells were negative for any of the tested markers, but were successfully amplified (based on GAPDH signal). This data, along with the variability in keratin expression observed provides an initial insight into the heterogeneity of CTCs. (Figure 73) Transcriptome sequencing of these single cells will likely reveal a much more complex picture, and has the potential to identify rare, but biologically important, subsets of CTCs.

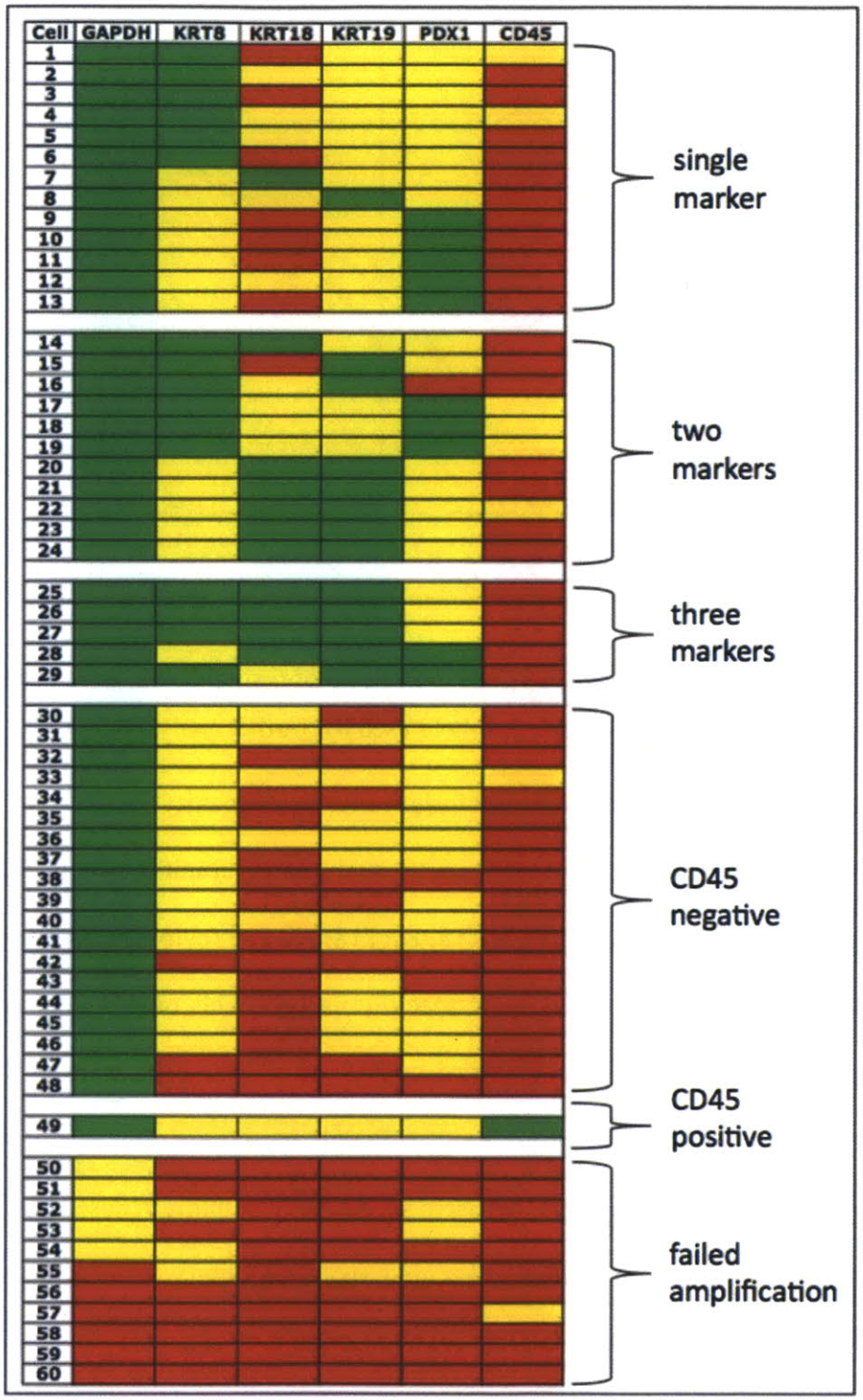

Figure 73. qPCR analysis of 60 single cells found in CTC enriched samples obtained from endogenous tumor bearing mice.

5.7 Conclusions

Here we presented an initial application of the MIMICS system to further our understanding of pancreatic cancer metastasis. CTCs from an endogenous pancreatic cancer mouse model were isolated using a modified negative depletion configuration. By optimizing the depletion of murine WBCs and interrogating the entire blood volume, we were able to recover CTCs in solution, in large numbers, and with high purity. This enabled single cell micromanipulation and transcriptome amplification. Initial qPCR analysis revealed broad heterogeneity amongst putative CTCs, with a range of cytokeratin expression levels and expression of the pancreatic-specific gene product PDX1. Perhaps most intriguing was the detection of PDX1 expressing cells with low or absent cytokeratin expression; these cells, found in whole blood, are presumably of tumorigenic origin yet lack expression of the traditional epithelial cytokeratin markers associated with CTCs, suggesting they may represent a subpopulation of CTCs undergoing EMT or may be otherwise implicated in the metastatic process. Ongoing work towards full transcriptome sequencing of these single cells will likely more fully reveal the heterogeneity within the CTC population and provide insights into the mechanisms of pancreatic cancer metastasis.

Chapter 6: Conclusions and outlook

In this thesis, two novel technologies are presented with the overall aim of enabling detailed characterization of circulating tumor cells with an array of immunophenotyping and molecular analysis tools.

6.1 Summary of contributions

Initially, we developed a novel biomaterial coating for microfluidic cell capture devices. As demonstrated, this coating facilitates cell capture with an efficiency comparable to standard chemistries, while enabling the release of virtually all captured cells upon degradation of the sacrificial coating. Importantly, the backbone degradation mechanism is innocuous to mammalian cells, and is demonstrated to have no effect on cell viability or proliferative potential. By dissolving the entire coating rather than targeting particular linkages, both specific (antibody-antigen) and non-specific (electrostatic) cell-surface linkages are cleaved, resulting in highly efficient release of captured cells. This study clearly demonstrated the utility of sacrificial coatings to enable the release of immunoaffinity captured cells from microfluidic cell capture devices.

Second, we present an entirely new CTC isolation technology, known as the MIMICS (Magnetophoretic Inertial Microfluidcs for Integrated Cell Sorting) system. This system integrates three microfluidic components – lossless debulking of whole blood, precise cell positioning using inertial forces, and highly sensitive magnetophoresis. As demonstrated, this system can be used for either positive selection (with > 90% yield of low EpCAM expressing PC3-9 cells) or negative depletion (> 90% yield of ultra-low EpCAM expressing LBX1 cells). The enriched CTCs are collected in solution, and in the case of negatively enriched cells, free of

any bound labels; this makes them readily compatible with a wide array of downstream assays. In an initial cohort of breast, prostate and lung patients, we are able to readily indentify CTCs using standard immunofluoresence methods and molecular profiling. Furthermore, review of papanicalaou stained samples by a board-certified cytopathologist revealed 'suspicious' and 'aberrant' cells likely of tumorigenic origin. Together, this initial data validates the functionality of the MIMICS system for CTC isolation from a clinical cohort; it further demonstrates the potential for highly sensitive, solution-based cell isolation to enable new downstream analyses which were previously technically limited. Most compelling is the development of a robust, sensitive 'negative depletion' approach to enable near lossless isolation of non-hematopoietic cell populations from whole blood, as this has the potential to reveal previously unstudied subpopulations of CTCs.

The MIMICS system was applied to an endogenous pancreatic mouse model to enable unbiased enrichment of CTCs, with the goal of better understanding the heterogeneity inherent in this rare cell population. CTCs were recovered with high purity, enabling single cell micromanipulation and gene expression analysis. Following single cell RNA extraction and cDNA amplification, qPCR analysis for a series of keratins (8, 18, 19) as well as PDX1 (a pancreatic specific marker) and CD45 (a leukocyte marker) was conducted. This initial screen revealed a notable number of 'classical' CTCs with high keratin expression and absent CD45 expression, while also highlighting a wide array of other phenotypes worthy of deeper characterization. Additionally, the study further demonstrates the flexibility of the MIMICS system as it was readily adapted to the mouse model.

6.2 Recommendations for future work

6.2.1 Sacrificial coatings for the release of immunoaffinity captured cells

The efforts towards release of immuno-affinity captured cells presented in this thesis clearly motivate the use of a sacrificial layer approach. While the work shown encompasses biomaterial development and validation, the key step needed to enable CTC capture and release is integrating the coating with the three-dimensional HB-chip micro-architecture in a conformal fashion. This is critical, as preservation of the microchip architecture is necessary to enable efficient rare cell capture. Potential coating approaches that should be explored include spraycoating and dipcoating; these are both robust, scalable techniques used to deposit biopolymers on substrates. Alternative approaches to forming sacrificial coatings should also be considered, as they may be more amenable to conformal coating. For instance, layer-by-layer (LBL) deposition is a well established method to form conformal hydrogels. (*70, 71*) By successively depositing polymers with opposing charges, a hydrogel may be formed as electrostatic forces hold the polymer layers together. Importantly, each layer is 'self-terminating' and thus conformal coatings may be easily formed. Another strategy to consider would be polymer vapor deposition; hydrogels formed using this approach have been demonstrated to conformally coat complex geometries. (*72, 73*) Key to the success of either of these approaches will be the selection of polymers and crosslinkers with rapidly degradable moieties to enable dissolution and cell release.

6.2.2 The MIMICS cell isolation system

The MIMICS system presented in this thesis represents a notable improvement in microfluidic immuno-based cell isolation. While promising, the system needs to be further validated using a larger clinical cohort and with direct comparisons to other CTC enrichment strategies, such as

the HB-Chip and the CellSearch system. Coupling the system with downstream lossless cell handling and plating methods would notably improve the utility of the technology. Further improvements should focus on advancing both the cell capture efficiency and purity. For 'positive selection', this may be achieved by exploring a variety of capture moieties beyond EpCAM. These could include antibodies or aptamers against disease-specific targets such as EGFR (lung cancer), HER2 (breast cancer), or PSMA (prostate cancer). Positive selection would also benefit from increases in purity through targeted removal of contaminating WBCs; possible approaches could include surface immuno-affinity capture or antibody directed photolysis.

Achieving another order of magnitude of purification in the 'negative depletion' mode would be an important advancement of the technology; this is imperative to enable molecular analyses of samples enriched in this manner. Multiple avenues exist to achieve this goal, including fluidic, magnetic and reagent enhancements. Based on the mathematical model presented previously (Figure 36), a minimum of 6-8 beads are needed to deflect white blood cells; this calculation, along with the probabilistic distribution of bead-cell interactions during the labeling process, suggests that many of the undeflected WBCs are labeled with magnetic beads, but in numbers below the deflection threshold. These cells could be magnetically removed from the sample using a secondary purification channel in which the residence time was increased by expanding the channel cross-section and therefore decreasing the magnetic load needed to deflect. As this approach would disrupt cell focusing, the WBCs would need to be deflected not to a side stream, but to the bottom of the channel, where they could be magnetically held in place while the target cells continued to the outlet. Another strategy to deplete cells with low levels of bead labeling would be to create a high-gradient magnetic field in the deflection region, thereby decreasing the magnetic load needed to deflect a cell to the side of the channel in the given residence time.

High gradient fields have been commonly used in bulk cell isolation technologies, and have recently been integrated into microfluidic circuits; the major obstacle is the complexity of patterning and aligning magnetizable materials at the microscale. (*74*) The third tactic that could be taken to improve the purity of the negative depletion product centers on modulating the reagents. While the 1 micron magnetic beads used here have a large magnetic moment, once a bead is bound to an antigen, surrounding antigens are sterically blocked from binding to additional beads; given that WBCs express millions of copies of CD45 on their surface, the effective copy number is dramatically reduced due to this steric hindrance. Therefore, using much smaller (~50 nm) highly magnetizable particles, which would not block surrounding antigens, has the potential to increase the overall magnetic loading on a cell. (*75*) Finally, it should be noted that while the vast majority of non-tumor cells found in whole blood express CD45 and CD15, there are other rare cell populations that exist in blood and lack these antigens, such as megakaryocytes and circulating endothelial progenitor cells; specific targeting of these cell populations should be considered. Similarly, should characterization of the undepleted WBCs reveal a specific subpopulation of leukocytes, direct targeting of this subpopulation through specific antigens would be warranted.

6.2.3 Single cell analysis of circulating tumor cells

The natural extension of the work presented in chapter 5 is full transcriptome sequencing of the amplified CTCs isolated from the endogenous pancreatic cancer mouse model; such an analysis has the potential to fundamentally advance our understanding of pancreatic cancer metastasis. If particular subpopulations of CTCs emerge (i.e., CTCs with stem cell or EMT characteristics), detailed study of these populations would be warranted. At a minimum, the transcriptome analysis efforts are likely to identify gene products that are highly expressed in CTCs, generating

a wealth of potential therapeutic candidates that merit biological characterization. Additionally, it is anticipated that with improvements in the purity of CTCs isolated from human blood samples using negative depletion, a similar characterization of human CTCs could be conducted, directly deepening our understanding of the role of CTCs in a wide variety of human cancers.

Chapter 7: References

1. M. Cristofanilli *et al.*, Circulating tumor cells, disease progression, and survival in metastatic breast cancer. *N Engl J Med* **351**, 781 (Aug 19, 2004).
2. G. Sakorafas, Safioleas, M., Breast cancer surgery: an historical narrative. Part I. From prehistoric times to Renaissance. *European Journal of Cancer Care,* (Jan 1, 2009).
3. T. R. Ashworth, A case of cancer in which cells similar to those in the tumours were seen in the blood after death. *The Medical Journal of Australia* **14**, 146 (1869).
4. M. Yu, S. Stott, M. Toner, S. Maheswaran, D. A. Haber, Circulating tumor cells: approaches to isolation and characterization. *J Cell Biol* **192**, 373 (Feb 7, 2011).
5. J. Kaiser, Cancer's circulation problem. *Science,* (Jan 1, 2010).
6. S. Kraeft *et al.*, Reliable and sensitive identification of occult tumor cells using the improved rare event imaging system. *Clinical Cancer Research,* (Jan 1, 2004).
7. D. Marrinucci *et al.*, Fluid biopsy in patients with metastatic prostate, pancreatic and breast cancers. *Physical Biology,* (Jan 1, 2012).
8. G. Vona *et al.*, Isolation by size of epithelial tumor cells: a new method for the immunomorphological and molecular characterization of circulating tumor cells. *American journal of pathology,* (Jan 1, 2000).
9. H. Lin *et al.*, Portable filter-based microdevice for detection and characterization of circulating tumor cells. *Clinical Cancer Research,* (Jan 1, 2010).
10. A. Bhagat, H. Hou, L. Li, C. Lim, J. Han, Pinched flow coupled shear-modulated inertial microfluidics for high-throughput rare blood cell separation. *Lab Chip,* (Jan 1, 2011).
11. K. Pantel, R. H. Brakenhoff, B. Brandt, Detection, clinical relevance and specific biological properties of disseminating tumour cells. *Nat Rev Cancer* **8**, 329 (May, 2008).
12. R. Rosenberg *et al.*, Comparison of two density gradient centrifugation systems for the enrichment of disseminated tumor cells in blood. *Cytometry,* (Jan 1, 2002).
13. A. Talasaz *et al.*, Isolating highly enriched populations of circulating epithelial cells and other rare cells from blood using a magnetic sweeper device. *Proceedings of the National Academy of Sciences,* (Jan 1, 2009).
14. M. Zborowski, J. J. Chalmers, Rare Cell Separation and Analysis by Magnetic Sorting. *Analytical Chemistry,* (2011).
15. P. Balasubramanian *et al.*, Confocal images of circulating tumor cells obtained using a methodology and technology that removes normal cells. *Molecular pharmaceutics* **6**, 1402 (2009).

16. S. Nagrath *et al.*, Isolation of rare circulating tumour cells in cancer patients by microchip technology. *Nature* **450**, 1235 (Dec 20, 2007).

17. S. L. Stott *et al.*, Isolation of circulating tumor cells using a microvortex-generating herringbone-chip. *Proceedings of the National Academy of Sciences of the United States of America* **107**, 18392 (Oct 26, 2010).

18. S. L. Stott *et al.*, Isolation and characterization of circulating tumor cells from patients with localized and metastatic prostate cancer. *Sci Transl Med* **2**, 25ra23 (Mar 31, 2010).

19. S. Maheswaran, L. Sequist, S. Nagrath, Detection of mutations in EGFR in circulating lung-cancer cells. *N Engl J Med*, (Jan 1, 2008).

20. D. Evanko, Microfluidics and a garden hose. *Nature methods*, (Jan 1, 2008).

21. S. Wang *et al.*, Highly Efficient Capture of Circulating Tumor Cells by Using Nanostructured Silicon Substrates with Integrated Chaotic Micromixers. *Angew. Chem. Int. Ed.* **50**, 3084 (Mar 4, 2011).

22. A. Carbonaro, S. Mohanty, H. Huang, L. Godley, L. Sohn, Cell characterization using a protein-functionalized pore. *Lab Chip*, (Jan 1, 2008).

23. X. Cheng *et al.*, A microfluidic device for practical label-free CD4+ T cell counting of HIV-infected subjects. *Lab Chip* **7**, 170 (Jan 1, 2007).

24. K. T. Kotz *et al.*, Clinical microfluidics for neutrophil genomics and proteomics. *Nat Med* **16**, 1042 (Sep 1, 2010).

25. U. Dharmasiri, M. A. Witek, A. A. Adams, S. A. Soper, Microsystems for the capture of low-abundance cells. *Annual Review of Analytical Chemistry* **3**, 409 (2010).

26. D. Pappas, K. Wang, Cellular separations: a review of new challenges in analytical chemistry. *Anal Chim Acta* **601**, 26 (Oct 3, 2007).

27. K. Wang, M. K. Marshall, G. Garza, D. Pappas, Open-tubular capillary cell affinity chromatography: single and tandem blood cell separation. *Analytical Chemistry* **80**, 2118 (Mar 15, 2008).

28. H. Wang *et al.*, Shear stress induces endothelial differentiation from a murine embryonic mesenchymal progenitor cell line. *Arterioscler Thromb Vasc Biol* **25**, 1817 (Sep 1, 2005).

29. A. A. Adams *et al.*, Highly efficient circulating tumor cell isolation from whole blood and label-free enumeration using polymer-based microfluidics with an integrated conductivity sensor. *Journal of the American Chemical Society* **130**, 8633 (2008).

30. U. Dharmasiri *et al.*, Highly efficient capture and enumeration of low abundance prostate cancer cells using prostate-specific membrane antigen aptamers immobilized to a polymeric microfluidic device. *Electrophoresis* **30**, 3289 (Sep 1, 2009).

31. D. M. Panchision *et al.*, Optimized flow cytometric analysis of central nervous system tissue reveals novel functional relationships among cells expressing CD133, CD15, and CD24. *Stem Cells* **25**, 1560 (Jun 1, 2007).

32. M. A. Cooperstein, H. E. Canavan, Biological cell detachment from poly(N-isopropyl acrylamide) and its applications. *Langmuir* **26**, 7695 (Jun 1, 2010).

33. A. M. Kloxin, A. M. Kasko, C. N. Salinas, K. S. Anseth, Photodegradable hydrogels for dynamic tuning of physical and chemical properties. *Science* **324**, 59 (Apr 3, 2009).

34. A. Hatch, G. Hansmann, S. K. Murthy, Engineered Alginate Hydrogels for Effective Microfluidic Capture and Release of Endothelial Progenitor Cells from Whole Blood. *Langmuir*, (2011).

35. H. G. Gordan, N. L. Larson, *American Journal of Clinical Pathology*, 613 (1955).

36. Recommendations of the International Council for Standardization in Haematology for Ethylenediaminetetraacetic Acid Anticoagulation of Blood for Blood Cell Counting and Sizing. International Council for Standardization in Haematology: Expert Panel on Cytometry. *American Journal of Clinical Pathology* **100**, 371 (Oct 1, 1993).

37. S. M. Lewis, C. T. Stoddart, Effects of anticoagulants and containers (glass and plastic) on the blood count. *Lab Pract* **20**, 787 (Oct 1, 1971).

38. M. Berridge, Calcium signalling, a spatiotemporal phenomenon. *New Comprehensive Biochemistry*, (Jan 1, 2007).

39. K. Machaca, Ca(2+) signaling, genes and the cell cycle. *Cell Calcium* **48**, 243 (Nov 1, 2010).

40. A. D. Augst, H. J. Kong, D. J. Mooney, Alginate Hydrogels as Biomaterials. *Macromol. Biosci.* **6**, 623 (Aug 7, 2006).

41. R. S. Ashton, A. Banerjee, S. Punyani, D. V. Schaffer, R. S. Kane, Scaffolds based on degradable alginate hydrogels and poly(lactide-co-glycolide) microspheres for stem cell culture. *Biomaterials* **28**, 5518 (Dec 1, 2007).

42. V. Breguet, U. von Stockar, I. W. Marison, Characterization of alginate lyase activity on liquid, gelled, and complexed states of alginate. *Biotechnol Prog* **23**, 1223 (Jan 1, 2007).

43. Y. Xia, G. Whitesides, SOFT LITHOGRAPHY. *Annual Review of Materials Science* **28**, 153 (1998).

44. O. Jeon, K. H. Bouhadir, J. M. Mansour, E. Alsberg, Photocrosslinked alginate hydrogels with tunable biodegradation rates and mechanical properties. *Biomaterials* **30**, 2724 (May 1, 2009).

45. K. Haraguchi, H.-J. Li, Control of the coil-to-globule transition and ultrahigh mechanical properties of PNIPA in nanocomposite hydrogels. *Angew Chem Int Ed Engl* **44**, 6500 (Oct 14, 2005).

46. S. Nayak, L. A. Lyon, Soft nanotechnology with soft nanoparticles. *Angew Chem Int Ed Engl* **44**, 7686 (Dec 2, 2005).

47. W. A. Comisar, S. X. Hsiong, H.-J. Kong, D. J. Mooney, J. J. Linderman, Multi-scale modeling to predict ligand presentation within RGD nanopatterned hydrogels. *Biomaterials* **27**, 2322 (Apr 1, 2006).

48. W. A. Comisar, N. H. Kazmers, D. J. Mooney, J. J. Linderman, Engineering RGD nanopatterned hydrogels to control preosteoblast behavior: a combined computational and experimental approach. *Biomaterials* **28**, 4409 (Oct 1, 2007).

49. D. C. Danila *et al.*, Circulating tumor cell number and prognosis in progressive castration-resistant prostate cancer. *Clin Cancer Res* **13**, 7053 (Dec 1, 2007).

50. V. Muller *et al.*, Circulating tumor cells in breast cancer: correlation to bone marrow micrometastases, heterogeneous response to systemic therapy and low proliferative activity. *Clin Cancer Res* **11**, 3678 (May 15, 2005).

51. S. Riethdorf *et al.*, Detection of circulating tumor cells in peripheral blood of patients with metastatic breast cancer: a validation study of the CellSearch system. *Clin Cancer Res* **13**, 920 (Feb 1, 2007).

52. L. Yang *et al.*, Optimization of an enrichment process for circulating tumor cells from the blood of head and neck cancer patients through depletion of normal cells. *Biotechnol. Bioeng.* **102**, 521 (Feb 1, 2009).

53. D. Marrinucci *et al.*, Case study of the morphologic variation of circulating tumor cells. *Hum Pathol* **38**, 514 (Mar, 2007).

54. M. Yu *et al.*, A developmentally regulated inducer of EMT, LBX1, contributes to breast cancer progression. *Genes Dev* **23**, 1737 (Aug 1, 2009).

55. J. A. Davis *et al.*, Deterministic hydrodynamics: taking blood apart. *Proceedings of the National Academy of Sciences of the United States of America* **103**, 14779 (Oct 3, 2006).

56. L. Huang, E. Cox, R. Austin, J. C. Sturm, Continuous particle separation through deterministic lateral displacement. *Science*, (Jan 1, 2004).

57. R. Huang *et al.*, A microfluidics approach for the isolation of nucleated red blood cells (NRBCs) from the peripheral blood of pregnant women. *Prenat Diagn* **28**, 892 (Oct, 2008).

58. G. Fonnum, C. Johansson, A. Molteberg, S. Morup, E. Aksnes, Characterisation of Dynabeads® by magnetization measurements and Mössbauer spectroscopy. *Journal of magnetism and magnetic materials*, (Jan 1, 2005).

59. D. Di Carlo, D. Irimia, R. G. Tompkins, M. Toner, Continuous inertial focusing, ordering, and separation of particles in microchannels. *Proceedings of the National Academy of Sciences* **104**, 18892 (2007).

60. A. F. Hezel, A. C. Kimmelman, B. Z. Stanger, N. Bardeesy, R. A. Depinho, Genetics and biology of pancreatic ductal adenocarcinoma. *Genes Dev* **20**, 1218 (May 15, 2006).

61. E. Rozenblum *et al.*, Tumor-suppressive pathways in pancreatic carcinoma. *Cancer Res* **57**, 1731 (May 1, 1997).

62. S. R. Hingorani *et al.*, Trp53R172H and KrasG12D cooperate to promote chromosomal instability and widely metastatic pancreatic ductal adenocarcinoma in mice. *Cancer Cell* **7**, 469 (May, 2005).

63. A. J. Aguirre *et al.*, Activated Kras and Ink4a/Arf deficiency cooperate to produce metastatic pancreatic ductal adenocarcinoma. *Genes Dev* **17**, 3112 (Dec 15, 2003).

64. N. Bardeesy *et al.*, Both p16(Ink4a) and the p19(Arf)-p53 pathway constrain progression of pancreatic adenocarcinoma in the mouse. *Proc Natl Acad Sci U S A* **103**, 5947 (Apr 11, 2006).

65. N. Bardeesy *et al.*, Smad4 is dispensable for normal pancreas development yet critical in progression and tumor biology of pancreas cancer. *Genes Dev* **20**, 3130 (Nov 15, 2006).

66. M. Yu, Ting, David, Wnt Paper. *Nature*, (2012).

67. Andrew D. Rhim *et al.*, EMT and Dissemination Precede Pancreatic Tumor Formation. *Cell* **148**, 349 (Jan 20, 2012).

68. M. Yu, et. al., Detection of both epithelial and mesenchymal markers in metastatic breast cancer patient CTCs. *In preparation.*, (2012).

69. F. Tang *et al.*, mRNA-Seq whole-transcriptome analysis of a single cell. *Nat Methods* **6**, 377 (May, 2009).

70. E. Verploegen *et al.*, Reversible Switching of the Shear Modulus of Photoresponsive Liquid-Crystalline Polymers. *Angew. Chem. Int. Ed.* **48**, 3494 (Apr 27, 2009).

71. N. Zacharia, G. Rutledge, P. Hammond, Spraying asymmetry into functional membranes layer-by-layer. *Nat Mater*, (Jan 1, 2009).

72. M. E. Alf *et al.*, Chemical Vapor Deposition of Conformal, Functional, and Responsive Polymer Films. *Adv. Mater.* **22**, 1993 (Dec 4, 2009).

73. H. Tekin *et al.*, Responsive microgrooves for the formation of harvestable tissue constructs. *Langmuir*, (2011).

74. D. Inglis, R. Riehn, J. C. Sturm, R. Austin, Microfluidic high gradient magnetic cell separation. *Journal of Applied physics*, (April 2006, 2006).

75. R. Grass, E. Athanassiou, W. Stark, Covalently functionalized cobalt nanoparticles as a platform for magnetic separations in organic synthesis. *Angewandte Chemie Intl Edition*, (2007).